Controlling the buckling behavior of bilayered systems

Thesis by
Paul Mazur

In Partial Fulfillment of the Requirements for the
Degree of
Doctor of Philosophy

Caltech

CALIFORNIA INSTITUTE OF TECHNOLOGY
Pasadena, California

2019
Defended August 10, 2018

© 2019

Paul Mazur
ORCID: 0000-0002-2837-9716

All rights reserved

ACKNOWLEDGEMENTS

All this research wouldn't have been possible without the help of my advisor Professor Kaushik Bhattacharya. I am very grateful for all his scientific ideas, his mentorship, his support, and his kindness. During all 5 years of this PhD, every time I encountered a persistent difficulty, his door was always open and he always had more brilliant scientific intuition to overcome this difficulty. I also want to thank him for always being such a nice person, not only in our work environment but also outside of work when organizing events for the entire group. All those aspects have made my work during those 5 years very enjoyable, and I continue to feel very lucky for the opportunity to have accomplished all this research with him. I also want to thank my thesis committee: Professor Guruswami Ravichandran, whose words and comments have always been a great support during those 5 years; Professor Basile Audoly, who gave me very precious research materials through his publications and through the conversations we had related to energy computation; and Professor Chiara Daraio for her work regarding the interactions between materials' physical properties and structural deformations.

A lot of my inspiration during those years came from being a part of Kaushik's research group. I am very grateful to all my companions: Cindy, Sri, Vinamra, Mauricio, Lincoln, Jin, Paul, Dingyi, Chun-Jen, Louisa, Tori, Ying Shi, Hao, Sai, Kevin, Swarnava, Stella, Noy and many others for always making time for me whenever I needed a practice exam, a practice presentation, and feedback about my calculations and methods.

Those years were also made happy by the people from SOPS and the MCE department. I want to thank Dingyi Sun, Natalie Schaal, Tori Lee, Louisa Avel- lar, William Schill, Kevin Korner, and all other SOPS directory board members for the socials, the barbecues, and the banquets in which they brought plenty of joy and laughs through the years. I also want to thank the MCE administrative people: Carolina Oseguera, Lynn Seymour, Holly Golcher, and Sonya Lincoln. In particular, I would like to express my gratitude for Jenni Campbell, who is in charge of Kaushik's group, and Leslie Rico before her, who helped me with a lot of organizational work.

This program would not have been possible without the Arts et Métiers Paris Tech Foundation and the SAFRAN company who put everything together to help me in my application and my funding. I want to thank them for all their efforts and the trust they placed in me.

I want to thank the Pasadena Rugby Club for taking me in the very first month I arrived in California and giving me 5 seasons of amazing games with extraordinary teammates.

Finally, none of my success would have been possible without the support of my family. My parents and my brothers not only called and sent messages of support, but they also came to California to visit me. I am very grateful for all their kindness and for always making me happy despite the distance.

ABSTRACT

A bilayered system is an assembly of two different materials and has the form of flat and thin layers. The two materials are attached to each other at the surface. The attachment method varies depending on the materials properties. Bilayered systems made of materials with different dimensions and stiffness have been widely studied and used for different applications. The characteristic scale of this kind of system can go from hundreds of km in the case of geological layers on the Earth surface to some μm in the case of very small electronic systems or microlenses.

The behavior of a bilayered system, when submitted to a stimulus, is characterized by the conflict between the preferred response of each material and the constraint that one imposes on the other. As a result, the deformation of the bilayered system will be different from that which could be obtained when the materials are taken separately. Of particular interest is the buckling of such systems: when submitted to a particular stress distribution, one material will expand significantly more than the other, but as the two materials are attached at the interface surface, the material displacements must be continuous through this interface. The conflict between the continuity of displacement and the need to expand differently may result in nonlinear patterns at this interface. Those unstable situations can be used to define a limit of constraint for the materials or can be used as actuators for a desired surface pattern. Many studies have focused on characterizing homogeneous buckling within an entire surface due to homogeneous strain distribution within the top surface. This characterization was performed theoretically, numerically, and experimentally. But, some studies have shown different possibilities of evolution of the buckling patterns known today. As a consequence, we can pose two questions: 1) Is there a possibility to modify non-linear patterns regardless of what is imposed by mechanical properties and dimensions? 2) What happens in the case of a non-uniform state of constraints within the bilayered system?

This thesis explores those questions for the case of a thin stiff film attached to a compliant thick substrate. The first part of this thesis serves to describe the initial buckling theory in the case of uniform strain and explains how to define the loading threshold resulting in uniform buckling at the surface characterized by a finite number of spatial frequencies. The second part of the thesis studies the consequences of a non-uniform loading within the surface. A numerical method based on the theory of the first part is implemented to show the emergence of new frequencies due to the discontinuous loading distribution. The third part focuses on the possibility of tuning a uniform buckling by including an electromechanical coupling into the bilayered system. This coupling makes the materials sensitive to electric fields, thus creating a new energy term to interfere with the mechanical energy of deformation, thereby modifying the resulting spatial frequency of the buckling. This study is done theoretically and numerically by finite element modeling.

TABLE OF CONTENTS

Acknowledgements iii
Abstract v
Table of Contents vii
List of Illustrations ix
List of Tables xi
Chapter I: Introduction 1
  1.1 Overview of a bilayered system 1
  1.2 Fields of application of buckling deformation 2
    1.2.1 Flow control 2
    1.2.2 Flexible electronics 5
    1.2.3 Microlens arrays 5
    1.2.4 Material characterization and metrology 7
    1.2.5 Phase grating 7
  1.3 Literature review 8
  1.4 Thesis motivation and outline 9
Chapter II: Instabilities in bilayered systems 11
  2.1 Bilayered system 11
    2.1.1 Föppl-von Kármán theory 11
    2.1.2 Energy brought by the substrate 12
    2.1.3 Loading 15
  2.2 Possible instabilities 16
    2.2.1 Buckling 16
    2.2.2 Deformation patterns 16
    2.2.3 Theory for unidirectional wrinkles 17
  2.3 Experimental studies 18
Chapter III: Numerical method for discontinuous buckling 21
  3.1 Liquid-crystalline substrates 21
  3.2 Minimizing the total energy 22
    3.2.1 Non-dimensionalization 23
    3.2.2 Transfer to the Fourier domain 25
    3.2.3 Use of the Augmented Lagrangian 25
  3.3 Results 31
    3.3.1 Case of a uniform strain 31
    3.3.2 Influence of quadratic constraint on convergence 33
    3.3.3 Case of discontinuous strain 40
    3.3.4 Limit of the interface dimension 44
    3.3.5 Study of a symmetric interface with a small error 50
Chapter IV: Wrinkling control by electric field: small deformation theory . . 52
  4.1 Electromechanical coupling and bilayered systems 52

- 4.2 Energy of the system 53
- 4.3 Case of unidirectional wrinkles 59
- 4.4 Case of bidirectional wrinkles 61

Chapter V: Wrinkling control by electric field: finite deformation simulations 64
- 5.1 Strain mismatch-induced wrinkles 64
  - 5.1.1 Computational setting 64
  - 5.1.2 Buckling method 66
  - 5.1.3 Results 68
- 5.2 Dielectric material modeling 74
- 5.3 Results 78
  - 5.3.1 Results with varying elasticity of the substrate 79
  - 5.3.2 Different options for deformation gradient tensor and mesh size 84
  - 5.3.3 Results with varying thickness of film 85
  - 5.3.4 Results for gold film and PDMS substrate 89

Chapter VI: Conclusion 91
- 6.1 General conclusion 91
- 6.2 Future work 95

Bibliography 98

Appendix A: Augmented Lagrangian code 104

Appendix B: Abaqus bilayered system code 121

Appendix C: Substrate energy code 148

LIST OF ILLUSTRATIONS

Number *Page*
1.1 Example of multilayered material 1
1.2 Example of buckling of a bilayered system. 2
1.3 Modeling of flow streamlines over an aircraft 3
1.4 Ducted rubber coating 4
1.5 Example of elastic electronic surface made on a polymer substrate . . 6
1.6 Magnified optical profile of microlens surface 6
2.1 Bilayered system consisting of a thin film attached to a thick substrate. 11
2.2 Schematics of buckling mode shapes in bilayered systems 17
2.3 Schematic of three types of morphological instability 17
2.4 Experimental method to generate wrinkles: example 1 19
2.5 Experimental method to generate wrinkles: example 2 19
3.1 Converged 1D deflection for uniform strain using Augmented Lagrangian method 32
3.2 Representation of deflection at different iterations 34
3.3 Converged 2D deflection for uniform strain using Augmented Lagrangian method 35
3.4 Relative error of the amplitude as a function of the sampling 35
3.5 Representation of deflection for varying scale 36
3.6 Evolution of the norm of the residue distribution for different values of quadratic penalty coefficient β. 39
3.7 Example of uniform deflection depending on both x and y coordinates. The final converged out-of-plane displacement is on the left, and the evolution of the norm of the associated residue is on the right. 40
3.8 Converged deflection for varying angle distributions. 42
3.9 Converged deflection for symmetric strain angle through the interface. 42
3.10 Converged deflection for multiple symmetric interfaces. 43
3.11 Converged deflection for multiple non-symmetric interfaces. 43
3.12 Converged deflection for different angles of the strain mismatch . . . 45
3.13 Energy density functions distributions for the case of uniform wrinkles. 46
3.14 Energy density functions distributions for the case of wrinkles with one non-symmetric interface. 47

3.15 Energy density functions distributions for the case of symmetric wrinkles. 48
3.16 Multiplication of the number of strain orientation discontinuities on a surface 49
3.17 Angle difference to generate branching along the interface 51
4.1 Principle of operation of dielectric elastomers 53
4.2 Evolution of wrinkles wavenumber for varying external voltage . . . 60
4.3 Evolution of wrinkles amplitude for varying external voltage 61
4.4 Illustration of the influence of the electric field on multi directional wrinkles 63
5.1 ABAQUS mesh illustration 65
5.2 Steps for wrinkles generation in ABAQUS 67
5.3 Fourier analysis of post-buckling behavior 69
5.4 ABAQUS evolution of wrinkles with temperature 70
5.5 ABAQUS wrinkles for different stiffness ratios 71
5.6 Numerical and theoretical results for wavelength 72
5.7 Numerical and theoretical results for amplitude 73
5.8 ABAQUS results for gold film attached to PDMS substrate 74
5.9 Study of the accuracy of the user element 76
5.10 Study of the accuracy of the user element for different Young moduli 77
5.11 Steps for electric field generation in ABAQUS 78
5.12 Comparison of amplitude of wrinkles for constant and varying wavelengths as a function of applied electric field. 80
5.13 ABAQUS subroutine result 80
5.14 ABAQUS results for varying substrate elasticity 81
5.15 Comparison of theory results and ABAQUS results for varying substrate elasticity 83
5.16 Amplitude vs external applied electric field for different gradient deformation tensor formats. 85
5.17 Amplitude vs external applied electric field for mesh sizes. 86
5.18 ABAQUS results for varying thickness 87
5.19 Comparison of theory results and ABAQUS results for varying thickness 88
5.20 Amplitude vs external applied electric field for gold film attached to PDMS substrate. 90

LIST OF TABLES

Number *Page*
1.1 Representative dielectric elastomer materials performance (Zheng [84]). 10
3.1 1D converged deflection characteristics with the Augmented Lagrangian method. 32
3.2 Converged two-dimensional deflection characteristics with the Augmented Lagrangian method. 35
3.3 Minimum norm of the residue and computational cost for different values of quadratic penalty coefficient β. 38
4.1 Table of the numerical values of physical parameters. 60
5.1 Possible sets of units in ABAQUS. 65
5.2 Physical parameters of the film and the substrate in ABAQUS. 65
5.3 Comparison between numerical values and theoretical values of wrinkles'wavelengths. 72
5.4 Comparison between numerical values and theoretical values of wrinkle amplitudes. 73
5.5 Datas used to model gold film attached to PDMS substrate. 74
5.6 Physical parameters of the film and the substrate for amplitude comparison. 79
5.7 Comparison of linear approximation of amplitude with theory coefficients for varying substrate elasticity. 82
5.8 Comparison of linear approximation of amplitude with theoretical coefficients for varying thickness. 86
5.9 Set of units in the case of a film made of gold. 89

Chapter 1

INTRODUCTION

1.1 Overview of a bilayered system

The combination of different materials to obtain a system with specific deformation properties represents a large field of study and research in the engineering domain. A common example is composite materials as illustrated in Figure 1.1. The simplest possible system is a bilayered system that consists of two materials attached to each other on a single large common surface. A bilayered system as it is considered in this thesis consists of a thin film attached to a thick substrate as shown in Figure 1.2. The interest in such a system comes from the study of instabilities when the substrate and the film are made of completely different solids with linear elastic properties in different ranges. Specifically, it is the strain mismatch between the two materials that tunes the instability at the surface. Another point to be considered is the dimensions of such a system: even though the film is very thin compared to the substrate, the thickness of the substrate is taken to be very small compared to its dimensions along the two other axes. This consideration allows simplifications in the study of deformations such as the use of plane strain assumptions.

Those considerations about the thickness of the two components result in the film being considered as a plate and the substrate as a semi-infinite elastic solid. To illustrate the deformations that can happen in case of buckling of a bilayered system, a simple example of wrinkles is shown in Figure 1.2. Those instability modes can

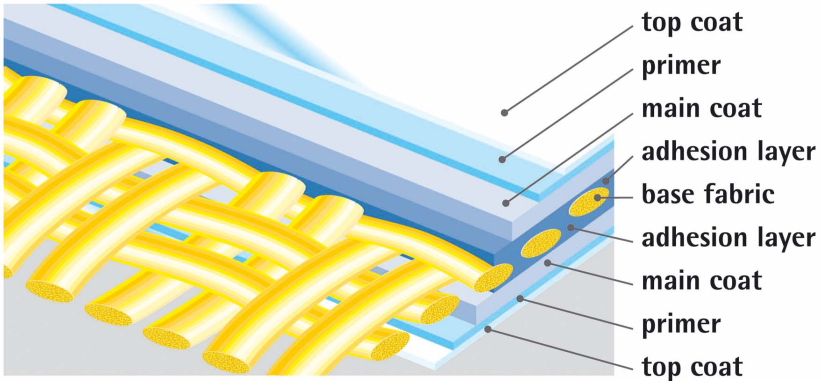

Figure 1.1: Example of multilayered material taken from [60].

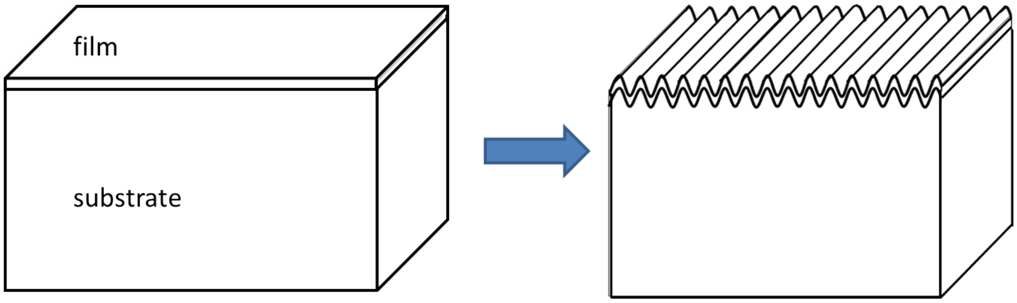

Figure 1.2: Example of buckling of a bilayered system.

appear in many situations observed in nature as listed by Genzer and Groenewold [32]: the case of mountains, with Earth's crust attached to Earth's mantle; the case of human skin, with the epidermis on top of the dermis; the case of fruits, in which the skin of the fruit can wrinkle on top of its flesh. They also pointed out that such instabilities are not only resulting from a plate film on top of a substrate, but can also come out of rods on top of a soft substrate, like in the case of rails buckling while attached to the soil. As mentioned by Hong et al. [41], those instabilities can be associated with the failure of the bilayered system, like in the case of creasing on a tire leading to fatigue failure if the phenomena is repetitive, or in the case of the film being damaged by creasing while it is supposed to cover and protect the substrate. The buckling of rails attached to the ground is also a failure and can cause very serious damages. On the other hand, many potential fields of application have been explored to discover an instability mode of a bilayered system. A tunable nonlinear deformation on a surface has several interesting uses.

1.2 Fields of application of buckling deformation

1.2.1 Flow control

The influence of boundary layer flow over energy consumption for a system in motion has been studied from theoretical, numerical, and experimental perspectives. In order to improve the efficiency of a system, several engineering problems have focused on the influence of the drag generated by the interaction between a solid structure and a fluid flow. Over the last century, the speed of all vehicles has increased, triggering more and more turbulent flow situations over the surface of those vehicles. The result is a higher fuel consumption to provide the necessary extra energy to compensate for the effects of turbulent flow [81, 26] and the risk of deterioration of the surface in contact with the flow. The situation is more critical in an aeronautic structure. The boundary layer affects lift and drag and can be the

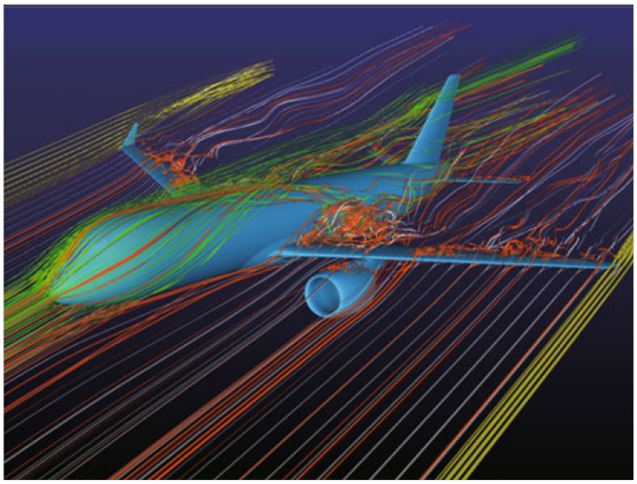

Figure 1.3: Flow streamlines over an aircraft. From Chen et al. [23]

difference between flight and staling.

There have been multiple studies of the interaction between large surfaces and flows. The main parameter used and measured for characterization is the velocity vector of the flow. The velocity field within a flow is determined by solving the Navier Stokes equations. The components of this vector are the streamwise velocity, the normal velocity, and the spanwise velocity. Starting from this vector, more specific characterization parameters like the Mach number, the Reynolds shear stress, or the overall drag coefficient can be defined.

The reduction of the drag related to the surface shear stress generated by the flow is the main objective of those studies. The theoretical study of drag uses the Navier Stokes equation combined with the conservation of mass. It results in the distinction of different types of drags as discussed in [28]. The numerical studies on turbulent flow over an aircraft have been performed on multiple occasions with diverse models. Each model can result in a different result in terms of drag representationm as emphasized in [23] and as illustrated in Figure 1.3.

To address the problem of drag reduction, studies have focused on the surface characteristics. Different methods have been used to specify surface property and its potential influence on drag reduction. In particular, one strategy that has been widely studied is the use of a compliant surface: initially, Kramer [50] introduced the idea of a distributed damping surface by the intermediary of a ducted rubber coating, illustrated in Figure 1.4, that would be in contact with a flow. His experiments resulted in a reduced drag coefficient compared to a rigid surface. Based on

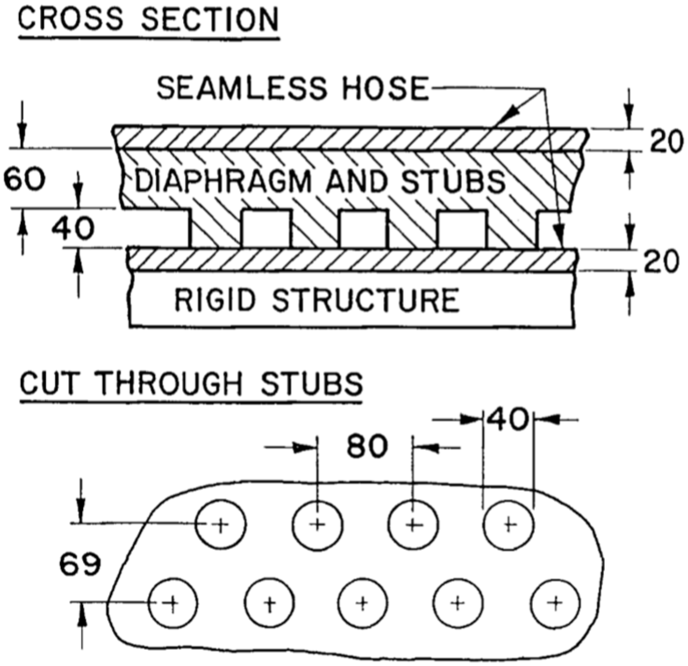

Figure 1.4: Ducted rubber coating from Kramer [50] (Dimensions in 1/1000 inch).

those results, further studies brought more types of compliant surfaces and more experimental observations.

The most common way to model a compliant surface is by considering it as a surface supported by springs and dampers. Those springs and dqmpers are associated with spring stiffness and a damping coefficient. The displacements of the wall can then be described by equation of motion relating the displacements, the spring and dumper coefficientsm and the wall stresses induced by the flow. The displacement field of this compliant surface results in different types of waves appearing within the flow in contact with the surface. The characterization of those waves gives a different approach to the influence of a compliant wall on the drag: Gad-El-Hak [35] and Carpenter [19] showed that even if the drag could be delayed by the effect of a compliant surface on the growth rate of Tollmien-Schlichting instabilities, the effect of the surface displacement could generate additional flow induced instabilities. Although Carpenter [20] managed to develop optimization criteria taking into account the different types of instabilities, the number of unknowns and the non-linearity of the Navier Stokes equation in the case of a turbulent flow makes the design of an ideal compliant surface very challenging.

In more recent studies performed by Luhar et al. [55, 56] it was emphasized that the waves associated with the wall-normal velocity and the wall pressure cover a large region in the spectral domain. It is possible to come up with an admittance relating the wall normal velocity and the wall pressure, but the main difficulty comes from the fact that it is necessary to optimize the wall performance for an entire range of wavenumbers and frequencies.

1.2.2 Flexible electronics

The design of coating made of metallic film attached to compliant polymer substrate is used in the design of electronics for smart sensory devices. Some very concrete examples are quoted by Lumelsky et al [57], like the design of a skin for smart floor or a machine skin for personal robots. Going more into detail of those electronics, Lacour et al [51] realized a mechanical and electrical characterization of a stretchable electronic surface and built a device based on the bilayered concept supporting an electric circuit. The principle was that the polymer substrate would be the support of both the active device cells containing circuit components like transistors and the metal interconnects (see Figure 1.5). The cells would be supported by a rigid islandm but the key to this system was the metal interconnects: the buckling of the bilayered system made of those interconnects and the substrate would make the circuit capable of handling up to 12 % stretch and avoiding fracture. The metal used for interconnects was gold and would buckle in a reversible way while still conserving its electrical properties. Another example is the design of metal-semiconductor-metal photodetectors based on buckled nanoribbons. This device's properties are well characterized by Sun et al [69], showing that the material properties of the Gallium arsenide nanoribbons, when attached to polymer substrate, result in a buckling behavior. This buckling behavior can be exploited in terms of bending when the nanoribbons are fully embedded inside the polymer material.

1.2.3 Microlens arrays

The importance of the physical properties of the materials, especially the elasticity modulus in the nonlinear deformation of bilayered systems, is taken advantage of in the design of microlenses: by controlling the dimensions of the film deposited on a substrate, it is possible to obtain a particular targeted shape for the bilayered system and then the film after the buckling occurs. This particular shape can be controlled to be concave or convex and then result in the microlenses desired. To generate microlenses through buckling, Chan and Crosby [21] developed a process : after modifying the linear elasticity of a polymer substrate along its surface by

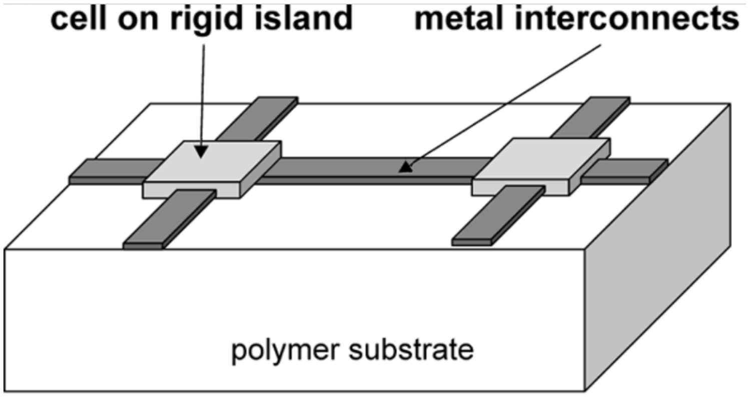

Figure 1.5: Example of elastic electronic surface made on a polymer substrate. From Lacour et al. [51]

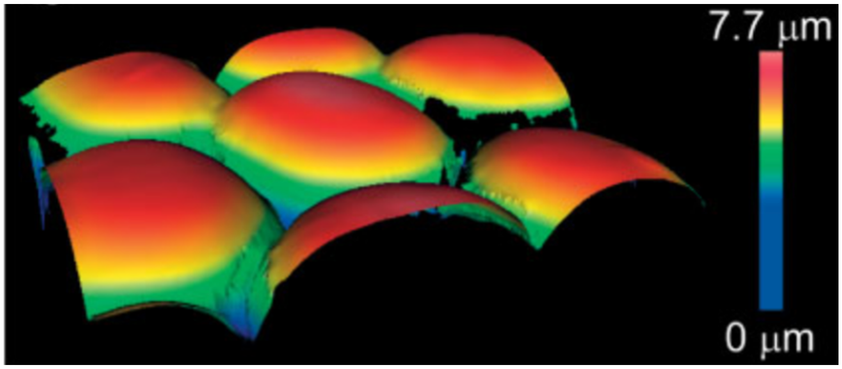

Figure 1.6: Magnified optical profile of microlens surface. From Chan and Crosby [21].

ultraviolet/ozone oxydation creating silicate regions, they attached this bilayered system to acrylate monomer in order to generate a swelling of the substrate. The specific regions with silicate on top of the polymer were then subject to buckling due to difference of elastic modulus between the polymer and the silicate. The control of the dimensions of the oxidized regions associated with the knowledge of the different elasticity modulus was the key to obtain the microlenses of the desired size, as illustrated in Figure 1.6. In order to build microlenses that would be less rigid and whose shape would be reversible, Chandra et al. [22] developed another method by applying a silicate layer through a copper mask on a pre-stretched polymer substrate. After releasing the substrate, the difference of elasticity modulus between the polymer and the silicate would trigger the wrinkling process, and the dimension of the microlens could be controlled by modifying the dimensions of the copper mask.

1.2.4 Material characterization and metrology

The previous sections have shown that the deformations observed on bilayered systems result from the difference of elastic modulus between materials. This fact can be used as a basis to determine the elastic properties of a film based on measured deformation when subjected to a known stretch and attached to a well-characterized substrate. The technique was used by Stafford et al. [66] when they created a film with an elastic modulus gradient resulting from the combination of two different polystyrene sub-films with varying thicknesses assembled together. This film consisting of two materials was then attached to a pre-stretched thick substrate, and the wavelength of the resulting observed surface wrinkles was measured by small angle light scattering. This wavelength could then be used to calculate the modulus of the film at every position. This is not the only application that can be made using bilayered systems. In their review, Chung et al. [27] also mention the possibility of using this system as a force sensor in biology studies: if the deformation properties of the film and substrate materials are known, the force exerted by the film on the substrate can be deduced from a measure of resulting deformation. The authors also describe the possibility of using the wrinkling phenomena on top of a bilayered system to measure over a time evolution the viscoelastic properties of a chosen polymer.

1.2.5 Phase grating

Another interesting application of those non-linear deformations is as diffraction tools: for a particular type of buckling consisting of wrinkles, the top surface of a bilayered system can (if the dimensions allow it) be turned into a phase grating. An example of such use was given by Harrison et al. [36] as they attached atactic polystyrene films to prestretched polydimethylsiloxane to generate buckling. They used the resulting deformed surface to diffract a coherent beam by generating a phase shift to the light proportional to the amplitude of the wrinkles on the surface of the bilayered system. One of the possible uses of a phase grating that refers to the previous section on metrology is described by Ma et al. [59]. They created a bilayered phase grating combining gold and polydimethylsiloxane and used the diffracted light as a way to measure thermal strain applied to a silicon sample attached to the phase grating.

1.3 Literature review

The interest in the bilayered system has led to a number of experimental, theoretical, and computational studies. Biot [9] studied a different bilayered system where an infinite beam, instead of a thin film, was attached to the substrate. In his study, the deflection of the beam, when submitted to a particular load, ended up being nonlinear as a consequence of the difference of elastic properties between the beam and the substrate. He also showed the importance of the assumption of a two-dimensional substrate and a three-dimensional substrate.

Then Allen [3] completed a study closer to the system illustrated in Figure 1.2, focusing on sandwich panels. His work depicted both the bending and the buckling of the panels. He emphasized the contribution of the core and the faces in different scenarios, including our scenario of interest involving a very thin face.

Using the developed theory on the buckling phenomena, experimental studies were performed, motivated by the potential applications described in the previous sections. The most commonly studied engineering system consists of a thin metal film attached to a thick polymer. Bowden et al. [10] and Wagner et al. [76] would attach a gold film to a polydimethylsiloxane (PDMS) substrate. Instead of gold, it is also possible to consider thin silicon ribbons [46, 47]. Iacopi et al. [45] used a Ta film attached to a polymer core. It is also possible to oxidize the surface of a PDMS substrate to obtain a thin layer on top with a Young's modulus completely different from the original Young's modulus of the PDMS [11]. A different approach would consist of having both the substrate and the film made of gels with different compositions and properties [67].

The experimental studies were then followed by more research by Huang [42, 43], Li et al. [53].

Another research motivation in the experimental field is the observation of bilayered systems at many occasions in biological patterns. The study of brain deformation [64, 15, 71] involving the differential growth of the cortex attached to the subcortex is a field of investigation on which the Föppl-von Kármán theory is an appropriate tool. It is also the case for mucosa deformation [52] as the study of its deformation can help us to understand medical issues and lead to new treatment approaches.

On the numerical field, Chen and Hutchinson [24] studied a more complex type of buckling using ABAQUS to show that the nonlinear deformation depends on the minimum energy state. Cao and Hutchinson [18] emphasized the influence of the value of the critical buckling strain on the resulting buckling pattern. Tallinen and Biggins [70] studied the folding of the bilayered system near and far from the buckling threshold. Cai et al. [16] completed a comparative study between experimental results and numerical results on the creasing phenomena on top of a bilayered system.

This possibility for different buckling states due to energy minimization was then developed in theory by Audoly and Boudaoud [4, 5, 6]. Hutchinson then studied the stability of wrinkling in bilayered system [44]. Wang and Zhao [77] emphasized the distinction between all initial and advanced instability modes of bilayered systems, including buckling delamination, by realizing phase diagrams.

1.4 Thesis motivation and outline

The key question explored in this thesis concerns the control of instability by heterogeneous stimuli and electric fields.

Chapter 2 of this thesis reviews the possible deformation of a bilayered system consisting of a thin film attached to a thick substrate. The film is treated as a Föppl-von Kármán plate and the substrate as a semi-infinite elastic solid.

In Chapter 3, we provide a numerical method to study instabilities, and we use this numerical method on a surface subjected to a discontinuous heterogeneous external stretch. The key idea of the numerical method is to optimize the total energy by turning it into a quadratic form of the displacement by expressing the energy in the Fourier domain.The non-linear terms of the deflection are treated with the introduction of an auxiliary variable linked to the deformation by a constraint treated using the augmented Lagrangian method. The convergence of this model using heterogeneous external stretch gives a precise picture of the behavior of a bilayered system subjected to a varying load.

Chapter 4 goes into an active coating whose deformations can be modified. The tool used to control the deflection of a surface is the electromechanical coupling. Considering dielectric elastomers as the substrate of the bilayered system, the chapter presents a theoretical study of the total energy of this system, taking into account an extra term in the expression of the energy resulting from an external applied electric field [30]. The optimization of the energy gives an amplitude of the deflection depending on the applied electric field. This enables the potential control of instabilities using an applied electric field. The choice of the dielectric elastomers for the substrate is also motivated by the fact that their mechanical properties, such

Elastomer	***Elastic energy density*** (J/cm^3)	***Actuation pressure*** (MPa)	***Thickness strain***(%)	***Young's modulus*** (MPa)	***Electric field*** (V/μm)	***Dielectric constant***	***Coupling efficiency*** (%)
Silicone	0.22	1.36	32	1.0	235	3.2-9.8	54
Polyurethane	0.087	1.6	11	17	160	7.0	21
Fluoroelastomer	0.0046	0.11	8	2.5	32	12.7	15
Latex rubber	0.0059	0.11	11	0.85	67	2.7	21

Table 1.1: Representative dielectric elastomer materials performance (Zheng [84]).

as Young's modulus are close to those of the solids found in literature used for the role of substrate as illustrated in Table 1.1.

Chapter 5 keeps exploring the concept of an active bilayered system, but from a finite deformation numerical perspective. Using finite element modeling via ABAQUS, a bilayered system made of a thin stiff film attached to a thick compliant substrate is modeled, and the non-linear deformation resulting from buckling is generated. The Maxwell stress related to the dielectric elastomer model is introduced through a subroutine and incorporated into a linear elastic material to add the effect of an external electric field. The resulting evolution of the deformation gives a complementary approach to the theoretical results of Chapter 4.

Chapter 6 explores the different directions and possibilities offered by the results of this thesis.

Chapter 2

INSTABILITIES IN BILAYERED SYSTEMS

This chapter formulates the problem of deformation of bilayered systems and recalls key results in the literature associated to those systems.

2.1 Bilayered system

Consider the bilayered system shown in Figure 2.1. The thickness h of the film is assumed to be very small compared to the thickness H of the substrate. Therefore, we treat the thin film as a Föppl-von Kármán plate and the substrate as a semi-infinite solid. The two are coupled by the continuity of displacement across the interface.

2.1.1 Föppl-von Kármán theory

Since the thickness is small, we consider all components of the displacement to be independent of the thickness coordinate (we may regard this to be the mid-plane displacement). The energy $\mathscr{E}_{el}$ consists of a stretching energy $\mathscr{E}_{st}$ and a bending energy $\mathscr{E}_b$ [31, 75]:

$$\mathscr{E}_{el} = \mathscr{E}_{st} + \mathscr{E}_b \tag{2.1}$$

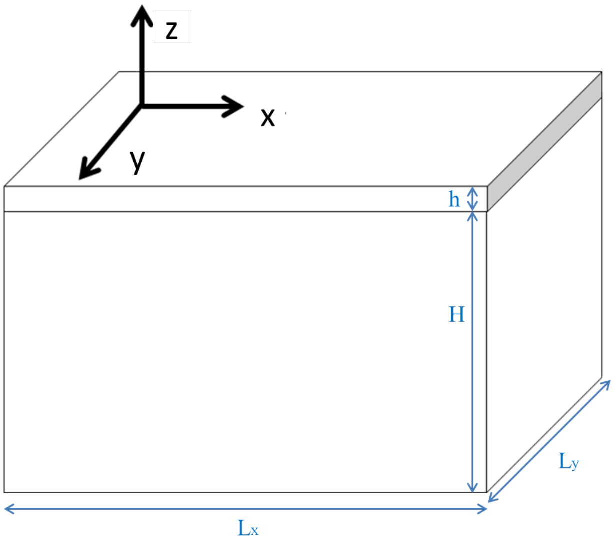

Figure 2.1: Bilayered system consisting of a thin film attached to a thick substrate.

with

$$\mathscr{E}_{st} = \frac{Eh}{2(1-\nu^2)} \int\int (\epsilon_{xx} + \epsilon_{yy})^2 - 2(1-\nu^2)(\epsilon_{xx}\epsilon_{yy} - \epsilon_{xy}^2)\ dx\ dy \tag{2.2}$$

and

$$\mathscr{E}_b = \frac{D}{2} \int\int (\Delta w)^2 - 2(1-\nu)(\frac{\partial^2 w}{\partial x^2}\frac{\partial^2 w}{\partial y^2} - (\frac{\partial^2 w}{\partial x \partial y})^2)\ dx\ dy \tag{2.3}$$

where w is the out of plane deflection, u, v are the two components of the in-plane displacement, $\epsilon_{xx} = \frac{\partial u}{\partial x} + \frac{1}{2}(\frac{\partial w}{\partial x})^2$, $\epsilon_{yy} = \frac{\partial v}{\partial y} + \frac{1}{2}(\frac{\partial w}{\partial y})^2$, $\epsilon_{xy} = \frac{1}{2}(\frac{\partial u}{\partial y} + \frac{\partial v}{\partial x} + \frac{\partial w}{\partial x}\frac{\partial w}{\partial y})$ are the components of the strain tensor, E is the Young modulus of the film, D is the bending modulus of the film, ν is the Poisson ratio of the film. We note that the out of plane deflection can result in stretching as shown by the extra term of the ϵ expressions.

The governing equations of the plate are then obtained by minimizing the elastic energy with respect to displacements u, v, w:

$$\frac{\partial \sigma_{\alpha\beta}}{\partial x_\beta} = 0 \tag{2.4}$$

$$D\Delta^2 w - h\frac{\partial^2 w}{\partial x_\alpha \partial x_\beta}\sigma_{\alpha\beta} = 0 \tag{2.5}$$

with $\sigma_{\alpha\beta}$ the components of the stress tensor.

The shape of the plate results from a competition between the stretching energy and the bending energy.

2.1.2 Energy brought by the substrate

The substrate is considered as a semi-infinite linear elastic material. The expression of the substrate energy can be simplified depending on the situation: for example, in the case of a substrate in sandwich panels, Allen [3] showed that considering this energy first as a sum of stretching energy and shear energy and then considering all in-plane strains to be negligible compared to the strains in the z direction, the energy of the substrate could be reduced to terms only related to the shear strains in the z direction. In our case, we want to start from a general approach and express the energy of the substrate without neglecting any terms. It is possible to do so starting from the general elastic energy of the substrate :

$$\mathscr{E}_{sub} = \int_{-\infty}^{\infty}\int_{-\infty}^{\infty}\int_{-\infty}^{0} \frac{1}{2}\sigma_{ij}\ \epsilon_{ij}\ dz\ dx\ dy. \tag{2.6}$$

This can be expressed in terms of the substrate displacements u_s,v_s,w_s as

$$\mathscr{E}_{sub} = \frac{1}{L_xL_y}\frac{E_s}{2}\int_{-\infty}^{\infty}\int_{-\infty}^{\infty}\int_{-\infty}^{0}\frac{1}{2}\frac{1-\nu_s}{(1+\nu_s)(1-2\nu_s)}((\frac{\partial u_s}{\partial x})^2 + (\frac{\partial v_s}{\partial y})^2 + (\frac{\partial w_s}{\partial z})^2)$$
$$+ \frac{1}{2}\frac{1}{1+\nu_s}((\frac{\partial u_s}{\partial y} + \frac{\partial v_s}{\partial x})^2 + (\frac{\partial u_s}{\partial z} + \frac{\partial w_s}{\partial x})^2 + (\frac{\partial v_s}{\partial z} + \frac{\partial w_s}{\partial y})^2)dx\ dy\ dz. \quad (2.7)$$

The equilibrium equations associated with this energy are the Navier equations

$$(\lambda+\mu)grad\ \ div\begin{pmatrix} u_s \\ v_s \\ w_s \end{pmatrix} + \mu\begin{pmatrix} \Delta u_s \\ \Delta v_s \\ \Delta w_s \end{pmatrix} = 0 \quad (2.8)$$

with λ and μ being the Lame coefficients of the material which can be expressed as functions of the Young modulus and the Poisson coefficient as follows:

$$\lambda = \frac{E_s\nu_s}{(1+\nu_s)(1-2\nu_s)}, \quad (2.9)$$
$$\mu = \frac{E_s}{2(1+\nu_s)}. \quad (2.10)$$

Equation (2.8) gives

$$(\lambda+\mu)(\frac{\partial^2 u_s}{\partial x^2} + \frac{\partial^2 v_s}{\partial x\partial y} + \frac{\partial^2 w_s}{\partial x\partial z}) + \mu(\frac{\partial^2 u_s}{\partial x^2} + \frac{\partial^2 u_s}{\partial y^2} + \frac{\partial^2 u_s}{\partial z^2}) = 0, \quad (2.11)$$
$$(\lambda+\mu)(\frac{\partial^2 u_s}{\partial x\partial y} + \frac{\partial^2 v_s}{\partial y^2} + \frac{\partial^2 w_s}{\partial x\partial z}) + \mu(\frac{\partial^2 v_s}{\partial x^2} + \frac{\partial^2 v_s}{\partial y^2} + \frac{\partial^2 v_s}{\partial z^2}) = 0, \quad (2.12)$$
$$(\lambda+\mu)(\frac{\partial^2 u_s}{\partial x\partial z} + \frac{\partial^2 v_s}{\partial y\partial z} + \frac{\partial^2 w_s}{\partial z^2}) + \mu(\frac{\partial^2 w_s}{\partial x^2} + \frac{\partial^2 w_s}{\partial y^2} + \frac{\partial^2 w_s}{\partial z^2}) = 0. \quad (2.13)$$
$$(2.14)$$

We seek to solve these equations subjected to the deflection of the film $u_s(z=0) = u$, $v_s(z=0) = v$, $w_s(z=0) = w$ and zero displacement as $z \longrightarrow \infty$. By naming $f' = \frac{\partial f}{\partial z}$ and by transferring the previous equations into the Fourier domain for variables x and y, we obtain

$$(\lambda+\mu)((-k_x^2\hat{u_s}) + (-k_xk_y)\hat{v_s} + ik_x\hat{w_s}') + \mu(-k_x^2\hat{u_s} - k_y^2\hat{u_s} + \hat{u_s}'') = 0, \quad (2.15)$$

$$(\lambda+\mu)((-k_xk_y\hat{u_s}) + (-k_y^2)\hat{v_s} + ik_y\hat{w_s}') + \mu(-k_x^2\hat{v_s} - k_y^2\hat{v_s} + \hat{v_s}'') = 0, \quad (2.16)$$

$$(\lambda+\mu)((ik_x\hat{u_s}') + (ik_y)\hat{v_s}' + \hat{w_s}'') + \mu(-k_x^2\hat{w_s} - k_y^2\hat{w_s} + \hat{w_s}'') = 0. \quad (2.17)$$

This can be expressed with the form:

$$\begin{pmatrix} \hat{u_s} \\ \hat{v_s} \\ \hat{w_s} \\ \hat{u_s}' \\ \hat{v_s}' \\ \hat{w_s}' \end{pmatrix}' = \begin{pmatrix} 0 & 0 & 0 & 1 & 0 & 0 \\ 0 & 0 & 0 & 0 & 1 & 0 \\ 0 & 0 & 0 & 0 & 0 & 1 \\ k_x^2 \frac{\lambda+2\mu}{\mu} + k_y^2 & \frac{\lambda+\mu}{\mu} k_x k_y & 0 & 0 & 0 & -ik_x \frac{\lambda+\mu}{\mu} \\ \frac{\lambda+\mu}{\mu} k_x k_y & k_y^2 \frac{\lambda+2\mu}{\mu} + k_x^2 & 0 & 0 & 0 & -ik_y \frac{\lambda+\mu}{\mu} \\ 0 & 0 & \frac{\mu}{\lambda+2\mu}(k_x^2+k_y^2) & -ik_x \frac{\lambda+\mu}{\lambda+2\mu} & -ik_y \frac{\lambda+\mu}{\lambda+2\mu} & 0 \end{pmatrix} \begin{pmatrix} \hat{u_s} \\ \hat{u_s} \\ \hat{u_s} \\ \hat{u_s}' \\ \hat{v_s}' \\ \hat{w_s}' \end{pmatrix} \tag{2.18}$$

or $U' = AU$. The linear operator A of Equation (2.18) has eigenvalues k_z and $-k_z$ each one with multiplicity 3 and

$$k_z = \sqrt{k_x^2 + k_y^2}. \tag{2.19}$$

The eigenspace associated with each of those two eigenvalues has dimension 2. As a consequence, Equation (2.18) presents the following forms as solutions:

$$\hat{u_s} = (u_1 + u_2 z)e^{k_z z} + (u_3 + u_4 z)e^{-k_z z}, \tag{2.20}$$

$$\hat{v_s} = (v_1 + v_2 z)e^{k_z z} + (v_3 + v_4 z)e^{-k_z z}, \tag{2.21}$$

$$\hat{w_s} = (w_1 + w_2 z)e^{k_z z} + (w_3 + w_4 z)e^{-k_z z}. \tag{2.22}$$

Injecting (2.20), (2.21), (2.22) into (2.15), (2.16), (2.17) gives a new set of equations to solve. As each coefficient associated with an exponential term must be brought to 0 to satisfy the condition as $z \longrightarrow \infty$, the expressions of substrate displacement are simplified:

$$\begin{aligned} \begin{pmatrix} \hat{u_s} \\ \hat{v_s} \\ \hat{w_s} \end{pmatrix} = e^{k_z z}\left(c_1 \begin{pmatrix} k_y \\ -k_x \\ 0 \end{pmatrix} + c_2 \begin{pmatrix} 0 \\ ik_z \\ k_y \end{pmatrix} + c_3 \begin{pmatrix} k_x z \\ \frac{k_z}{k_y} \frac{\lambda+3\mu}{\lambda+\mu} + k_y z \\ -ik_z z \end{pmatrix} \right) \\ + e^{-k_z z}\left(c_4 \begin{pmatrix} k_y \\ -k_x \\ 0 \end{pmatrix} + c_5 \begin{pmatrix} 0 \\ -ik_z \\ k_y \end{pmatrix} + c_6 \begin{pmatrix} k_x z \\ \frac{-k_z}{k_y} \frac{\lambda+3\mu}{\lambda+\mu} + k_y z \\ ik_z z \end{pmatrix} \right) \end{aligned} \tag{2.23}$$

The constants of integration can be determined using the boundary conditions: the substrate is considered semi-infinite, then c_4, c_5, c_6 are all 0 and the displacements at z=0 are equal to the displacements u, v, w of the film; then c_1, c_2, c_3 are functions of $\hat{v}$,$\hat{u}$,$\hat{w}$:

$$\hat{u} = k_y \; c_1 \tag{2.24}$$

$$\hat{w} = k_y\ c_2 \tag{2.25}$$

$$\hat{v} = -k_x\ c_1 + ik_z\ c_2 + \frac{k_z}{k_y}\frac{\lambda + 3\mu}{\lambda + \mu}\ c_3 \tag{2.26}$$

To be able to use those expressions, it is first necessary to use the Plancherel theorem to transfer the in-plane spatial domain into the Fourier domain in Equation (2.7):

$$\begin{aligned}\mathscr{E}_{sub} = \frac{1}{L_x L_y}\frac{1}{2}\int_{-\infty}^{\infty}\int_{-\infty}^{\infty}\int_{-\infty}^{0} &(2\mu + \lambda)(k_x^2|\hat{u}_s|^2 + k_y^2|\hat{v}_s|^2 + |\hat{w}_s{'}|^2)\\ &+ \lambda(k_x k_y \hat{u}_s \hat{v}_s{}^* + k_x k_y \hat{v}_s \hat{u}_s{}^* + ik_x \hat{u}_s \hat{w}_s{'^*} - ik_x \hat{u}_s{}^* \hat{w}_s{'} + ik_y \hat{v}_s \hat{w}_s{'^*} - ik_y \hat{v}_s{}^* \hat{w}_s{'})\\ &+ \mu(|ik_y \hat{u}_s + ik_x \hat{v}_s|^2 + |ik_x \hat{w}_s + \hat{u}_s{'}|^2 + |ik_y \hat{w}_s + \hat{v}_s{'}|^2)\ dz\ dk_x\ dk_y. \end{aligned}\tag{2.27}$$

By substituting the expressions of $\hat{v}_s$,$\hat{u}_s$,$\hat{w}_s$, the final form of the substrate energy is finally obtained:

$$\mathscr{E}_{sub} = \frac{1}{L_x L_y}\int_{-\infty}^{\infty}\int_{-\infty}^{\infty}\begin{pmatrix}\hat{u}^*\\ \hat{v}^*\\ \hat{w}^*\end{pmatrix}\frac{E_s(1-\nu_s)}{(1+\nu_s)(3-4\nu_s)}\ \underline{\underline{T}}\ \begin{pmatrix}\hat{u}\\ \hat{v}\\ \hat{w}\end{pmatrix} dk_x\ dk_y, \tag{2.28}$$

with

$$\underline{\underline{T}} = \begin{pmatrix} \frac{k_x^2}{k_z} + \frac{3-4\nu_s}{1-\nu_s}\frac{k_y^2}{4k_z} & \frac{1}{1-\nu_s}\frac{k_x k_y}{4k_z} & -\frac{1-2\nu_s}{1-\nu_s}\frac{ik_x}{2}\\ \frac{1}{1-\nu_s}\frac{k_x k_y}{4k_z} & \frac{k_y^2}{k_z} + \frac{3-4\nu_s}{1-\nu_s}\frac{k_x^2}{4k_z} & -\frac{1-2\nu_s}{1-\nu_s}\frac{ik_y}{2}\\ \frac{1-2\nu_s}{1-\nu_s}\frac{ik_x}{2} & \frac{1-2\nu_s}{1-\nu_s}\frac{ik_y}{2} & k_z \end{pmatrix}. \tag{2.29}$$

The details of the calculation just depicted can also be found in Appendix C.

If we assume that u, v are small then

$$\mathscr{E}_{sub} = \frac{1}{L_x L_y}\int_{-\infty}^{\infty}\int_{-\infty}^{\infty} E_s^*|\hat{w}|^2\ dk_x\ dk_y \tag{2.30}$$

with $E_s^* = \frac{E_s(1-\nu_s)}{(1+\nu_s)(3-4\nu_s)}$. This recovers expression given by the work of Audoly and Boudaoud [4].

2.1.3 Loading

When the bilayered system is submitted to a load, the total energy receives an extra term associated with this load. Of particular interest in this thesis is the situation when there is a mismatch in the stress-free strain between the film and the substrate. We introduce this by modifying the strain tensor as follows:

$$\epsilon_{xx} = -\eta_x + \frac{\partial u}{\partial x} + \frac{1}{2}(\frac{\partial w}{\partial x})^2, \tag{2.31}$$

$$\epsilon_{yy} = -\eta_y + \frac{\partial v}{\partial y} + \frac{1}{2}(\frac{\partial w}{\partial y})^2, \tag{2.32}$$

$$\epsilon_{xy} = -\eta_{xy} + \frac{1}{2}(\frac{\partial u}{\partial y} + \frac{\partial v}{\partial x} + \frac{\partial w}{\partial x}\frac{\partial w}{\partial y}) \tag{2.33}$$

with η_x, η_y, η_{xy} being the components of the strain mismatch tensor.

2.2 Possible instabilities

2.2.1 Buckling

The system above has an equilibrium solution with $w = 0$. However, as the mismatch η increases, this solution becomes unstable at a critical η_c. We obtain deformation patterns as post-buckled states.

2.2.2 Deformation patterns

Using the separation of variable and superposition, Allen [3] looked for solution w of the form

$$w = \sum_m \sum_n A_{mn}\ sin(k_m\ x)\ sin(k_n\ y) \tag{2.34}$$

where A_{mn} is the amplitude and k_m, k_n the wavenumbers of the mn^{th} mode.

The simplest form of w is the cylindrical pattern characterized by one coefficient A and one wavenumber k. This situation occurs when the plane strain applied to the bilayered system is uni-directional and with an amplitude within a specific range. This form is one of the most observed and studied experimentally and numerically [12, 46, 65, 18]. But more complex patterns can be observed when the stretching of the system becomes bi-axial. The possibilities have been well-described by Audoly and Boudaoud [4, 5, 6], who explained that by adding a second main direction for the plane stretch field within the bilayered system, the initial uni-directional wrinkle deflection could turn into undulating stripes or a checkerboard pattern. They also explained that a higher magnitude of in plane strain could lead to the formation of a herringbone pattern. Those different options are depicted in Figure 2.2.

Those different types of deformation occur for an external load near the buckling threshold and depend mainly on the orientation of the stretch. But other types of patterns can result from uni-directional in-plane strain: if the magnitude of the strain goes very high beyond the buckling threshold, the uni-directional wrinkles will be

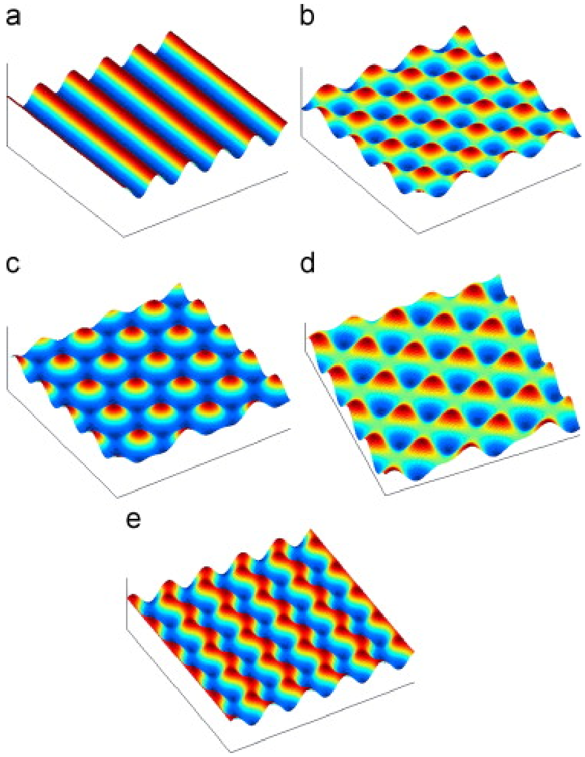

Figure 2.2: Schematics of mode shapes: (a) 1D wrinkling mode, (b) square checkerboard mode, (c) hexagonal mode, (d) triangular mode, and (e) herringbone mode. Image from[17].

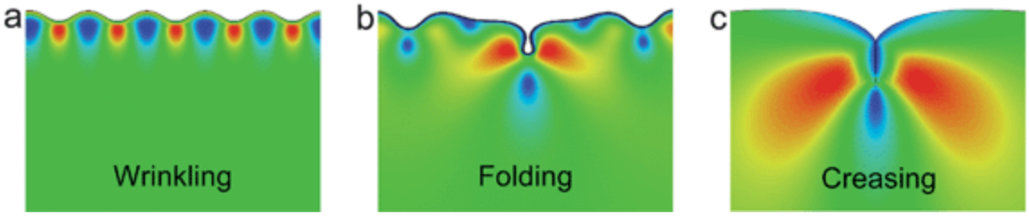

Figure 2.3: Schematic of three types of morphological instability: (a) wrinkling, (b) folding, and (c) creasing. Image from[54].

folded [68]. It is also possible to observe a period-doubling (a doubling of the periodicity) of the original wrinkles [14, 18], and for particular cases of stiffness ratio, a creasing behavior will be observed beyond the buckling threshold (see Figure 2.3).

2.2.3 Theory for unidirectional wrinkles

In their work, Audoly and Boudaoud [4] start from the assumption that the deflection would be of the form $w = A\ cos(kx)$ and use the simplified form of the substrate energy. They obtain

$$\mathscr{E}_{el} = \frac{Eh}{2(1-\nu^2)}(\eta_x^2 + \eta_y^2 + 2\nu\eta_x\eta_y - \frac{\eta_x + \nu\eta_y}{2}k^2A^2 + \frac{1}{16}k^4A^4) + \frac{E}{2(1+\nu)}\eta_{xy}^2 + \frac{1}{4}Dk^4A^2 + \frac{1}{2}E_s^*kA^2. \quad (2.35)$$

The expressions of the amplitude and wavenumber characterizing the wrinkles are obtained by optimizing Equation (2.35) with respect to A and k:

$$\frac{d\mathscr{E}_{el}}{dk} = 0 \Rightarrow k = (\frac{E_s^*}{D})^{1/3} \quad (2.36)$$

$$\frac{d\mathscr{E}_{el}}{dA} = 0 \Rightarrow A = \sqrt{(\eta_x + \nu\eta_y)\frac{4}{k^2} - h^2} \quad (2.37)$$

Equations (2.36) and (2.37) show that the wavelengths of wrinkles are independent of the external stretch η applied to the bilayered system, and they also give an expression for the minimum stretch required for the buckling to happen: $(\eta_x + \nu\eta_y)\frac{4}{k^2} - h^2 > 0$ means that $(\eta_x + \nu\eta_y) > \frac{h^2k^2}{4}$ represent the condition on η for wrinkles to appear.

The results regarding the amplitude of those wrinkles must be considered very carefully. The theory explained by Koiter [37] shows that there is another method to express the amplitude and it gives very different results compared to Equation (2.37).

2.3 Experimental studies

To confirm all the theories developed in the previous sections of this chapter, many experimental studies have been realized. The details of those experimental studies are indicative of the range of physical parameters that can be considered for further investigation.

Regarding the materials used in the experimental studies, we notice that the material used the most often as a substrate is the PDMS which is a silicon-based organic polymer. The advantage of this polymer is that its stiffness can vary depending on the way the sample is prepared. Although the substrate is in most cases made of PDMS, the material for the film is different from one study to another: as mentioned in Section 1.3, it can be made of gold, silicon, or gels. Another possibility used by Brau et al [12] and Auguste et al[7] is to start from the PDMS substrate and to create the film on top of the substrate by uniformly oxidizing the top surface of the substrate using ultra violet rays combined with ozone as illustrated in Figure 2.4. The ozone will modify the rigidity of the surface, resulting in a thin film with a higher stiffness already attached to the substrate.

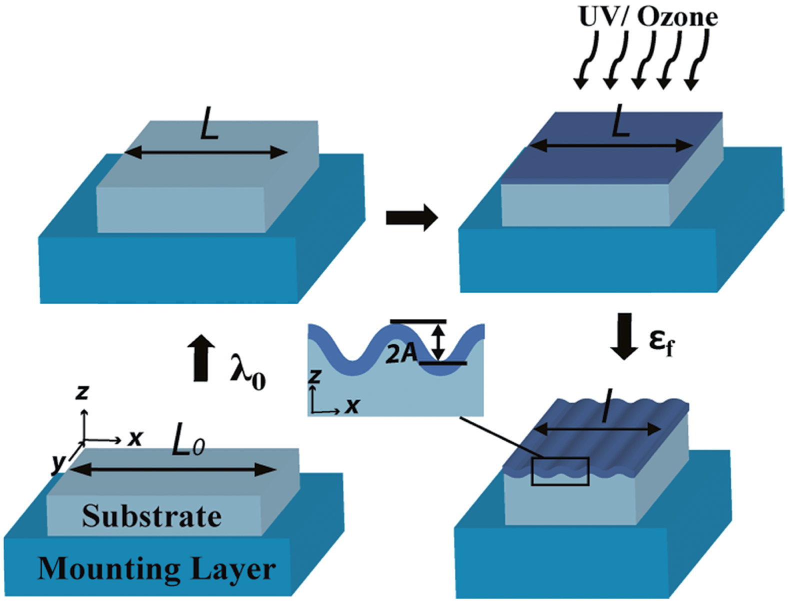
UV/ Ozone
L
L
2A
z
x
λ0
εf
z
x
y
L0
l
Substrate
Mounting Layer

Figure 2.4: Generating wrinkles in a bilayered system by oxidation using ultra violet and ozone. Image from[7].

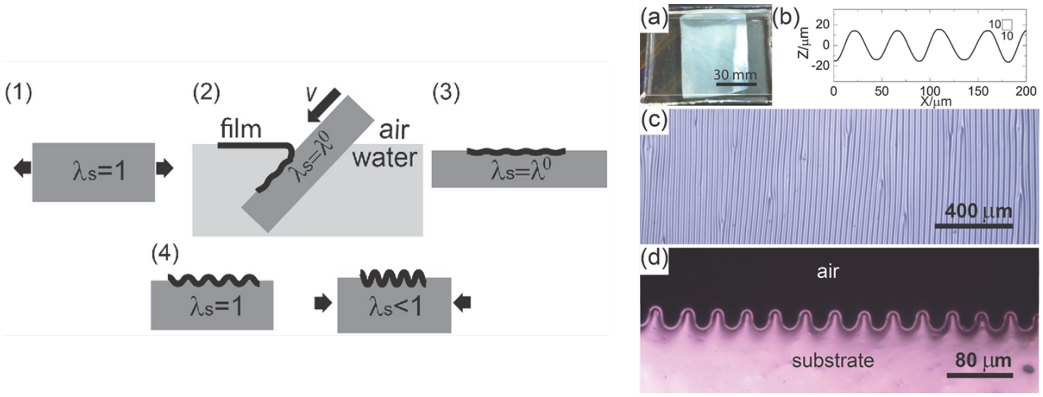
(1)
λs=1
(2)
film
v
λs=λ0
air
water
(3)
λs=λ0
(4)
λs=1
λs<1
(a)
30 mm
(b)
Z/μm
20
0
-20
10
10
0
50
100
150
200
X/μm
(c)
400 μm
(d)
air
substrate
80 μm

Figure 2.5: Generating wrinkles in a bilayered system by spin coating and dip coating. Image from[25].

In case the film is not created from the surface of the substrate, different techniques can be used to generate it: Jin et al [48] used spin coating to generate a thin film made of uncured PDMS and then placed the film into an oven at 120° C before attaching it to a PDMS substrate at 40°C. Chen and Crosby [25] also used a spin coating method to generate a polystyrene film, but used a dip coating method to attach it to the substrate, as illustrated in Figure 2.5.

The choice of the method for engineering the bilayered system is also related to the method used to generate the differential strain. Different modes of compression for such a system are listed by Holland et al [40]: either the two materials are already attached together, and then everything is submitted to the same a strain resulting in a different load due to the stiffness mismatch, or one of the two materials is pre-stretched before being attached to the other, and then this pre-stretch is turned off after attachment. It is also possible to have both materials attached, but then external stretch is only applied to one material. This was the case in the work of Breid and Crosby [13]: they used the ultra violet method to generate the stiff film on top of the substrate, and then injected a solvent vapor inside the substrate to swell it while the stiff film maintained its original volume. This method resulted in in a differential stress at the interface film substrate.

The measurement part can also involve different methods. In their work, Auguste et al [7] used optical profilometry with laser scanning confocal fluorescence microscopy to characterize the shape of the wrinkles.

Chapter 3

NUMERICAL METHOD FOR DISCONTINUOUS BUCKLING

This chapter presents a numerical method for a situation where the mismatch strain is possibly heterogeneous. We apply it to the case of liquid crystalline substrates.

3.1 Liquid-crystalline substrates

A potential materials for the substrate of the bilayered system is the liquid crystal elastomer (LCE). LCEs are rubbery networks of polymer chains with a long-range mobile crystalline order, and they show enormous (0.1-1) strains depending on temperature [78]. Specifically on cooling, we observe compression along the nematic director and extension perpendicular to it. Studying very thin (35 nm) polystyrene film attached to a thicker (0.36 mm) LCE substrate, Agrawal [2] observed the formation of surface wrinkles parallel to the nematic director of the LCE if the bilayer is cooled by 20°C and perpendicular to the nematic director and if the bilayer is heated by 10°C. When the bilayer is brought back to its initial temperature, the surface deformation returns to the initial state. It is observed that the wavelength of the wrinkles varies linearly with the thickness of the polystyrene film, and beyond sufficiently high thickness for the film, the wrinkling instability is replaced by reversible curling. The role of the thickness is also emphasized in the work of Verduzco [74] who studied the defomation of a nematic gel.

The thermal expansion technique is also the base of the experimental study of Kang et al [49]. In this work, the liquid crystalline material is a reactive mesogen solution (RMS) and is attached to a polyimide (PI) film before being exposed to plasma. The PI film is rubbed before attachment in order to make the RMS molecules align along the rubbing direction once in contact with the film. This technique shows the importance of molecular alignment: when the PI film is not rubbed, the resulting wrinkles formed after plasma exposure were isotropic while a rubbed film would result in a one directional wrinkle aligned with the rubbing direction. In Kang's paper, it is speculated that the necessary strain for wrinkling comes from thermal heating due to the plasma. It is also shown that a longer exposure time to plasma (100 seconds instead of 60 seconds) would result in higher amplitude for the resulting wrinkles. This paper links each characteristic of the wrinkling phenomena to a particular experimental parameter: the wrinkling directionality is linked to the molecular alignment of the liquid crystal, the amplitude of wrinkles is connected to the plasma exposure time generating higher strain. The wavelength of the wrinkles results from the thicknesses and the elastic modulus ratio.

Even though the thermal expansion property is key in generating the differential strain triggering the wrinkles, the very particular wrinkling pattern (direction, complexity) depends on the preparation of the liquid crystalline material. This fact is emphasized in the work of de Haan [34], showing that polymerization by photoalignment of liquid crystal opens the door to different possibilities of wrinkle orientations. This photopolymerization by UV light irradiation allows the director alignment to be heterogeneous or a function of space. It results in wrinkles changing directions in different regions of the very same sample. Even more complex patterns are also obtained using photomasks during the polymerization. This method is also used in the work of Ma [58] where it is also shown that the duration of the UV radiation can influence the final wavelength and amplitude of the resulting wrinkles: the longer the exposure to UV, the larger the wavelength and the amplitude of the wrinkles are.

3.2 Minimizing the total energy

We consider the situation where the strain mismatch η between the film and the substrate varies with space (x,y). The total energy of the bilayered system is

$$
\begin{aligned}
\mathscr{E}_{el} &= \mathscr{E}_{sf} + \mathscr{E}_{bf} + \mathscr{E}_{sub} \\
&= \frac{1}{L_x L_y}\Big(\int\int \frac{Eh}{2(1-\nu^2)}\Big(-\eta_x + \frac{\partial u}{\partial x} + \frac{1}{2}\Big(\frac{\partial w}{\partial x}\Big)^2 - \eta_y + \frac{\partial v}{\partial y} + \frac{1}{2}\Big(\frac{\partial w}{\partial y}\Big)^2\Big)^2 \\
&- \frac{Eh}{1+\nu}\Big(-\eta_x + \frac{\partial u}{\partial x} + \frac{1}{2}\Big(\frac{\partial w}{\partial x}\Big)^2\Big)\Big(-\eta_y + \frac{\partial v}{\partial y} + \frac{1}{2}\Big(\frac{\partial w}{\partial y}\Big)^2\Big) \\
&+ \frac{Eh}{1+\nu}\Big(-\eta_{xy} + \frac{1}{2}\Big(\frac{\partial u}{\partial y} + \frac{\partial v}{\partial x}\Big) + \frac{\partial w}{\partial x}\frac{\partial w}{\partial y}\Big)^2 \, dx \, dy \\
&+ \int\int \frac{D}{2}(\Delta w)^2 \, dx \, dy + \int\int E_s^* \sqrt{k_x^2 + k_y^2}\,|\hat{w}|^2 \, dk_x \, dk_y\Big).
\end{aligned}
\tag{3.1}
$$

Finding the equilibrium state of this system is achieved by finding the displacements u, v and w that minimizes this total energy. In this expression, the part of the energy associated with the bending phenomenon is different from Equation 2.3: for simplicity, we only keep the term $(\Delta w)^2$.

3.2.1 Non-dimensionalization

The expression of the energy involves a lot of different variables and parameters. The number of parameters can be reduced using non-dimensionalization to simplify the expression of the energy. Another advantage is that this process will allow us to introduce a set of coefficients associated with each type of energy. Those coefficients will make it more convenient to control the influence of one particular energy compared to the two others.

In our case, the variables are u, v, w, x, y, η_x and η_y. The parameters are E, h, ν and E_s*. Expressions of the undimensionalized variables are written:

$$\bar{x} = \frac{x}{x_0}; \;\; \bar{y} = \frac{y}{y_0}; \;\; \bar{u} = \frac{u}{u_0}; \;\; \bar{v} = \frac{v}{v_0}; \;\; \bar{w} = \frac{w}{w_0}; \;\; \bar{\eta_x} = \frac{\eta_x}{\eta_{x0}}; \;\; \bar{\eta_y} = \frac{\eta_y}{\eta_{y0}};$$

$$\bar{\eta_{xy}} = \frac{\eta_{xy}}{\eta_{xy0}}.$$

We must be careful about the frequency domain and be sure that the non-dimensionalization of this domain is equivalent to the Fourier transform of the non-dimensionalized space domain.

$$\begin{aligned} \hat{w} &= \int w(x,y)\ exp(-i(k_x x + k_y y)) dx\ dy \\ &= \int w_0\ \bar{w}\ exp(-i(k_{x0}\ \bar{k_x}\ x_0\ \bar{x} + k_{y0}\ \bar{k_y}\ y_0\ \bar{y}))\ x_0\ d\bar{x}\ y_0\ d\bar{y} \\ &= w_0\ x_0\ y_0 \int \bar{w}\ exp(-i(k_{x0}\ x_0\ \bar{k_x}\ \bar{x} + k_{y0}\ y_0\ \bar{k_y}\ \bar{y}))\ d\bar{x}\ d\bar{y} \end{aligned} \tag{3.2}$$

If we define $k_{x0} = \frac{1}{x_0}$, $k_{y0} = \frac{1}{y_0}$ and $\hat{\bar{w}} = \int \bar{w}\ exp(-i(\bar{k_x}\ \bar{x} + \bar{k_y}\ \bar{y}))$ then $\hat{w} = w_0\ x_0\ y_0\ \hat{\bar{w}}$.

Substituting all those variables in the expression of energy, we obtain

$$\begin{aligned} L_x\ L_y\ \mathscr{E} = \int & \frac{Eh}{2(1-\nu^2)}(-\eta_{x0}\ \bar{\eta_x} + \frac{u_0}{x_0}\frac{\partial \bar{u}}{\partial \bar{x}} + \frac{1}{2}(\frac{w_0}{x_0})^2(\frac{\partial \bar{w}}{\partial \bar{x}})^2 - \eta_{y0}\ \bar{\eta_y} + \frac{v_0}{y_0}\frac{\partial \bar{v}}{\partial \bar{y}} \\ & + \frac{1}{2}(\frac{w_0}{y_0})^2(\frac{\partial \bar{w}}{\partial \bar{y}})^2)^2 - \frac{Eh}{1+\nu}(-\eta_{x0}\ \bar{\eta_x} + \frac{u_0}{x_0}\frac{\partial \bar{u}}{\partial \bar{x}} + \frac{1}{2}(\frac{w_0}{x_0})^2(\frac{\partial \bar{w}}{\partial \bar{x}})^2)(-\eta_{y0}\ \bar{\eta_y} + \frac{v_0}{y_0}\frac{\partial \bar{v}}{\partial \bar{y}} \\ & + \frac{1}{2}(\frac{w_0}{y_0})^2(\frac{\partial \bar{w}}{\partial \bar{y}})^2) + \frac{Eh}{1+\nu}(-\eta_{xy0}\ \bar{\eta_{xy}} + 0.5\ (\frac{u_0}{y_0}\frac{\partial \bar{u}}{\partial \bar{y}} + \frac{v_0}{x_0}\frac{\partial \bar{v}}{\partial \bar{x}}) \\ & + \frac{1}{2}\frac{w_0}{x_0}\frac{w_0}{y_0}\frac{\partial \bar{w}}{\partial \bar{x}}\frac{\partial \bar{w}}{\partial \bar{y}})^2) + \frac{D}{2}(\frac{w_0}{x_0^2}\frac{\partial^2 \bar{w}}{\partial \bar{x}^2} + \frac{w_0}{y_0^2}\frac{\partial^2 \bar{w}}{\partial \bar{y}^2})^2\ x_0\ y_0\ d\bar{x}\ d\bar{y} \\ & + \int E_s^* \sqrt{k_{x0}^2\ \bar{k_x}^2 + k_{y0}^2\ \bar{k_y}^2} w_0^2\ x_0^2\ y_0^2\ \hat{\bar{w}}\hat{\bar{w}}^*\ k_{x0}\ d\bar{k_x}\ k_{y0}\ d\bar{k_y}. \end{aligned}$$

Because of the symmetry along the axes x and y within the bilayered system, we take $x_0 = y_0$ and $k_{x0} = k_{y0}$. Then the previous equation gives

$$
\begin{aligned}
&\frac{1}{x_0 y_0}\frac{2}{D}\frac{x_0^4}{w_0^2}L_x\ L_y\ \mathscr{E} = \int \frac{12}{h^2}\frac{x_0^4}{w_0^2}(-\eta_{x0}\ \bar{\eta_x}+\frac{u_0}{x_0}\frac{\partial \bar{u}}{\partial \bar{x}}+\frac{1}{2}(\frac{w_0}{x_0})^2(\frac{\partial \bar{w}}{\partial \bar{x}})^2-\eta_{y0}\ \bar{\eta_y}+\frac{v_0}{y_0}\frac{\partial \bar{v}}{\partial \bar{y}} \\
&+\frac{1}{2}(\frac{w_0}{y_0})^2(\frac{\partial \bar{w}}{\partial \bar{y}})^2)^2-2(1-\nu)\frac{12}{h^2}\frac{x_0^4}{w_0^2}(-\eta_{x0}\ \bar{\eta_x}+\frac{u_0}{x_0}\frac{\partial \bar{u}}{\partial \bar{x}}+\frac{1}{2}(\frac{w_0}{x_0})^2(\frac{\partial \bar{w}}{\partial \bar{x}})^2)(-\eta_{y0}\ \bar{\eta_y}+\frac{v_0}{y_0}\frac{\partial \bar{v}}{\partial \bar{y}} \\
&+\frac{1}{2}(\frac{w_0}{y_0})^2(\frac{\partial \bar{w}}{\partial \bar{y}})^2)+2(1-\nu)\frac{12}{h^2}\frac{x_0^4}{w_0^2}(-\eta_{xy0}\ \bar{\eta_{xy}}+0.5\ (\frac{u_0}{y_0}\frac{\partial \bar{u}}{\partial \bar{y}}+\frac{v_0}{x_0}\frac{\partial \bar{v}}{\partial \bar{x}})+\frac{1}{2}\frac{w_0}{x_0}\frac{w_0}{y_0}\frac{\partial \bar{w}}{\partial \bar{x}}\frac{\partial \bar{w}}{\partial \bar{y}})^2) \\
&+(\frac{\partial^2 \bar{w}}{\partial \bar{x}^2}+\frac{\partial^2 \bar{w}}{\partial \bar{y}^2})^2\ d\bar{x}\ d\bar{y}+\int \frac{E_s^*}{x_0 y_0}\frac{2}{D}\frac{x_0^4}{w_0^2}|k_{x0}|\sqrt{\bar{k_x}^2+\bar{k_y}^2}w_0^2\ x_0^2\ y_0^2\ \hat{\bar{w}}\hat{\bar{w}}^*\ k_{x0}^2\ d\bar{k_x}\ d\bar{k_y}.
\end{aligned}
$$

We introduce dimensionless numbers α_{bend}, $\alpha_{stretch}$ and α_{subs} and set

$$
\begin{aligned}
x_0 &= (\frac{\alpha_{subs}}{\alpha_{bend}}\frac{D}{2E_s^*})^{\frac{1}{3}}, \\
w_0 &= \sqrt{\frac{\alpha_{stret}}{\alpha_{bend}}\frac{h^2}{12}}, \\
u_0 = v_0 &= \sqrt{\frac{\alpha_{stret}}{\alpha_{bend}}\frac{h^2 w_0^2}{12 x_0^2}}, \\
\eta_{x0} = \eta_{y0} = \eta_{xy0} &= \sqrt{\frac{\alpha_{stret}}{\alpha_{bend}}\frac{h^2 w_0^2}{12 x_0^4}}, \\
\bar{\mathscr{E}} &= \alpha_{bend}\frac{2}{D}\frac{x_0^3}{y_0 w_0^2}L_x L_y \mathscr{E}.
\end{aligned}
$$

Then the expression of the undimensionalized energy is

$$
\begin{aligned}
\bar{\mathscr{E}} = \int \alpha_{stret}(-\bar{\eta_x}+\frac{\partial \bar{u}}{\partial \bar{x}}+\frac{1}{2}(\frac{\partial \bar{w}}{\partial \bar{x}})^2-\bar{\eta_y}+\frac{\partial \bar{v}}{\partial \bar{y}}+\frac{1}{2}(\frac{\partial \bar{w}}{\partial \bar{y}})^2)^2-2\alpha_{stret}(1-\nu)(-\bar{\eta_x}+\frac{\partial \bar{u}}{\partial \bar{x}} \\
+\frac{1}{2}(\frac{\partial \bar{w}}{\partial \bar{x}})^2)(-\bar{\eta_y}+\frac{\partial \bar{v}}{\partial \bar{y}}+\frac{1}{2}(\frac{\partial \bar{w}}{\partial \bar{y}})^2)+2\alpha_{stret}(1-\nu)(-\bar{\eta_{xy}}+0.5\ (\frac{\partial \bar{u}}{\partial \bar{y}}+\frac{\partial \bar{v}}{\partial \bar{x}})+\frac{1}{2}\frac{\partial \bar{w}}{\partial \bar{x}}\frac{\partial \bar{w}}{\partial \bar{y}})^2 \\
+\alpha_{bend}(\frac{\partial^2 \bar{w}}{\partial \bar{x}^2}+\frac{\partial^2 \bar{w}}{\partial \bar{y}^2})^2\ d\bar{x}\ d\bar{y}+\int \alpha_{subs}\sqrt{\bar{k_x}^2+\bar{k_y}^2}\hat{\bar{w}}\hat{\bar{w}}^*\ d\bar{k_x}\ d\bar{k_y}. \quad (3.3)
\end{aligned}
$$

3.2.2 Transfer to the Fourier domain

The expression of this energy is a non-linear function of the displacement and of the gradient of the displacements. This expression mixes integrals over the space domain and the Fourier domain. To simplify this, we recall Plancherel's theorem, which presents two dimensions

$$\int_{-\infty}^{+\infty}\int_{-\infty}^{+\infty}|f(x,y)|^2 dx\ dy = \frac{1}{4\pi^2}\int_{-\infty}^{+\infty}\int_{-\infty}^{+\infty}|\hat{f}(k_x,k_y)|^2 dk_x\ dk_y \tag{3.4}$$

where $\hat{f}(k)$ denotes the non-unitary angular frequency version of the Fourier transform of a function $f(x,y)$

This theorem allows us to transform the stretching energy and the bending energy of the film taken from Equation (3.1):

$$\begin{aligned}\bar{\mathscr{E}}_{fs} = \frac{\alpha_{stret}}{4\pi^2}\int |-\hat{\bar{\eta}}_x + i\bar{k}_x\hat{u} + \frac{1}{2}\widehat{(\frac{\partial\bar{w}}{\partial\bar{x}})^2} - \hat{\bar{\eta}}_y + i\bar{k}_y\hat{\bar{v}} + \frac{1}{2}\widehat{(\frac{\partial\bar{w}}{\partial\bar{y}})^2}|^2 - (1-\nu)(-\hat{\bar{\eta}}_x \\ + i\bar{k}_x\hat{\bar{u}} + \frac{1}{2}\widehat{(\frac{\partial\bar{w}}{\partial\bar{x}})^2})^*(-\hat{\bar{\eta}}_y + i\bar{k}_y\hat{\bar{v}} + \frac{1}{2}\widehat{(\frac{\partial\bar{w}}{\partial\bar{y}})^2}) - (1-\nu)(-\hat{\eta}_x + ik_x\hat{u} + \frac{1}{2}\widehat{(\frac{\partial\bar{w}}{\partial\bar{x}})^2})(-\hat{\bar{\eta}}_y + \\ i\bar{k}_y\hat{\bar{v}} + \frac{1}{2}\widehat{(\frac{\partial\bar{w}}{\partial\bar{y}})^2})^* + 2(1-\nu)|-\hat{\bar{\eta}}_{xy} + \frac{1}{2}(i\bar{k}_y\hat{\bar{u}} + i\bar{k}_x\hat{\bar{v}}) + \frac{1}{2}\widehat{\frac{\partial\bar{w}}{\partial\bar{x}}\frac{\partial\bar{w}}{\partial\bar{y}}}|^2\, d\bar{k}_x\, d\bar{k}_y,\end{aligned} \tag{3.5}$$

$$\mathscr{E}_{fb} = \frac{1}{4\pi^2}\int |(\bar{k}_x^2 + \bar{k}_y^2)\hat{\bar{w}}|^2\, d\bar{k}_x\, d\bar{k}_y \tag{3.6}$$

where * denotes the complex conjugate.

3.2.3 Use of the Augmented Lagrangian

We would like to use this to rewrite the total energy in the form

$$\bar{\mathscr{E}} = \bar{\mathscr{E}}_{fb} + \bar{\mathscr{E}}_{fs} + \bar{\mathscr{E}}_s = \int \begin{pmatrix}\hat{\bar{u}}\\ \hat{\bar{v}}\\ \hat{\bar{w}}\end{pmatrix}^{t*} \underline{\underline{A}} \begin{pmatrix}\hat{\bar{u}}\\ \hat{\bar{v}}\\ \hat{\bar{w}}\end{pmatrix} + (\underline{B}^t)^* \begin{pmatrix}\hat{\bar{u}}\\ \hat{\bar{v}}\\ \hat{\bar{w}}\end{pmatrix} + C\, d\bar{k}_x\, d\bar{k}_y. \tag{3.7}$$

However, this is not possible due to the terms $\widehat{(\frac{\partial\bar{w}}{\partial\bar{x}})^2}$, $\widehat{(\frac{\partial\bar{w}}{\partial\bar{y}})^2}$ and $\widehat{\frac{\partial\bar{w}}{\partial\bar{x}}\frac{\partial\bar{w}}{\partial\bar{y}}}$. In order to solve this problem, we introduce auxiliary variables ξ_1, ξ_2 and impose the constraint $\xi_1 = \frac{\partial w}{\partial x}$, $\xi_2 = \frac{\partial w}{\partial y}$. We use the augmented Lagrangian to enforce the constraint.

General description of Augmented Lagrangian

The AL is an iterative way to optimize a constrained problem. In order to describe it properly, it is necessary to start from the penalty function method:

When considering the optimization of a function $f(x)$ subjected to a constraint $c(x) = 0$, the penalty function method consists of setting a penalty function sequence g_n(x):

$$g_n(x) = f(x) + \frac{n}{2}\, c(x)^2. \tag{3.8}$$

The optimization is solved by finding the limit of the sequence of the minima x_n as n goes to ∞

The AL described by Hestenes [39], is an improvement of the penalty function method that can be sensitive to local minima and might result in the constraint $c(x)$ not converging to 0. It builds upon the penalty function parameter by adding a Lagrange multiplier λ associated with the constraint $c(x)$. The new function to optimize becomes

$$g_n(x) = f(x) + \lambda_n c(x) + \frac{\beta}{2}\, c(x)^2. \tag{3.9}$$

The quadratic penalty parameter β can be taken as a sequence β_n or can be maintained a constant positive. The theorems associated with the convergence of λ_n have been depicted by Hestenes [39], then by Gill et al [33], and later Nocedal and Wright [61]. The iterations of g_n and λ_n are described by the following procedure:

```
Result: Minimized function $f(x_n)$ and its associated minimizer $x_n$
Choose initial values of $\lambda_0$, $\beta$ and a convergence criteria $\tau$ ;
$n$=0 ;
while $|c(x_n)| < \tau$ do
    Determine $x$ solving $\frac{dg_n(x)}{dx}$=0;
    $x_n$=$x$;
    $\lambda_{n+1} = \lambda_n + \beta c(x_n)$;
    $g_{n+1}(x) = f(x) + \lambda_{n+1} c(x) + \frac{\beta}{2} c(x)^2$;
    $n = n + 1$;
end
```

Algorithm 1: Functional minimization algorithm using Augmented Lagrangian.

Application to the bilayered system energy

The optimization problem $\bar{\mathscr{E}}(\bar{u}, \bar{v}, \bar{w})$ we are interested in is

$$\begin{gathered} min_{\bar{u},\bar{v},\bar{w}} \quad \bar{\mathscr{E}}_2(\bar{u}, \bar{v}, \bar{w}, \xi_1, \xi_2) \quad subject \quad to \\ \frac{\partial \bar{w}}{\partial \bar{x}} - \xi_1 = 0, \\ \frac{\partial \bar{w}}{\partial \bar{y}} - \xi_2 = 0 \end{gathered}$$

with

$$\begin{aligned} \bar{\mathscr{E}}_2(\bar{u}, \bar{v}, \bar{w}, \xi_1, \xi_2) = \int \alpha_{stret}(-\bar{\eta}_x + \frac{\partial \bar{u}}{\partial \bar{x}} + \frac{1}{2}\xi_1^2 - \bar{\eta}_y + \frac{\partial \bar{v}}{\partial \bar{y}} + \frac{1}{2}\xi_2^2)^2 - 2\alpha_{stret}(1-\nu)(-\bar{\eta}_x \\ + \frac{\partial \bar{u}}{\partial \bar{x}} + \frac{1}{2}\xi_1^2)(-\bar{\eta}_y + \frac{\partial \bar{v}}{\partial \bar{y}} + \frac{1}{2}\xi_2^2) + 2\alpha_{stret}(1-\nu)(-\bar{\eta}_{xy} + 0.5\,(\frac{\partial \bar{u}}{\partial \bar{y}} + \frac{\partial \bar{v}}{\partial \bar{x}}) + \frac{1}{2}\xi_1\xi_2)^2 \\ + \alpha_{bend}(\frac{\partial^2 \bar{w}}{\partial \bar{x}^2} + \frac{\partial^2 \bar{w}}{\partial \bar{y}^2})^2 \, d\bar{x}\, d\bar{y} + \int \alpha_{subs}\sqrt{\bar{k_x}^2 + \bar{k_y}^2}\,\hat{\bar{w}}\hat{\bar{w}}^* \, d\bar{k}_x\, d\bar{k}_y. \quad (3.10) \end{aligned}$$

Following the procedure of the AL, a new function $\mathscr{A}$ is created:

$$\mathscr{A} = \bar{\mathscr{E}}_2 + \int -\lambda_1(\frac{\partial \bar{w}}{\partial \bar{x}} - \xi_1) - \lambda_2(\frac{\partial \bar{w}}{\partial \bar{y}} - \xi_2) + \frac{\beta}{2}((\frac{\partial \bar{w}}{\partial \bar{x}} - \xi_1)^2 + (\frac{\partial \bar{w}}{\partial \bar{y}} - \xi_2)^2)\, d\bar{x}\, d\bar{y}. \quad (3.11)$$

In order to minimize $\mathscr{A}$ with respect to $\bar{u}, \bar{v}, \bar{w}$, it is necessary to transfer all the terms into the Fourier domain to create a quadratic form

$$\begin{aligned}\mathscr{A} = \int \frac{\alpha_{stret}}{4\pi^2}(|-\hat{\hat{\eta}}_x + i\bar{k}_x\hat{u} + \frac{1}{2}\widehat{\xi_1^2} - \hat{\hat{\eta}}_y + i\bar{k}_y\hat{\hat{v}} + \frac{1}{2}\widehat{\xi_2^2}|^2 \\ -(1-\nu)(-\hat{\hat{\eta}}_x + i\bar{k}_x\hat{\hat{u}} + \frac{1}{2}\widehat{\xi_1^2})^*(-\hat{\hat{\eta}}_y + i\bar{k}_y\hat{\hat{v}} + \frac{1}{2}\widehat{\xi_2^2}) - (1-\nu)(-\hat{\eta}_x + i\bar{k}_x\hat{\hat{u}} + \frac{1}{2}\widehat{\xi_1^2})(-\hat{\hat{\eta}}_y + \\ i\bar{k}_y\hat{\hat{v}} + \frac{1}{2}\widehat{\xi_2^2})^* + 2(1-\nu)|-\hat{\hat{\eta}}_{xy} + \frac{1}{2}(i\bar{k}_y\hat{\hat{u}} + i\bar{k}_x\hat{\hat{v}}) + \frac{1}{2}\widehat{\xi_1\xi_2}|^2) \\ + \frac{1}{4\pi^2}|(\bar{k}_x^2 + \bar{k}_y^2)\hat{\hat{w}}|^2 + \alpha_{subs}\sqrt{\bar{k_x}^2 + \bar{k_y}^2}\hat{\hat{w}}\hat{\hat{w}}^* - \frac{1}{4\pi^2}\hat{\lambda}_1^*(i\bar{k}_x\hat{w} - \hat{\xi}_1) \\ - \frac{1}{4\pi^2}\hat{\lambda}_2^*(i\bar{k}_y\hat{\hat{w}} - \hat{\xi}_2) + \frac{\beta}{2}\frac{1}{4\pi^2}(|i\bar{k}_x\hat{w} - \hat{\xi}_1|^2 + |i\bar{k}_y\hat{\hat{w}} - \hat{\xi}_2|^2)\, d\bar{k}_x\, d\bar{k}_y. \end{aligned} \quad (3.12)$$

Now, thanks to the new variables ξ_1 and ξ_2, it is possible to write $\mathscr{A}$ with a quadratic form of $\hat{\hat{u}}$,$\hat{\hat{v}}$,$\hat{\hat{w}}$:

$$\mathscr{A} = \int \begin{pmatrix} \hat{\hat{u}} \\ \hat{\hat{v}} \\ \hat{\hat{w}} \end{pmatrix}^{t*} \underline{\underline{A}} \begin{pmatrix} \hat{\hat{u}} \\ \hat{\hat{v}} \\ \hat{\hat{w}} \end{pmatrix} + (\underline{B}^t)^* \begin{pmatrix} \hat{\hat{u}} \\ \hat{\hat{v}} \\ \hat{\hat{w}} \end{pmatrix} + C\, d\bar{k}_x\, d\bar{k}_y \quad (3.13)$$

with

$$\underline{\underline{A}} = \frac{1}{4\pi^2}\begin{pmatrix} 2\alpha_{stret}(\bar{k}_x^2 + \frac{1-\nu}{2}\bar{k}_y^2) & \alpha_{stret}(1+\nu)\bar{k}_x\bar{k}_y & 0 \\ \alpha_{stret}(1+\nu)\bar{k}_x\bar{k}_y & 2\alpha_{stret}(\bar{k}_y^2 + \frac{1-\nu}{2}\bar{k}_x^2) & 0 \\ 0 & 0 & 2\alpha_{bend}(k_x^2+k_y^2)^2 + 2\alpha_{subs}4\pi^2\sqrt{k_x^2+k_y^2} \\ & & +\beta(k_x^2+k_y^2) \end{pmatrix} \quad (3.14)$$

and

$$\underline{B}^* = \begin{pmatrix} \frac{\alpha stret}{4\pi^2}((2ik_x)(-\hat{\hat{\eta}}_x^* + \frac{1}{2}\widehat{\xi_1^2}^* - \hat{\hat{\eta}}_y^* + \frac{1}{2}\widehat{\xi_2^2}^*) - (2ik_x)(1-\nu)(-\hat{\hat{\eta}}_y^* + \frac{1}{2}\widehat{\xi_2^2}^*) + (2ik_y)(1-\nu)(-\hat{\hat{\eta}}_{xy}^* + \frac{1}{2}\widehat{\xi_1\xi_2}^*)) \\ \frac{\alpha stret}{4\pi^2}((2ik_x)(-\hat{\hat{\eta}}_x^* + \frac{1}{2}\widehat{\xi_1^2}^* - \hat{\hat{\eta}}_y^* + \frac{1}{2}\widehat{\xi_2^2}^*) - (2ik_y)(1-\nu)(-\hat{\hat{\eta}}_y^* + \frac{1}{2}\widehat{\xi_2^2}^*) + (2ik_x)(1-\nu)(-\hat{\hat{\eta}}_{xy}^* + \frac{1}{2}\widehat{\xi_1\xi_2}^*)) \\ \frac{1}{4\pi^2}(-ik_x)\hat{\lambda}_1{}^* + \frac{1}{4\pi^2}(-ik_x)\hat{\lambda}_2{}^* + \frac{1}{4\pi^2}\frac{\beta}{2}(-2ik_x)\hat{\xi}_1{}^* + \frac{1}{4\pi^2}\frac{\beta}{2}(-2ik_y)\hat{\xi}_2{}^* \end{pmatrix} \quad (3.15)$$

The distribution $\hat{\hat{u}}$,$\hat{\hat{v}}$,$\hat{\hat{w}}$ minimizing $\mathscr{A}$ is given by:

$$\begin{pmatrix} \hat{\hat{u}} \\ \hat{\hat{v}} \\ \hat{\hat{w}} \end{pmatrix} = -\underline{\underline{A}}^{-1}\underline{B}. \quad (3.16)$$

The AL iterative loop must be adapted to take into account the ξ_1 and ξ_2 in the energy minimization: the two distributions cannot remain fixed at their initial values: ξ_1 and ξ_2 must be calculated at each iteration to minimize $\mathscr{A}$. It could be possible to consider a larger quadratic form in the Fourier domain, but it is more straightforward in that case to optimize $\mathscr{A}$ with respect to ξ_1 and ξ_2 in the spatial domain. As a result, at each iteration, ξ_1 and ξ_2 are determined by solving the equations:

$$\frac{\partial \mathscr{A}}{\partial \xi_1} = 0, \tag{3.17}$$

$$\frac{\partial \mathscr{A}}{\partial \xi_1} = 0 \tag{3.18}$$

which are equivalent to solving

$$\begin{aligned}\alpha_{stret}(2\xi_1(-\bar{\eta}_x + \frac{\partial \bar{u}}{\partial \bar{x}} + \frac{1}{2}\xi_1^2 - \bar{\eta}_y + \frac{\partial \bar{v}}{\partial \bar{y}} + \frac{1}{2}\xi_2^2) - 2(1-\nu)\xi_1(-\bar{\eta}_y + \frac{\partial \bar{v}}{\partial \bar{y}} + \frac{1}{2}\xi_2^2)\\ + 2(1-\nu)\xi_2(-\bar{\eta}_{xy} + \frac{1}{2}(\frac{\partial \bar{u}}{\partial \bar{y}} + \frac{\partial \bar{v}}{\partial \bar{x}}) + \frac{1}{2}\xi_1\xi_2)) + \lambda_1 - \beta(\frac{\partial \bar{w}}{\partial \bar{x}} - \xi_1) = 0,\end{aligned} \tag{3.19}$$

$$\begin{aligned}\alpha_{stret}(2\xi_2(-\bar{\eta}_x + \frac{\partial \bar{u}}{\partial \bar{x}} + \frac{1}{2}\xi_1^2 - \bar{\eta}_y + \frac{\partial \bar{v}}{\partial \bar{y}} + \frac{1}{2}\xi_2^2) - 2(1-\nu)\xi_2(-\bar{\eta}_x + \frac{\partial \bar{u}}{\partial \bar{x}} + \frac{1}{2}\xi_1^2)\\ + 2(1-\nu)\xi_1(-\bar{\eta}_{xy} + \frac{1}{2}(\frac{\partial \bar{u}}{\partial \bar{y}} + \frac{\partial \bar{v}}{\partial \bar{x}}) + \frac{1}{2}\xi_1\xi_2)) + \lambda_2 - \beta(\frac{\partial \bar{w}}{\partial \bar{x}} - \xi_2) = 0.\end{aligned} \tag{3.20}$$

Ultimately, the iterative procedure of the AL applied to the bilayered system is described by the following algorithm:

```
Result: Distribution of $u$, $v$, $w$ minimizing the total energy.
Definition step: Choose all physical parameters of the bilayered system and
  the value of the non-dmensionalized coefficients $\alpha_{bend}$, $\alpha_{stret}$ and $\alpha_{sub}$. Using
  those parameters, the space domain, the frequency domain, the
  undimensionalized coefficients $x_0$, $w_0$, $u_0 = v_0$, $\eta_{x0} = \eta_{y0} = \eta_{xy0}$, $\bar{\mathscr{E}}$ and the
  quadratic tensor $\underline{\underline{A}}$ can be defined. Choose the parameters of the loop: the
  maximum number of iterations, the convergence criteria $\tau$, the coefficient of
  quadratic penalty $\beta$., the initial value of the Lagrange multipliers $\lambda_1^0$ and $\lambda_2^0$.
  Choose the initial distributions for undimensionalized displacements $\bar{u_0}$, $\bar{v_0}$,
  and $\bar{w_0}$. ;
$n$=0 ;
while $\frac{\partial \bar{w}_{n+1}}{\partial \bar{x}} - \xi_{1(n+1)} < \tau$ and $\frac{\partial \bar{w}_{n+1}}{\partial \bar{y}} - \xi_{2(n+1)} < \tau$ do
    Solve Equations (3.19) and (3.20) to determine $\xi_{1(n+1)}$ and $\xi_{2(n+1)}$;

    Transfer all distributions $\bar{u}_n$, $\bar{v}_n$, $\bar{w}_n$, $\lambda_1 n$,$\lambda_2 n$,$\xi_{1n}^2$, $\xi_{2n}^2$, $\xi_{1n}\xi_{2n}$ into the Fourier
      domain;

    Compute $\underline{\underline{B}}_{n+1}$ using (3.15);

    Compute $\hat{\hat{u}}_{n+1}$, $\hat{\hat{v}}_{n+1}$, $\hat{\hat{w}}_{n+1}$ using (3.16);

    Transfer $\hat{\hat{u}}_{n+1}$, $\hat{\hat{v}}_{n+1}$, $\hat{\hat{w}}_{n+1}$ into the space domain ;

    Compute $\nabla\bar{u}_{n+1}$,$\nabla\bar{v}_{n+1}$,$\nabla\bar{w}_{n+1}$ ;

    Compute $\lambda_{1(n+1)} = \lambda_{1(n)} - \beta(\frac{\partial \bar{w}_{n+1}}{\partial \bar{x}} - \xi_{1(n+1)})$ ;
    Compute $\lambda_{2(n+1)} = \lambda_{2(n)} - \beta(\frac{\partial \bar{w}_{n+1}}{\partial \bar{y}} - \xi_{2(n+1)})$ ;

    $n = n + 1$;
end
```

Algorithm 2: Energy minimization algorithm using Augmented Lagrangian in the Fourier domain.

We implement the algorithm in Matlab. Since we discretize the problem, it is important that the discretization be chosen to include the frequencies of interest. Further, Matlab uses unitary ordinary frequency instead of the unitary angular frequency used here.

3.3 Results

In all cases, the initial distributions for displacements u, v and w are taken to be random, the initial distributions λ_1^0 and λ_2^0 are taken to be 0 and the value of the penalty coefficient β is maintained constant through the entire procedure. The thickness of the film is taken to be 30 μm, the Poisson coefficient of the film is set to 0.3, and the Poisson coefficient of the substrate is set to 0.4

3.3.1 Case of a uniform strain

We seek to verify the method by comparing the converged results in the case of a homogeneous strain with the analytic results shown in Chapter 2.

One dimensional deformation

In one dimension, we consider in-plane displacement u and deflection w depending only on the space variable x. We still allow strain in the y direction η_y to be applied as it is a uniform field independent of directions. There is only one constraint $\frac{\partial w}{\partial x}$, and as a consequence, there is only one Lagrange multiplier λ_1.

Several tests have been performed with different stiffness ratios and different values for the applied strain $\eta_x = \eta_y$. For every test, the sampling was taken to be 256 points, and the stopping criteria was taken to be:

$$\frac{|\frac{\partial w}{\partial x} - \xi_1|}{|\frac{\partial w}{\partial x}|} < 10^{-8}. \tag{3.21}$$

Every test converged to the stopping criteria and results in a single frequency mode for the deflection w as illustrated in Figure 3.1. This particular figure represents the case where the elasticity of the film is 10 GPa and the elasticity of the substrate is 10 MPa. Table 3.1 collects the results of all cases studied. We see excellent agreement between the numerical result and analytic result, thereby verifying the numerical method.

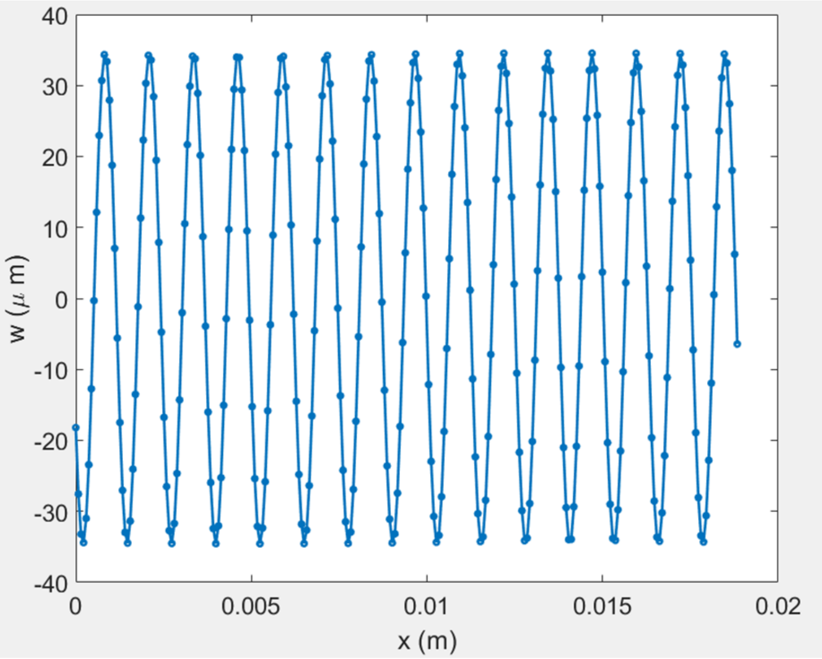

Figure 3.1: Plot of the converged deflection obtained using the Augmented Lagrangian method.

	Case 1	***Case 2***	***Case 3***	***Case 4***	***Case 5***	***Case 6***	***Case 7***	***Case 8***	***Case 9***
E_f (GPa)	1	3	5	7	10	10	10	10	10
E_s (MPa)	10	10	10	10	10	7	5	3	1
strain	0.03	0.03	0.03	0.02	0.01	0.01	0.009	0.009	0.009
converged wavelength (m^{-1})	10738	7445	6280	5613	4984	4425	3956	3337	2313
theoretical wavelength (m^{-1})	10738	7445	6280	5613	4984	4425	3956	3337	2313
converged amplitude (μm)	21.28	43.75	55.28	49.00	34.54	41.9	45.72	57.48	88.57
theoretical amplitude (μm)	21.28	43.75	55.28	49.00	34.54	41.9	45.72	57.48	88.57

Table 3.1: 1D converged deflection characteristics with the Augmented Lagrangian method.

Two-dimensional deformation

Figure 3.2 illustrates the evolution of a two-dimensional case by showing the first step with complete random distribution, and how the model manages to reach a converged configuration. We see some branching faults, but they eventually annihilate each other.

The main difficulty with the 2D case is the cost of calculation, especially since convergence requires usually around 40,000 iterations. As a consequence, the convergence criteria was taken to be 10^{-5} instead of 10^{-8}. The model also converged towards one mode frequency wrinkles as illustrated in Figure 3.3.

Another difficulty compared to the 1D case is the error with respect to the theory. We noticed that even though the wavelength of the wrinkles matched the expected theory value with a small relative difference, the value of the amplitude did not match exactly, and the relative difference was higher than 5%. The reason for that difference turned out to be the sampling of the model. When in 1D a sampling of more or less 18 value points per wrinkle period was enough to match the theory value, the 2D case would require 70 value points per wrinkle period. The influence of the sampling on the converged amplitude is shown in Figure 3.4. In order to reach that sampling, it was necessary to reduce the number of wrinkles observed on the whole data set as the option of increasing the number of points within the set requires high computational cost. The illustration of the number of wrinkles observed to improve the sampling is represented in Figure 3.5.

Being aware of this error depending on the sampling, the next step is to compare the theory with the numerical amplitude and wavelength for different scenarios of elasticity and applied strain. This comparison is illustrated in Table 3.2. When we compare the theoretical amplitude with the numerical converged solution, we must keep in mind that we are considering a unidirectional strain η which means that the strain in the other main direction will be zero. As a consequence, the theoretical expression of the amplitude, based on expression 2.37 will become

$$A = \sqrt{\eta \frac{4}{k^2} - h^2}. \tag{3.22}$$

3.3.2 Influence of quadratic constraint on convergence

The choice of the initial values for parameters and variables has an influence on the convergence of the model. The initial displacements are taken to be random

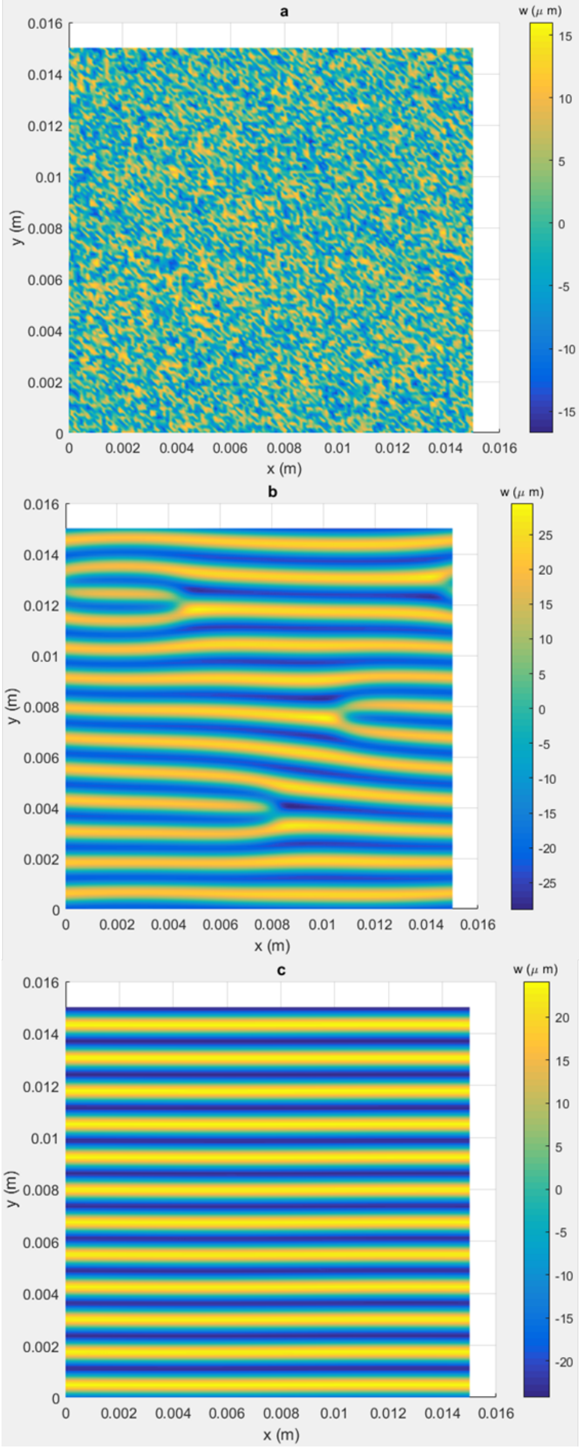

Figure 3.2: Evolution of the deflection w as a function of the number of iterations. Case a shows the deflection after one iteration; Case b shows the deflection after 4300 iterations; Case c shows the deflection after 16865 iterations.

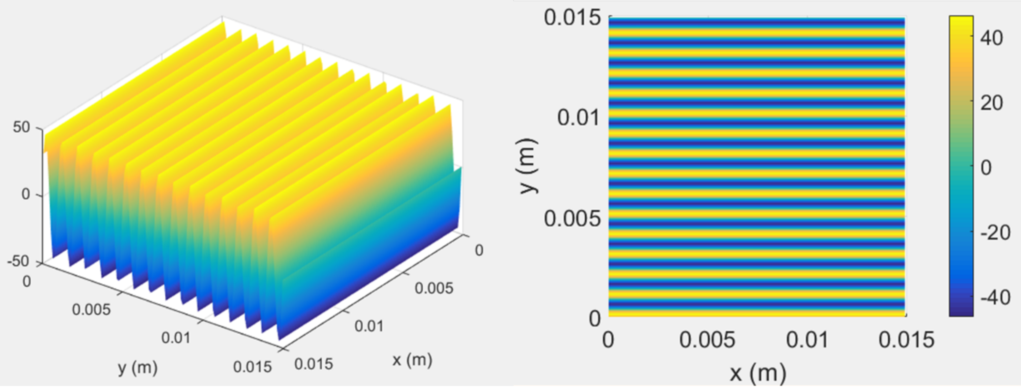

Figure 3.3: Plot of the converged deflection obtained using the Augmented Lagrangian method in 2D.

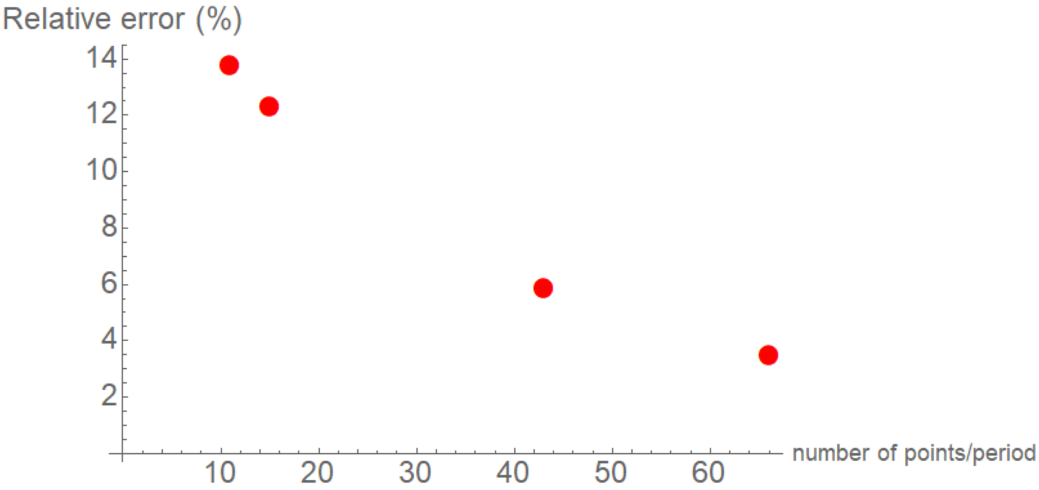

Figure 3.4: Relative error of the amplitude as a function of the sampling.

	Case 1	***Case 2***	***Case 3***	***Case 4***	***Case 5***	***Case 6***
E_f (GPa)	7	5	3	1	10	10
E_s (MPa)	10	10	10	10	1	10
strain η	0.01	0.03	0.03	0.03	0.003	0.01
converged wavelength (m^{-1})	5613	6286	7441	10740	2315	4982
theoretical wavelength (m^{-1})	5613	6279	7441	10738	2313	4984
sampling(number of points/period)	19	43	44	19	19	14
converged amplitude (μm)	16.96	43.79	33.56	10.52	32.67	23.36
theoretical amplitude (μm)	19.22	46.29	35.56	11.86	36.64	26.65

Table 3.2: Converged two-dimensional deflection characteristics with the Augmented Lagrangian method.

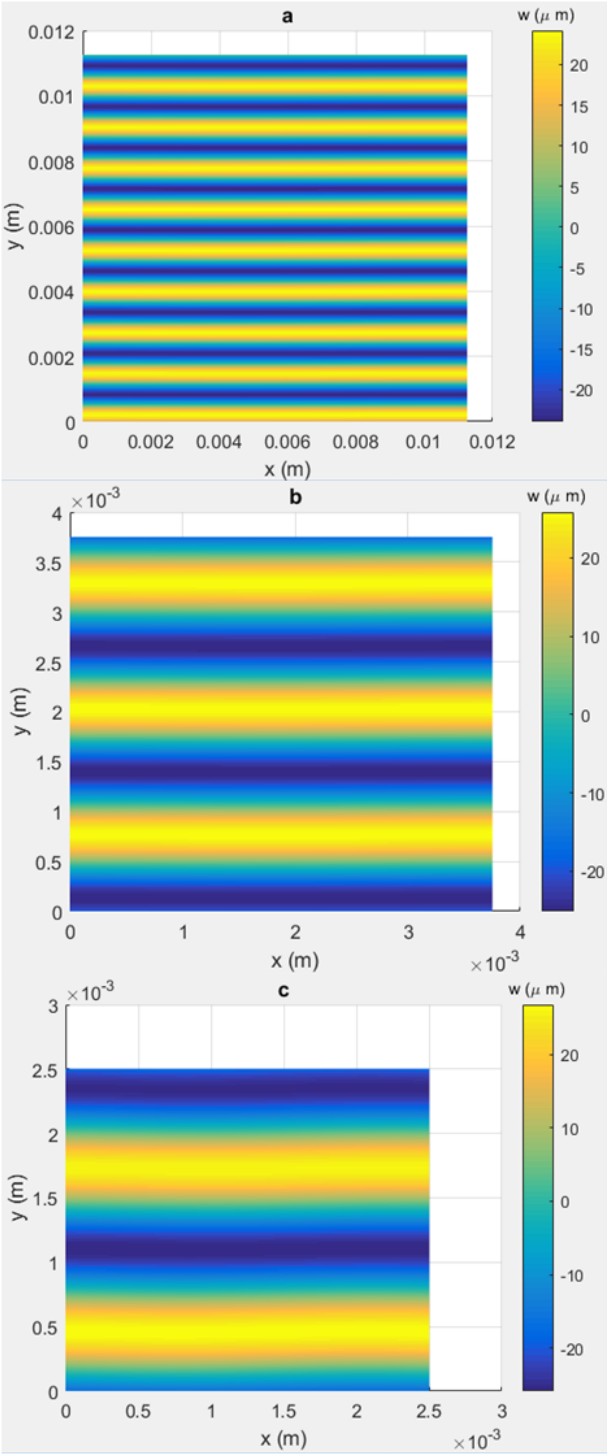

Figure 3.5: Change of sampling to improve the resolution and decrease the amplitude relative error. Case a shows 9 wrinkles for an error of 12.3%; Case b shows 3 wrinkles for an error of 5.85 %; Case c shows 2 wrinkles for an error of 3.48%.

distributions, and the initial Lagrange multipliers λ_1 and λ_2 are taken to be 0. Those choices are motivated by the fact that those values will evolve as the loop progresses. But regarding the quadratic penalty coefficient β, the choice is more important since β remains constant during the entire loop. When looking at the terms associated with β in the expressions (3.12) and (3.16), it is possible to determine the influence of β on the converged solution.

If β is significantly large, then the energy will be dominated by the quadratic penalty term $\frac{\beta}{2}(\nabla w - \xi)^2$. As a consequence, the minimization of the energy will make the residue $(\nabla w - \xi)$ very small to compensate the large value of β. This will result in a smaller converged residue and then more likely to satisfy the stopping loop criteria. But, the expression (3.16) indicates that in each successive increment, deflection w will be calculated as follow:

$$\hat{\hat{w}} = -4\pi^2 \frac{\frac{1}{4\pi^2}(ik_x)\hat{\lambda}_1 + \frac{1}{4\pi^2}(ik_x)\hat{\lambda}_2 + \frac{1}{4\pi^2}\frac{\beta}{2}(2ik_x)\hat{\xi}_1 + \frac{1}{4\pi^2}\frac{\beta}{2}(2ik_y)\hat{\xi}_2}{2\alpha_{bend}(k_x^2 + k_y^2)^2 + 2\alpha_{subs}4\pi^2\sqrt{k_x^2 + k_y^2} + \beta(k_x^2 + k_y^2)}. \tag{3.23}$$

And in the case of β being very large, this expression will then be dominated by the terms associated with β, and the influence of the other terms will be negligible. As a consequence, the convergence of w towards the form minimizing the energy will be very slow because the stretching and bending terms have a small influence at every increment compared to β. In conclusion, having β very large will ensure that the converged residue will be very small and will be more likely to match with the convergence criteria, but the final converged state will require a very large number of increments to be reached.

On the opposite side, if β is very small, the minimum value of the residue will be reached quicker, but might not be small enough to match with the stopping loop criteria. The influence of β is illustrated in Figure 3.6. In those plots, the norm of the residue distribution is calculated as:

$$|residue| = |\sqrt{r_1^2 + r_2^2}| \tag{3.24}$$

with

$$r_1 = \frac{\frac{\partial w}{\partial x} - \xi_1}{\frac{\partial w}{\partial x}}, \tag{3.25}$$

$$r_2 = \frac{\frac{\partial w}{\partial y} - \xi_2}{\frac{\partial w}{\partial y}}. \tag{3.26}$$

β	***Minimum residue norm***	***Increment of the minimum***
120	6.60×10^{-4}	8,019
400	1.16×10^{-4}	9,327
600	3.64×10^{-5}	15,775
800	2.21×10^{-5}	23,156
1000	1.31×10^{-5}	32,717
1200	9.84×10^{-6}	40,799
2000	3.28×10^{-6}	62,601
3000	1.45×10^{-6}	130,326

Table 3.3: Minimum norm of the residue and computational cost for different values of quadratic penalty coefficient β.

It is necessary to remember that ξ_1, ξ_2, $\frac{\partial w}{\partial x}$ and $\frac{\partial w}{\partial y}$ are distributions within the space domain as there is one value associated with each value of the displacement distribution within the space domain It can be observed that for β=120, the residue reached its minimum in less than 10,000 increments, but the norm of the residue distribution will not go lower than 0.005. By increasing β all the way until 4,000, one can see that the residue will take more than 130,000 increments to reach its minimum, but the minimum value of the norm of the residue will be lower than 10^{-5}. All the exact values of the minimum residue and associated increments are indicated in Table 3.3.

It is interesting to observe from Figure 3.6 that after reaching its minimum value, the residue starts increasing and diverges after more iterations. This phenomenon is due to the fact that the deflection w depends on only one variable. It means that its derivative with respect to the other variable will converge towards a zero distribution. At some point, both the derivative of w and the associated variable ξ will be so small that the relative error with respect to the derivative of w will become very unstable due to its very small values and will eventually start to diverge. This problem can be avoided by changing the orientation of the wrinkles to ensure that deflection w on both in-plane coordinates which will prevent $\frac{\partial w}{\partial x}$ or $\frac{\partial w}{\partial y}$ to tend to 0. This case is illustrated in Figure 3.7. We see that after a stabilization period, the residue norm will converge and reach the convergence criteria (in this case equal to 5×10^{-7}) set to stop the loop.

Case of gold film attached to PDMS substrate

In all previous sections, the values of the Young's modulus of the film are not the values that can be seen in the experimental work of Bowden et al [10]. If we take values indicated in the experimental studies: E = 82 GPa, E_s = 20 MPa, ν=

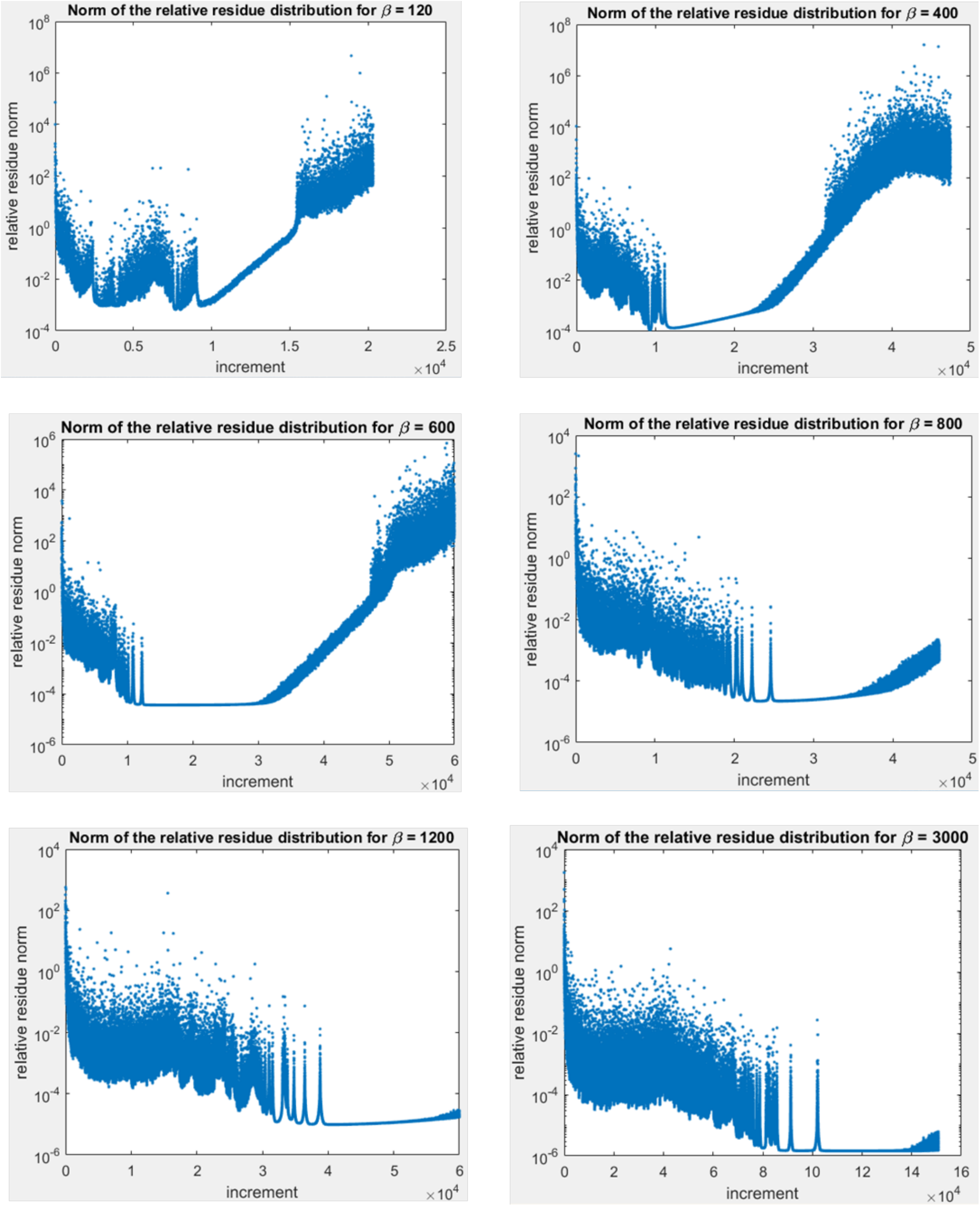

Figure 3.6: Evolution of the norm of the residue distribution for different values of quadratic penalty coefficient β.

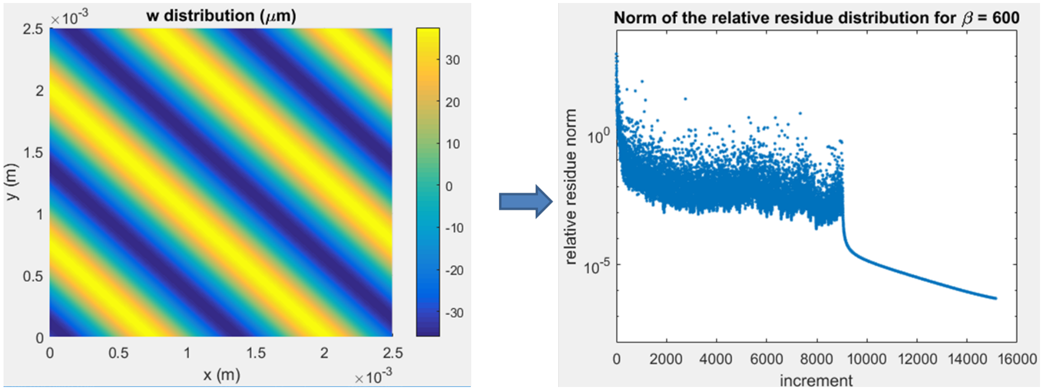

Figure 3.7: Example of uniform deflection depending on both x and y coordinates. The final converged out-of-plane displacement is on the left, and the evolution of the norm of the associated residue is on the right.

0.33, ν_s= 0.48, and a strain magnitude η = 0.005, the converged solution gives the expected wavelength but there is still some inaccuracy regarding the amplitude. For a thickness of 50 nm, as indicated in the experimental work, the converged model predicts an amplitude of around 50.54 nm while the theoretical value was 56 nm. This correspond to an error of 9.75 %. And if we take the thickness to be 100 nm, then the resulting numerical amplitude will be 101 nm while the expected theoretical amplitude is 111 nm. There is still an error of 9% and if we make the same study for a thickness of 400 nm, the resulting numerical amplitude is 404 nm and the theoretical amplitude is 444 nm making the error still 9%.

These results demonstrate that we can still obtain a converged model close to the theoretical model with parameters corresponding to experimental conditions.

3.3.3 Case of discontinuous strain

Importance of the substrate energy

One critical point to consider with the Matlab implemented AL method is that the Fourier transform of all variables ends up forcing all average values of strains to be zero regardless of the size of the surface. It is then necessary to be more careful with the contribution of the displacements in each energy, not only regarding the amount of resulting energy, but regarding the effect on the convergence of the final solution.

The substrate energy is then revisited to take into account the terms related to the in-plane strains. So we cannot use the simplified expression (2.30), but the full expression (2.28).

One parameter strain distribution

One of the key features here is the control of the direction of the wrinkling pattern along the surface. This control results from the stretching tensor

$$\underline{\eta} = \begin{pmatrix} \eta_x & \eta_{xy} \\ \eta_{xy} & \eta_y \end{pmatrix} \tag{3.27}$$

To reduce this tensor to one orientation parameter, we introduce the angle θ representing the orientation of the stretch with respect to the undimensionalized x-axis:

$$\underline{\eta} = \eta \begin{pmatrix} cos^2(\theta) & cos(\theta)\ sin(\theta) \\ cos(\theta)\ sin(\theta) & sin^2(\theta) \end{pmatrix} \tag{3.28}$$

In this representation, η will be considered as the loading parameter. We can generate a heterogeneous mismatch by creating an adequate distribution of the angle θ. This influence is illustrated in Figure 3.8. The left case of this figure is a simple interface with θ being $\pi/4$ on the left of the surface and $\pi/2$ on the right of the surface. The right case shows that multiple interfaces can be created as θ would switch from $\pi/2$ to $\pi/4$ two times on the same surface. We can observe spacing is at the expected value in each segment. This creates mismatch at the boundary, resulting in defects.

Another interesting case to observe is a case of symmetry of the parameter θ through the interface. As illustrated in Figure 3.9, the left part has wrinkles oriented with $\theta = \pi/4$ and the right part has wrinkles oriented with $\theta = -\pi/4$. In this case, we observe that symmetry of the angle results in wrinkles in phase through the interface. There is no need for branching as the positions of high amplitude deflections and low amplitude deflections are matching along the interface. This makes sense since the branching operation requires the presence of extra frequencies within the Fourier domain, which results in higher surface energy.

A more advanced case would consist of representing a more complex combination of interfaces. Figure 3.10 shows what happens when the surface is submitted to a particular angle variation making the final deflection go through a different set of interfaces with each one presenting a symmetry for the angle θ. Again it can be observed that the wrinkles will form in such a way that no branching is required through the interfaces.

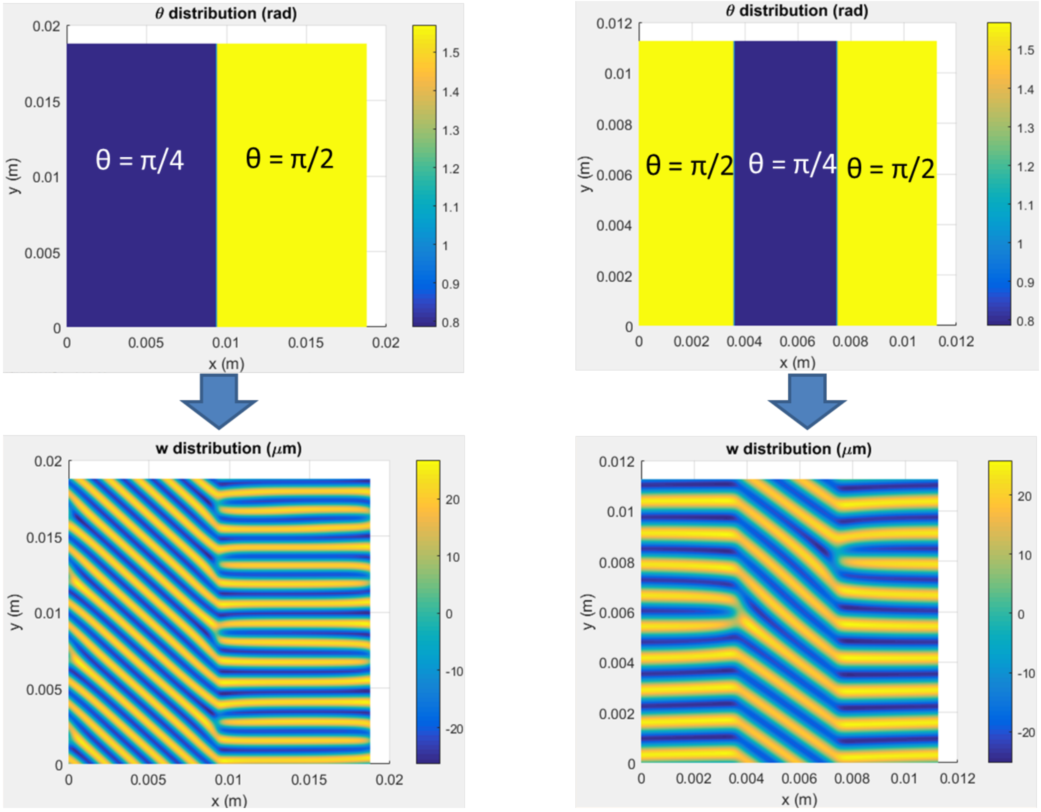

Figure 3.8: Converged deflection for varying angle distributions.

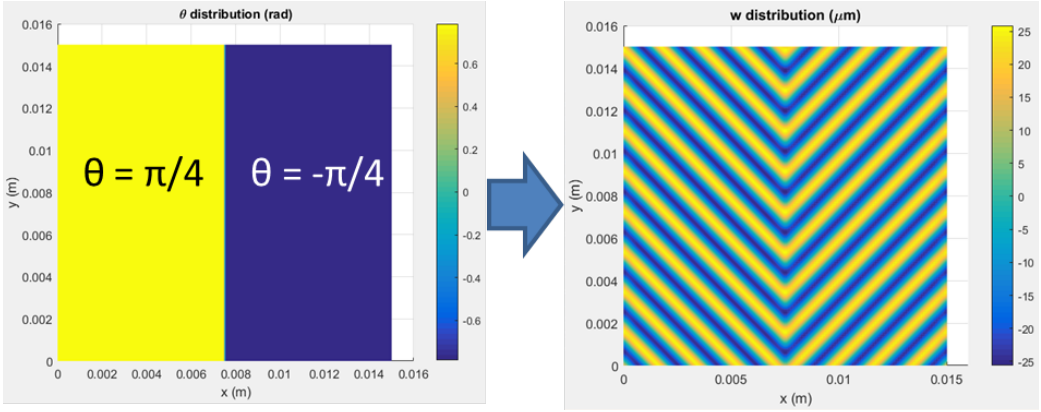

Figure 3.9: Converged deflection for symmetric strain angle through the interface.

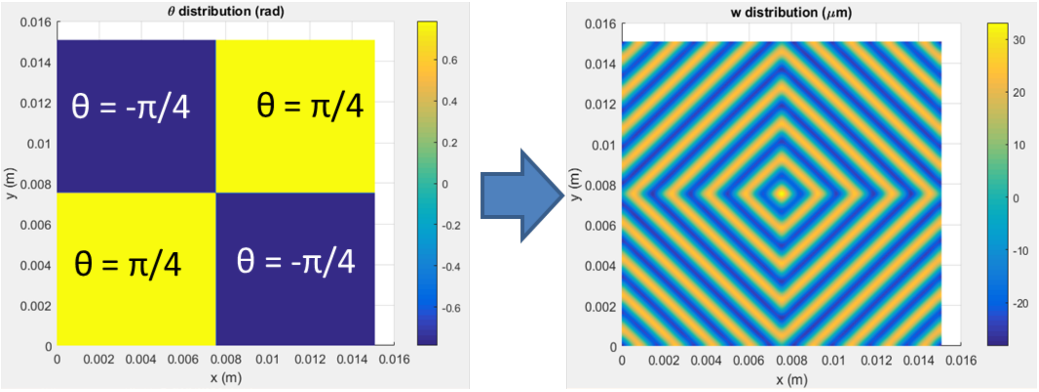

Figure 3.10: Converged deflection for multiple symmetric interfaces.

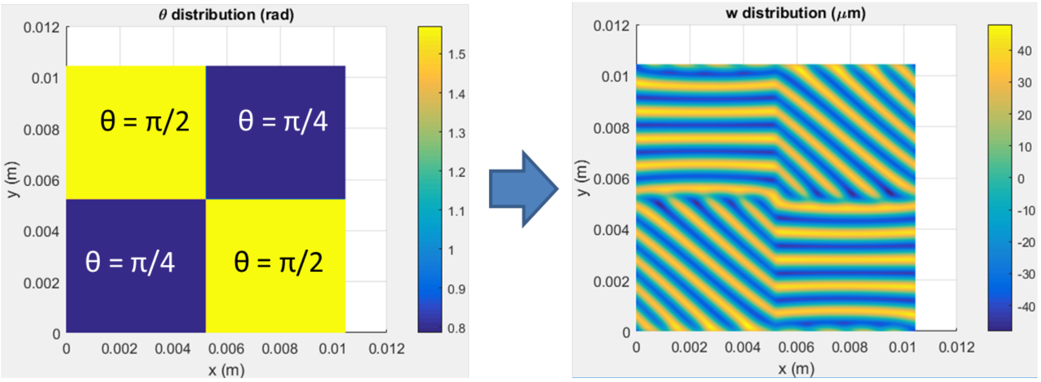

Figure 3.11: Converged deflection for multiple non-symmetric interfaces.

The last case we want to study in this section illustrates what happens when the periodicity at the edges is made impossible by the orientation of the wrinkles. Because of the Fourier transform, the model when returning to the space domain will have periodicity of the displacements between opposite edges of the surface. Strain orientation distribution depicted in Figure 3.11 results in 4 different regions with non-symmetric wrinkle directions. Observing closely the right part of the bottom edge, we can see that the deflection is continuous with the right part of the top edge but immediately branches towards the assigned direction of the region. This result indicates that when using this method, one should be careful and consider results represented away form the edges except if there is symmetry between the opposite edges.

Sensitivity to the angle of the strain

All results obtained in this thesis considered angles of the strain mismatch to be either $\theta = \frac{\pi}{2}$ and $\theta = \frac{\pi}{4}$. This choice resulted in a strain tensor with components either only along the y-axis or with equal axial and shear components:

$$\theta = \frac{\pi}{2} \quad \Rightarrow \quad \underline{\eta} = \begin{pmatrix} 0 & 0 \\ 0 & \eta \end{pmatrix}, \tag{3.29}$$

$$\theta = \frac{\pi}{4} \quad \Rightarrow \quad \underline{\eta} = \begin{pmatrix} \frac{\eta}{2} & \frac{\eta}{2} \\ \frac{\eta}{2} & \frac{\eta}{2} \end{pmatrix}. \tag{3.30}$$

But if we study the case of non-symmetric angles of strain orientation with respect to the x- and y-axes, we are going to see a difference in terms of converged amplitude. This is illustrated in Figure 3.12: we see that the converged maximum deflections for angles $\frac{\pi}{2}$ and $\frac{\pi}{4}$ are very close, and that there is a difference for angles $\frac{\pi}{3}$ and $\frac{\pi}{6}$. We can conclude that the numerical method is sensitive to the angle of orientation of the strain. To avoid inaccuracy in the results, we will consider only numerical values for angles $\frac{\pi}{2}$ and $\frac{\pi}{4}$ since those angles ensure the simplest forms of the strain tensor.

Energy at the interface

This method can now be used to characterize the energy behavior at the interface of the discontinuous strain. The case taken to make the comparison is the one with film elasticity being 10 GPa, substrate elasticity being 10 MPa, strain η being 0.01. Each energy is first computed separately using Equations (2.7) and (3.1) and then the total energy density functions are represented by summing the three energies. Figure 3.13 represents the reference case with no change of orientation angle, Figure 3.14 represents the case with the orientation angle going from $\pi/2$ to $\pi/4$, and Figure 3.14 represents the case with the orientation angle going from $\pi/4$ to $-\pi/4$. Figure 3.14 is the ideal illustration of the effect of branching at the interface on the energies. We see that overall, the branching has the effect of decreasing the energy variation at the interface. We can also see that the total energy variation is also decreased at the interface without any branching, but instead, a symmetric change of the orientation.

3.3.4 Limit of the interface dimension

The results obtained so far showed a surface divided in two or four parts. Of interest is the behavior of the material as the number of interfaces within the same surface

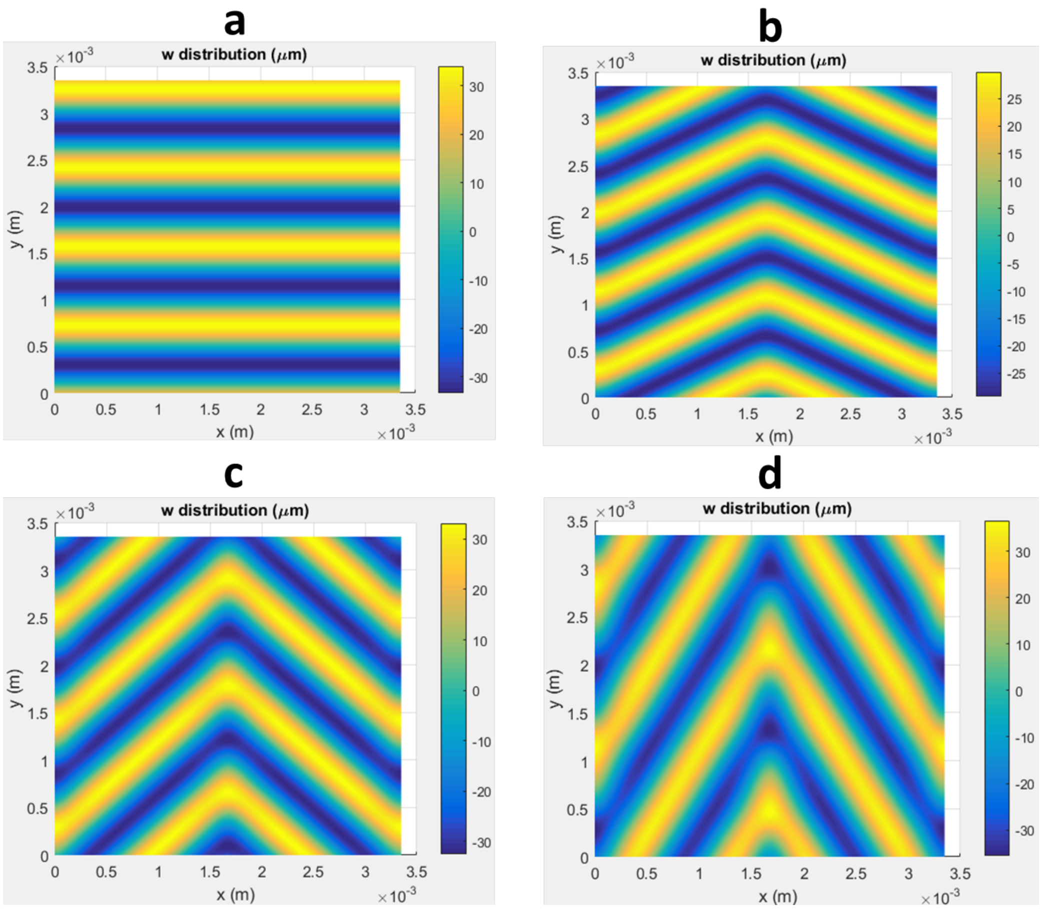

Figure 3.12: Converged deflection for different angles of the strain mismatch: case a: $\theta = \frac{\pi}{2}$;: case b: $\theta = \frac{\pi}{3}$;: case c: $\theta = \frac{\pi}{4}$;: case d: $\theta = \frac{\pi}{6}$.

are multiplied. This will reduce the space in which the wrinkles are allowed to form and will challenge the convergence of the final solution. This study is realized for a surface made of 256 × 256 nodes, and in every case a checkerboard is created for the orientation θ of the wrinkles as illustrated in the left figures in Figure 3.16. The different regions represent the angle θ switching from 0 to $\frac{pi}{2}$. The resulting converged deflection in each case is illustrated in the right figures in Figure 3.16.

In each case, the total dimension of the surface was taken so that eight wrinkles would have been observed in the case of a continuous strain distribution. We can see that for the case b, when the size of each sub-surface is the length of one period for the wrinkles, the deformation is still reflected correctly. But in case c, the distance between two interfaces is half this period and it becomes harder to distinguish precisely the discontinuities. We can then conclude that even if the

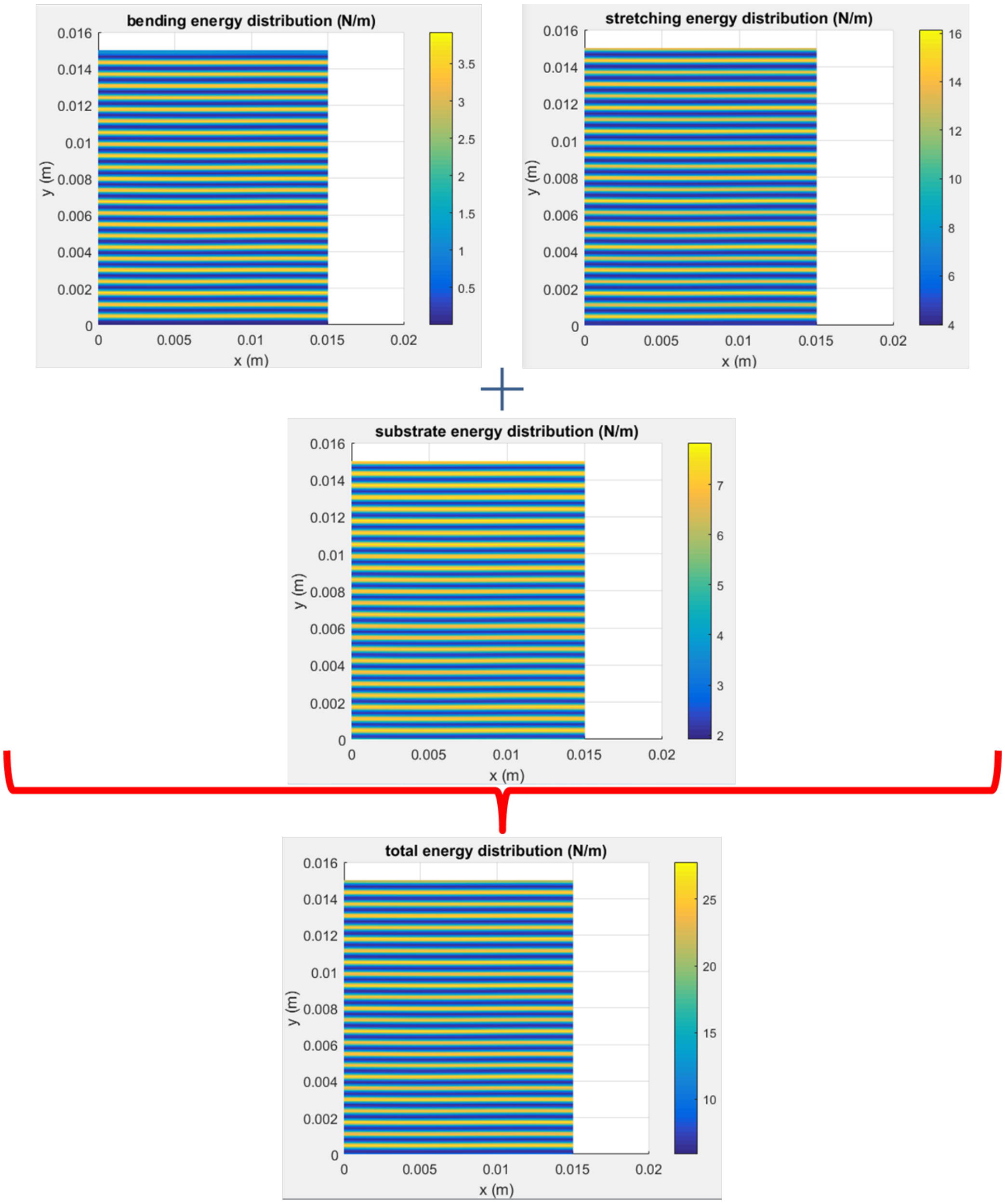

Figure 3.13: Energy density functions distributions for the case of uniform wrinkles.

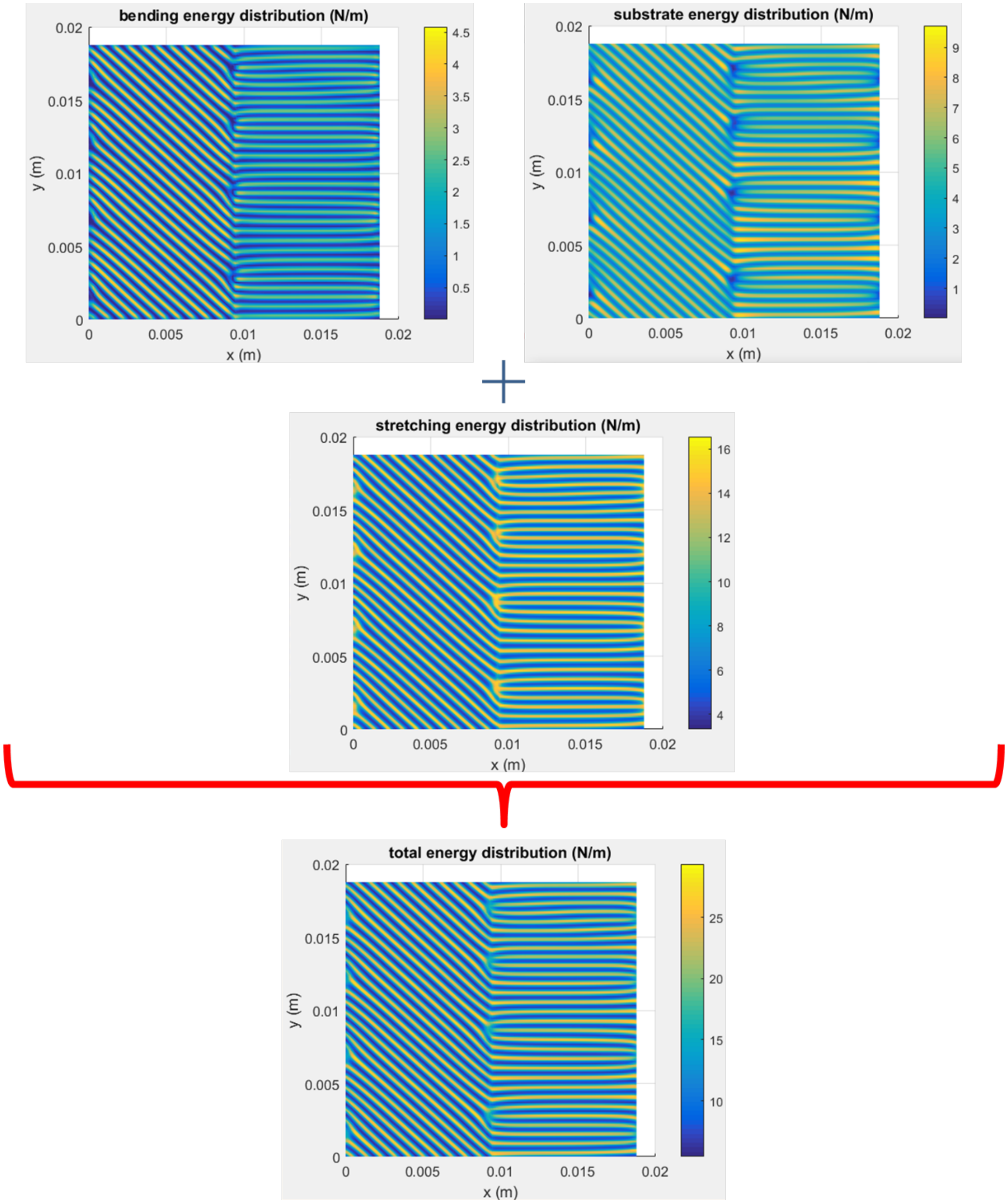

Figure 3.14: Energy density functions distributions for the case of wrinkles with one non-symmetric interface.

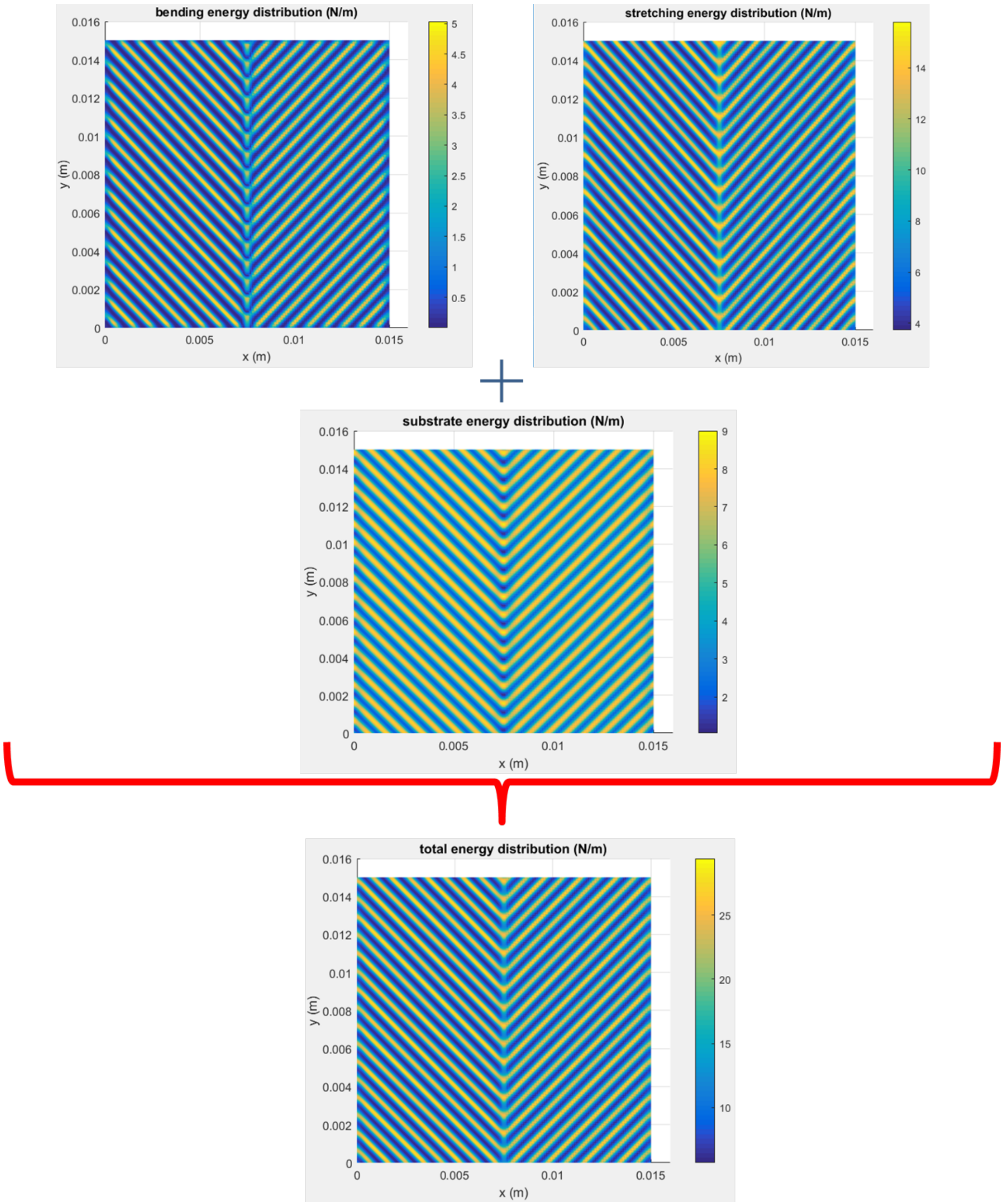

Figure 3.15: Energy density functions distributions for the case of symmetric wrinkles.

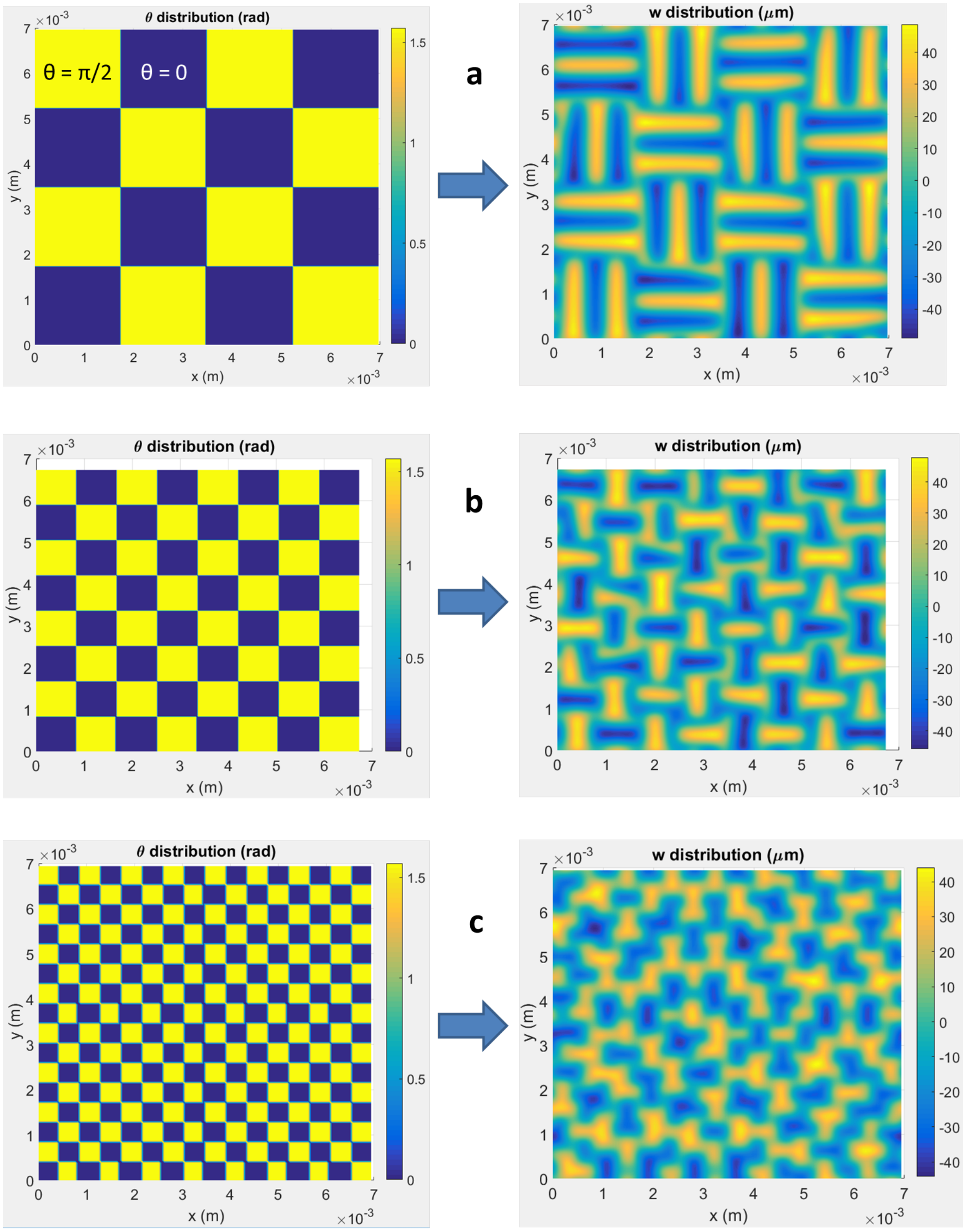

Figure 3.16: Strain orientation θ and resulting converged deflection w for three different number of interfaces within a surface. Case a: four different regions along each axis; case b: eight different regions along each axis; case c: sixteen different regions along each axis.

model still converges for small distances between interfaces, the clearness of the final disconitnuity will be very weak if this distance is lower than the wavelength associated with the wrinkles.

3.3.5 Study of a symmetric interface with a small error

The fact that symmetric strain orientations through the interface result in an interface without any branching or default brings another question: what angle difference across the interface will result in defaults along the interface? An approach to this problem consists of creating an interface with almost symmetric strain orientations. The test illustrated in Figure 3.17 shows the sensitivity of the branching phenomenon to a small prescribed difference of angles within the symmetry. As seen in the right figures, a 5% difference between the angles generates defaults at the interface, while in the right figures, a 1% difference yields no default in the final solution. In the 1% case, it appears that the wrinkles bend to match with the other half of the surface at the interface.

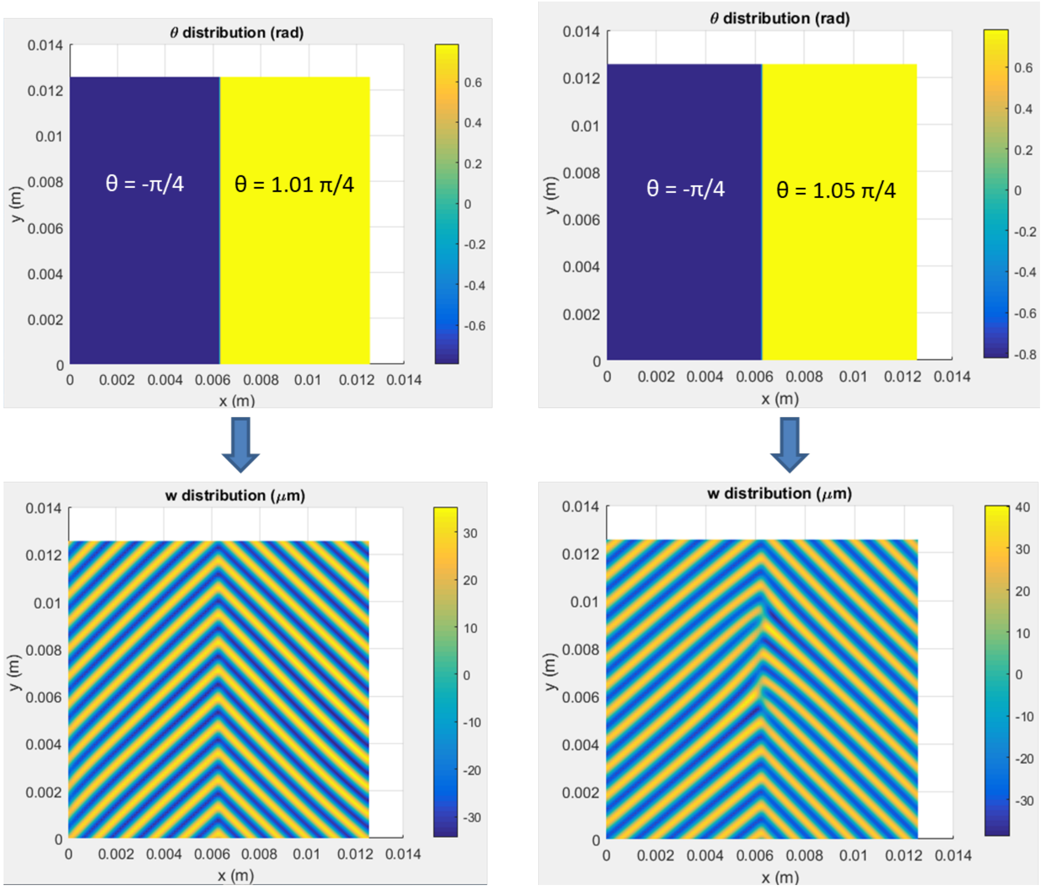

Figure 3.17: Comparison of two cases with slightly non-symmetric angles across the interface. The left part represents the case with a difference of 1% between the two angles accross the interface and the right part represents the case with a difference of 5%.

Chapter 4

WRINKLING CONTROL BY ELECTRIC FIELD: SMALL DEFORMATION THEORY

4.1 Electromechanical coupling and bilayered systems

Some applications, like phase grating, require the buckling of a bilayered system to be tunable and eventually reversible. One possibility for that is to use a dielectric elastomer as a substrate and then use the electromechanical coupling of this material to influence the buckling at the top surface.

Dielectric elastomers are part of the electroactive polymers. The use of such properties to trigger buckling has already been investigated in theoretical and experimental studies. The theory regarding dielectric elastomers started with the work of Toupin [73]. Dorfmann and Ogden [29] gave a summary of the constitutive equations for this type of material: when subjected to an external electric field, the dielectric elastomer sees a variation of its electric potential distribution. The electric field E and the electric displacement D resulting from this distribution are determined by the Maxwell's equations:

$$\nabla \cdot D = 0, \tag{4.1}$$

$$\nabla \times E = 0. \tag{4.2}$$

These electric fields and electric displacements result in mechanical forces in the body that are described by the Maxwell stress tensor τ_M.

$$\tau_M = D \otimes E - \frac{1}{2}\epsilon_0 E.E \quad . \tag{4.3}$$

This Maxwell stress tensor is added to the equilibrium equation of the elastomer and consequently has an influence on the equilibrium displacement field and the total equilibrium energy.

The first experimental studies of dielectric elastomers in a geometry similar to the systems in which we take interest in this thesis were to consider a polymer film attached to compliant electrodes on its top and bottom surfaces. This study was realized by Pelrine et al [63, 62] and showed that the effective pressure applied in the thickness direction and resulting from an external electric field would have the effect of reducing the thickness of the dielectric elastomer while expanding its area to ensure incompressibility (see Figure 4.1).

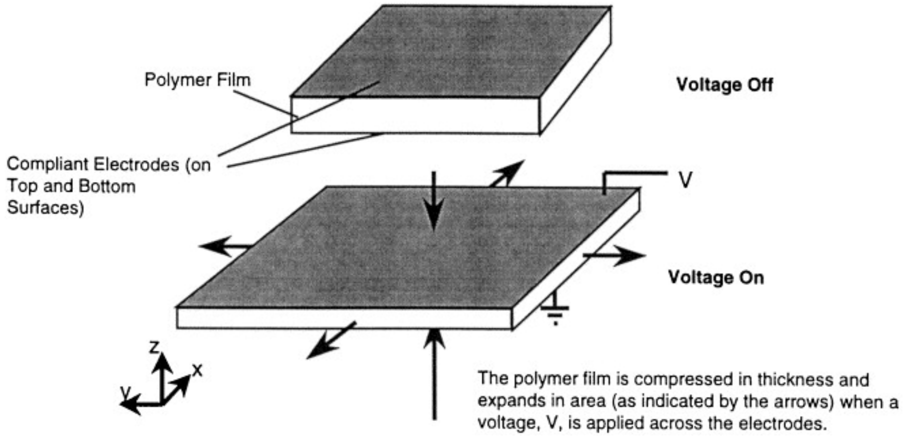
Polymer Film
Compliant Electrodes (on Top and Bottom Surfaces)
Voltage Off
V
Voltage On
z
x
y
The polymer film is compressed in thickness and expands in area (as indicated by the arrows) when a voltage, V, is applied across the electrodes.

Figure 4.1: Principle of operation of dielectric elastomers. Image from [62].

Our objective is different : the modification of buckling pattern. So we assume that the bottom electrode is rigid.

4.2 Energy of the system

The total energy of the system is the sum of the mechanical and electrostatic energies. The mechanical energy is that studied in Section 2.1.

$$\begin{aligned}\mathscr{E}_{mech} = \frac{Eh}{2(1-\nu^2)} \int\int & (-\eta_x + \frac{\partial u}{\partial x} + \frac{1}{2}(\frac{\partial w}{\partial x})^2 - \eta_y + \frac{\partial v}{\partial y} + \frac{1}{2}(\frac{\partial w}{\partial y})^2)^2 \\ & - 2(1-\nu)(-\eta_x + \frac{\partial u}{\partial x} + (\frac{\partial w}{\partial x})^2)(-\eta_y + \frac{\partial v}{\partial y} + (\frac{\partial w}{\partial y})^2) \\ & + 2(1-\nu)(-\eta_{xy} + \frac{1}{2}(\frac{\partial u}{\partial y} + \frac{\partial v}{\partial x}) + \frac{1}{2}\frac{\partial w}{\partial x}\frac{\partial w}{\partial y})^2 \, dx \, dy \\ + \frac{D}{2}\int\int (\Delta w)^2 - 2(1-\nu)(\frac{\partial^2 w}{\partial x^2}\frac{\partial^2 w}{\partial y^2} - (\frac{\partial^2 w}{\partial x \partial y})^2) & + \int\int E_s^* \sqrt{k_x^2 + k_y^2}\, |\hat{w}|^2 \, dk_x \, dk_y\end{aligned} \tag{4.4}$$

The electrostatic energy is

$$\mathscr{E}_e = \frac{1}{S}(\int_\Omega \frac{\alpha}{2}|P_0|^2 dV + \frac{\varepsilon_0}{2}\int_{y(\Omega)} |\nabla\varphi|^2 dv - \int_{y(S)} g(y)(-\varepsilon_0\nabla\varphi + P_0\chi(y(\Omega)))n_{electrode} dS) \tag{4.5}$$

according to Tian [72], with P_0 the polarization of the material, S the unit surface, φ the electric potential, g(y) the value of φ at the film, $n_{electrode}$ the vector normal to the electrode pointing towards the elastomer, Ω the entire system film-substrate α and ε_0 are permittivity constants defined by the relation

$$\varepsilon_r \varepsilon_0 = \varepsilon_0 + \frac{1}{\alpha}. \tag{4.6}$$

To simplify this expression, considering small deformation, we assume y(Ω)=Ω. Also the value of g(y) is a constant external applied voltage V, and it is possible to obtain an expression of the P_0 by using the variational principle to minimize the energy with respect to P_0. This variational principle performed by Tian [72] leads to

$$\frac{\partial \frac{\alpha}{2}|P_0|^2}{\partial P_0} + F^{-t}\nabla\varphi = 0 \tag{4.7}$$

which, considering very small deformations and then $F \approx Id$, is equivalent to

$$P_0 = \frac{-1}{\alpha}\nabla\varphi. \tag{4.8}$$

These simplifications lead to

$$\mathscr{E}_e = \frac{1}{S}\left(\int_\Omega \frac{1}{2}(\varepsilon_0 + \frac{1}{\alpha})|\nabla\varphi|^2 dV + \int_S V(\varepsilon_0 + \frac{1}{\alpha})\nabla\varphi . n_{electrode} dS\right). \tag{4.9}$$

Considering that the surface of the system film-substrate is at z=0 and that the depth of the substrate (associated to its thickness H) goes to -∞, the expression of the electric potential at the surface is initially $\varphi = \varphi_0(x, y, z = 0)$.

Then, the deflection w induces a perturbation φ_1 to this electric potential. The result is

$$\varphi = \varphi_0(x, y, w) + \varphi_1(x, w). \tag{4.10}$$

By doing a Taylor expansion of this expression we obtain

$$\varphi = \varphi_0(x, y, 0) + w\nabla\varphi_0(x, y, 0).e_z + \varphi_1(x, y, 0) + w\nabla\varphi_1(x, y, 0).e_z + o(w). \tag{4.11}$$

The term $w\nabla\varphi_1(x, y, 0).e_z$ is considered negligible as the deflection and the perturbation φ_1 are considered small. At the surface of the film-substrate, a constant voltage is applied. This means that the total electric potential φ is considered constant and equal to $\varphi_0(x, z = 0)$. Therefore, the Taylor expansion results in

$$w\nabla\varphi_0(x, y, 0).e_z + \varphi_1(x, y, 0) = 0, \tag{4.12}$$

which is equivalent to

$$-w\frac{\partial\varphi_0}{\partial z}(x, y, 0) = \varphi_1(x, y, 0). \tag{4.13}$$

This provides one boundary condition on φ_1. The governing equation of φ_1 is obtained from the Maxwell law:

$$\nabla_y \cdot \left[-\varepsilon_0 \nabla_y \varphi + P\chi\left(y(\Omega)\right)\right] = 0. \tag{4.14}$$

The Maxwell law leads to a simplification of the expression of $\mathscr{E}_e$:

$$\nabla \cdot \left[-\varepsilon_0 \nabla \varphi + P\chi\left(y(\Omega)\right)\right] = 0, \tag{4.15}$$

so that

$$\varphi \nabla \cdot \left[-\varepsilon_0 \nabla \varphi + P\chi\left(y(\Omega)\right)\right] = 0, \tag{4.16}$$

which gives

$$\nabla \cdot \left[-\varepsilon_0 \varphi \nabla \varphi + \varphi P\chi\left(y(\Omega)\right)\right] - \nabla \varphi \cdot \left(-\varepsilon_0 \nabla \varphi + P\chi\left(y(\Omega)\right)\right) = 0, \tag{4.17}$$

which gives

$$\int_\Omega \nabla \cdot \left[-\varepsilon_0 \varphi \nabla \varphi + \varphi P\chi\left(y(\Omega)\right)\right] dV - \int_\Omega \nabla \varphi \cdot \left(-\varepsilon_0 \nabla \varphi + P\chi\left(y(\Omega)\right)\right) dV = 0. \tag{4.18}$$

Then the divergence theorem gives

$$\int_S \left(-\varepsilon_0 V \nabla \varphi + V P\chi\left(y(\Omega)\right)\right) . n_{elastomer} dS = \int_\Omega \nabla \varphi \cdot \left(-\varepsilon_0 \nabla \varphi + P\chi\left(y(\Omega)\right)\right) dV. \tag{4.19}$$

But in that case, $n_{elastomer} = -n_{electrode}$ so we can inject the surface integral in the expression of $\mathscr{E}_e$ and also replace the polarization vector P by $\frac{-1}{\alpha}\nabla\varphi$. Finally

$$\mathscr{E}_e = -\frac{1}{S}\frac{1}{2}\int_\Omega (\varepsilon_0 + \frac{1}{\alpha})|\nabla \varphi|^2 dV. \tag{4.20}$$

Substituting the expression (4.10) into (4.20) we obtain

$$\mathscr{E}_e = -\frac{1}{L_x L_y}\frac{1}{2}\int_0^{L_x}\int_0^{L_y}\int_{-H}^0 (\varepsilon_0 + \frac{1}{\alpha})(|\nabla \varphi_0|^2 + |\nabla \varphi_1|^2 + 2\nabla \varphi_0 \cdot \nabla \varphi_1)\, dx\, dy\, dz. \tag{4.21}$$

The next step is to study the possible expressions of φ_0 and φ_1. We know that φ_0 is the electric potential in the case of the absence of deflection. φ_0 is then directly associated to the external voltage V and the electric field E_0 by the following expression:

$$E_0 = -\nabla \varphi_0 = -V/H. \tag{4.22}$$

From this, we can deduce

$$\nabla^2 \varphi_0 = 0. \tag{4.23}$$

Subjecting (4.8) into (4.15) we obtain that $\nabla^2 \varphi = 0$, and considering 4.23, we obtain

$$\nabla^2 \varphi_1 = 0. \tag{4.24}$$

This is a Laplace equation that can be solved by separation of variables:

$$\varphi_1 = f(x, y) g(z) \tag{4.25}$$

giving

$$\nabla^2 f + \lambda^2 f = 0 \tag{4.26}$$

and

$$g''(z) - \lambda^2 g(z) = 0 \tag{4.27}$$

with λ >0 which leads to

$$g(z) = C_1 e^{\lambda z} + C_2 e^{-\lambda z}. \tag{4.28}$$

But we recall that z goes to $-\infty$ as we consider the thickness H of the dielectric to be very large, which means that C_2 must be 0.

Now, regarding the function f in the equation (4.26), it is possible to perform a separation of variables again giving $f(x, y) = a(x)b(y)$ with

$$\frac{d^2 a}{dx^2} = -\delta^2 a, \tag{4.29}$$

$$\frac{d^2 b}{dy^2} = -\gamma^2 b, \tag{4.30}$$

$$\lambda^2 = \delta^2 + \gamma^2. \tag{4.31}$$

Solving equations (4.29) and (4.30) for all possible values of δ and γ give

$$\begin{aligned} a(x) &= \sum_{\delta} (M_\delta cos(\delta x) + N_\delta sin(\delta x)), \\ b(x) &= \sum_{\delta} (M_\gamma cos(\gamma y) + N_\gamma sin(\gamma y)) \end{aligned} \tag{4.32}$$

resulting in

$$\varphi_1 = \sum_{\delta,\gamma} e^{\lambda z}(A_\delta cos(\delta x) + B_\delta sin(\delta x))(A_\gamma cos(\gamma y) + B_\gamma sin(\gamma y)) \tag{4.33}$$

with $\lambda = \sqrt{\delta^2 + \gamma^2}$ Now considering the other boundary condition (4.13) combined with (4.22) we obtain

$$w = \frac{1}{E_0} \sum_{\delta,\gamma} (A_\delta cos(\delta x) + B_\delta sin(\delta x))(A_\gamma cos(\gamma y) + B_\gamma sin(\gamma y)). \tag{4.34}$$

This expression can also be seen as a Fourier cosine and sine decomposition. As w is considered to be periodic, it is then possible to write the following equivalence with the exponential Fourier decomposition:

$$w = \sum_{k_x,k_y=-\infty}^{+\infty} \hat{w}(k_x, k_y)\ e^{i(k_x\ x+k_y\ y)} \tag{4.35}$$

with

$$\begin{aligned} k_x &= \delta, \\ k_y &= \gamma \end{aligned} \tag{4.36}$$

As a consequence we have

$$\varphi_1 = E_0 \sum_{k_x,k_y=-\infty}^{+\infty} e^{\sqrt{k_x^2+k_y^2}z}\hat{w}(k_x, k_y)\ e^{i(k_x\ x+k_y\ y)}. \tag{4.37}$$

From this expression we can compute

$$\nabla\varphi_1 = \begin{pmatrix} E_0 \sum_{k_x,k_y=-\infty}^{+\infty} ik_x\ e^{\sqrt{k_x^2+k_y^2}z}\hat{w}(k_x, k_y)\ e^{i(k_x\ x+k_y\ y)} \\ \\ E_0 \sum_{k_x,k_y=-\infty}^{+\infty} ik_y\ e^{\sqrt{k_x^2+k_y^2}z}\hat{w}(k_x, k_y)\ e^{i(k_x\ x+k_y\ y)} \\ \\ E_0 \sum_{k_x,k_y=-\infty}^{+\infty} \sqrt{k_x^2 + k_y^2}\ e^{\sqrt{k_x^2+k_y^2}z}\hat{w}(k_x, k_y)\ e^{i(k_x\ x+k_y\ y)} \end{pmatrix} \tag{4.38}$$

and then we can compute

$$
\begin{aligned}
&|\nabla\varphi_1|^2 = \\
&\quad E_0^2 \sum_{k_x,k_y} ik_x \; e^{k_z\;z}\;\hat{w}(k_x,k_y)e^{i(k_x\;x+k_y\;y)} \sum_{n_x,n_y} -in_x\; e^{n_z\;z}\;\bar{\hat{w}}(n_x,n_y)e^{-i(n_x\;x+n_y\;y)} \\
&\quad + E_0^2 \sum_{k_x,k_y} ik_y \; e^{k_z\;z}\;\hat{w}(k_x,k_y)e^{i(k_x\;x+k_y\;y)} \sum_{n_x,n_y} -in_y\; e^{n_z\;z}\;\bar{\hat{w}}(n_x,n_y)e^{-i(n_x\;x+n_y\;y)} \\
&\quad + E_0^2 \sum_{k_x,k_y} k_z \; e^{k_z\;z}\;\hat{w}(k_x,k_y)e^{i(k_x\;x+k_y\;y)} \sum_{n_x,n_y} n_z\; e^{n_z\;z}\;\bar{\hat{w}}(n_x,n_y)e^{-i(n_x\;x+n_y\;y)} \\
&= \sum_{k_x,k_y}\sum_{n_x,n_y}(n_xk_x+n_yk_y+k_z\;n_z)e^{(k_z+n_z)z}\hat{w}(k_x,k_y)\bar{\hat{w}}(n_x,n_y)e^{i((k_x-n_x)\;x+(k_y-n_y)\;y)},
\end{aligned}
\tag{4.39}
$$

with

$$n_z = \sqrt{n_x^2+n_y^2}; \qquad k_z = \sqrt{k_x^2+k_y^2},$$

and

$$\nabla\varphi_1.\nabla\varphi_0 = -E_0^2 \sum_{k_x,k_y=-\infty}^{+\infty} \sqrt{k_x^2+k_y^2}\; e^{\sqrt{k_x^2+k_y^2}z}\hat{w}(k_x,k_y)\; e^{i(k_x\;x+k_y\;y)}. \tag{4.40}$$

We can now substitute (4.39) and (4.40) into (4.21). By recalling that the thickness H of the substrate is considered equivalent to ∞ then:

$$
\begin{aligned}
&\int_{-H}^{0} |\nabla\varphi_1|^2\;dz = \\
&E_0^2 \sum_{k_x,k_y}\sum_{n_x,n_y} \frac{n_xk_x+n_yk_y+k_z\;n_z}{(k_z+n_z)}\hat{w}(k_x,k_y)\bar{\hat{w}}(n_x,n_y)e^{i((k_x-n_x)\;x+(k_y-n_y)\;y)}.
\end{aligned}
\tag{4.41}
$$

This simplifies to:

$$
\begin{aligned}
&\int_0^{L_x}\int_0^{L_y}\int_{-H}^{0} |\nabla\varphi_1|^2\;dz\;dx\;dy = \\
&E_0^2 \sum_{k_x,k_y}\sum_{n_x,n_y} \tfrac{n_xk_x+n_yk_y+k_z\;n_z}{(k_z+n_z)}\hat{w}(k_x,k_y)\bar{\hat{w}}(n_x,n_y)\int_0^{L_x} e^{i(k_x-n_x)x}\;dx\int_0^{L_y} e^{i(k_y-n_y)y}\;dy \\
&\qquad = L_x\;L_y\;E_0^2\sum_{k_x,k_y}\frac{2(k_x^2+k_y^2)}{2\sqrt{k_x^2+k_y^2}}\hat{w}(k_x,k_y)\bar{\hat{w}}(k_x,k_y).
\end{aligned}
\tag{4.42}
$$

The next term to consider is $\nabla\varphi_1.\nabla\varphi_0$. It simplifies to

$$\begin{aligned}\int_0^{L_x}\int_0^{L_y}\int_{-H}^{0}\nabla\varphi_1.\nabla\varphi_0\;dz\;dx\;dy = {} & E_0^2\sum_{k_x,k_y}\hat{w}(k_x,k_y)\int_0^{L_x}e^{ikx}\;dx\int_0^{L_y}e^{iky}\;dy\\ = {} & 0.\end{aligned} \tag{4.43}$$

Then, substituting (4.42) and (4.43) into (4.21) , we obtain

$$\mathscr{E}_e = -\frac{1}{2}\varepsilon_0\varepsilon_r E_0^2(H+\sum_{k_x=-\infty}^{\infty}\sum_{k_y=-\infty}^{\infty}\sqrt{k_x^2+k_y^2}\;\hat{w}(k_x,k_y)\bar{\hat{w}}(k_x,k_y)). \tag{4.44}$$

The final step is to note that the sum over all possible frequencies k_x and k_y is actually equivalent to taking integrals over the entirety of the frequencies' domains. So the electrostatic energy is given by

$$\mathscr{E}_e = -\frac{1}{2}\varepsilon_0\varepsilon_r E_0^2(H+\int_{-\infty}^{\infty}\int_{-\infty}^{\infty}\sqrt{k_x^2+k_y^2}\;\hat{w}(k_x,k_y)\bar{\hat{w}}(k_x,k_y))\;dk_x\;dk_y. \tag{4.45}$$

When interpreting the two terms of expression (4.45), we see that the first term is a constant representing the linear electric field over the entire substrate, and the second term is the energy change resulting from the presence of deflection at the top of the dielectric material. More importantly, we notice that this second term is equal to the substrate energy up to constants. The minus sign of this electric energy term means that as the external voltage is increased, the electric energy will counteract the effect of the substrate on the buckling deformation.

Putting everything together, the total energy of the system is

$$\begin{aligned}\mathscr{E}_{total} = {} & \frac{Eh}{2(1-\nu^2)}\int\int(-\eta_x+\frac{\partial u}{\partial x}+\frac{1}{2}(\frac{\partial w}{\partial x})^2-\eta_y+\frac{\partial v}{\partial y}+\frac{1}{2}(\frac{\partial w}{\partial y})^2)^2\\ & -2(1-\nu)(-\eta_x+\frac{\partial u}{\partial x}+(\frac{\partial w}{\partial x})^2)(-\eta_y+\frac{\partial v}{\partial y}+(\frac{\partial w}{\partial y})^2)\\ & +2(1-\nu)(-\eta_{xy}+\frac{1}{2}(\frac{\partial u}{\partial y}+\frac{\partial v}{\partial x})+\frac{1}{2}\frac{\partial w}{\partial x}\frac{\partial w}{\partial y})^2\;dx\;dy\\ & +\frac{D}{2}\int\int(\Delta w)^2-2(1-\nu)(\frac{\partial^2 w}{\partial x^2}\frac{\partial^2 w}{\partial y^2}-(\frac{\partial^2 w}{\partial x\partial y})^2)\;dx\;dy\\ & +\int\int(E_s^*-\frac{1}{2}\varepsilon_0\varepsilon_r E_0^2)\sqrt{k_x^2+k_y^2}\;|\hat{w}|^2\;dk_x\;dk_y-\frac{1}{2}\varepsilon_0\varepsilon_r E_0^2 H.\end{aligned} \tag{4.46}$$

4.3 Case of unidirectional wrinkles

We can adopt the results of Audoly and Boudaoud [4] recalled in Chapter 2 to show that

physical parameter	***symbol***	***numerical value***
elasticity modulus of the film	E	1 GPa
Poisson coefficient of the film	ν	0.3
elasticity modulus of the substrate	E_s	1 MPa
Poisson coefficient of the substrate	ν_s	0.4
thickness of the film	h	30 μm
external buckling strain	$\eta_x = \eta_y$	0.01
relative permittivity	ε_r	7

Table 4.1: Table of the numerical values of physical parameters.

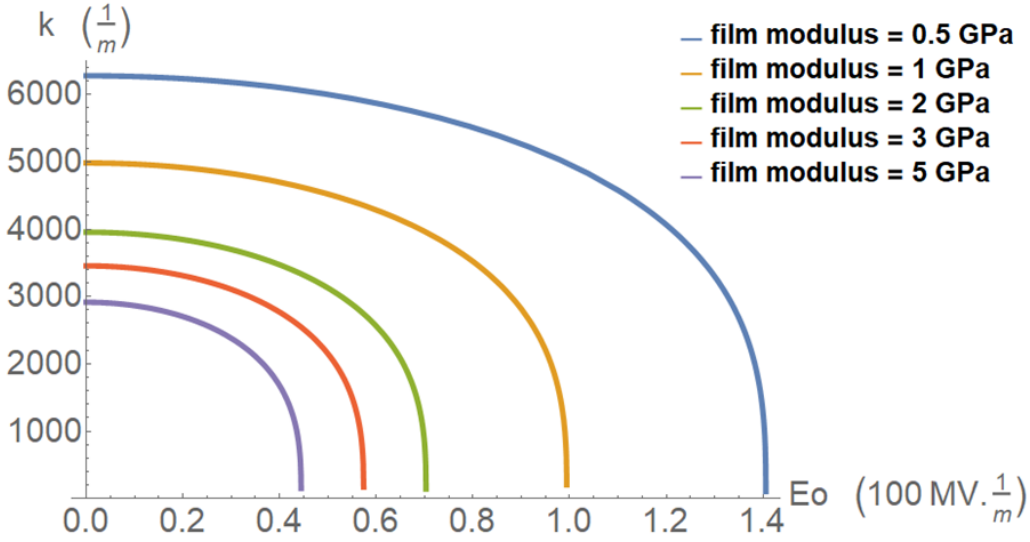

Figure 4.2: Wavenumber of wrinkles vs external electric field for different values of stiffness of the film.

$$\frac{d\mathscr{E}_{total}}{dk} = 0 \;\Rightarrow\; k = \left(\frac{E_s^* - \frac{1}{2}\varepsilon_0\varepsilon_r E_0^2}{D}\right)^{1/3}, \tag{4.47}$$

$$\frac{d\mathscr{E}_{total}}{dA} = 0 \;\Rightarrow\; A = \sqrt{(\eta_x + \nu\eta_y)\frac{4}{k^2} - h^2}. \tag{4.48}$$

Those two expressions show that as the external voltage increases, the wavenumber k will decrease and the amplitude A will increase. Taking the numerical values of Table 4.1, the influence of the voltage is illustrated in Figures 4.2 and 4.3.

More concretely, the consequence of the electric field will be that the number of wrinkles over a given surface will decrease, while the amplitude of those wrinkles will increase.

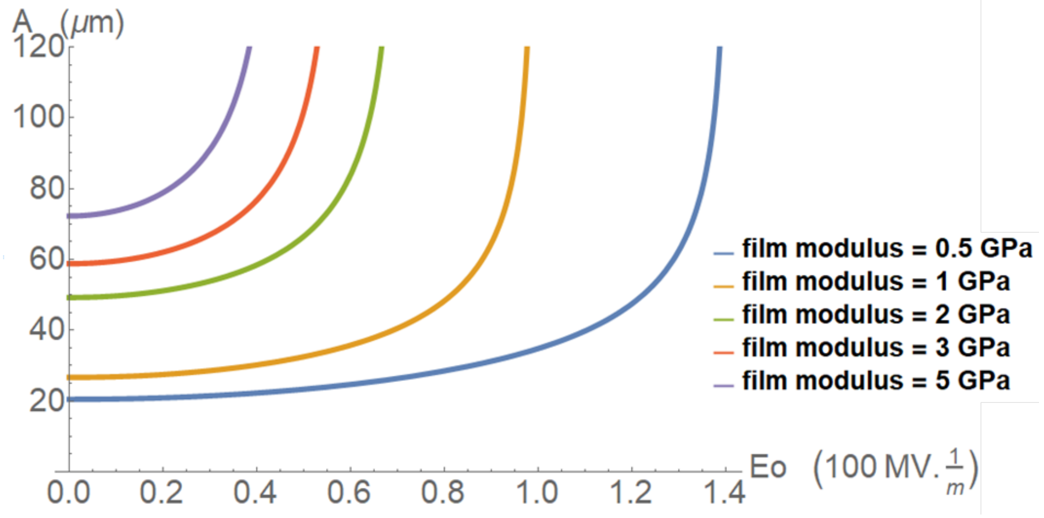

Figure 4.3: Amplitude of wrinkles vs external electric field for different values of stiffness of the film.

4.4 Case of bidirectional wrinkles

The effects described in the previous section can also be applied to a more complex buckling pattern. If the load triggering the buckling has more than one direction, the resulting surface deflection can depend on both the planar axes x and y. One simple example of such case is what is called the checkerboard deflection pattern:

$$w = A(cos(kx) + cos(ky)) \tag{4.49}$$

Considering only the purely mechanical part of the energy of deformation before applying an electric field, Audoly and Boudaoud showed that the different energies for the film and the substrate are:

$$\mathcal{E}_{substrate} = E_s^* k A^2 \tag{4.50}$$

$$\mathcal{E}_{bending} = \frac{1}{2} D k^4 A^2 \tag{4.51}$$

$$\mathcal{E}_{stretching} = \frac{Eh}{32(1-\nu)}(32\eta^2 - 16\eta A^2 k^2 + (3-\nu)A^4 k^4) \tag{4.52}$$

We can incorporate the effect of the electric field by modifying the substrate energy. We obtain

$$\frac{d\mathcal{E}_{total}}{dk} = 0 \Rightarrow k = (\frac{E_s^* - \frac{1}{2}\varepsilon_0 \varepsilon_r E_0^2}{D})^{1/3}, \tag{4.53}$$

$$\frac{d\mathscr{E}_{total}}{dA} = 0 \;\Rightarrow\; A = \sqrt{\frac{1}{3-\nu}\frac{8}{k^2}\eta - \frac{2h^2}{1+\nu}}. \tag{4.54}$$

The consequences illustrated in Figure 4.4 are again a higher amplitude of the deflection and a lower wavenumber.

It is tempting to think that the electric field can be increased to the point where there are no more wrinkles thanks to a sufficiently small wavenumber. But the situation is not that simple. For the models to hold, we must assume small deflection. It means that we must stay in a range of small deformation regarding the amplitude.

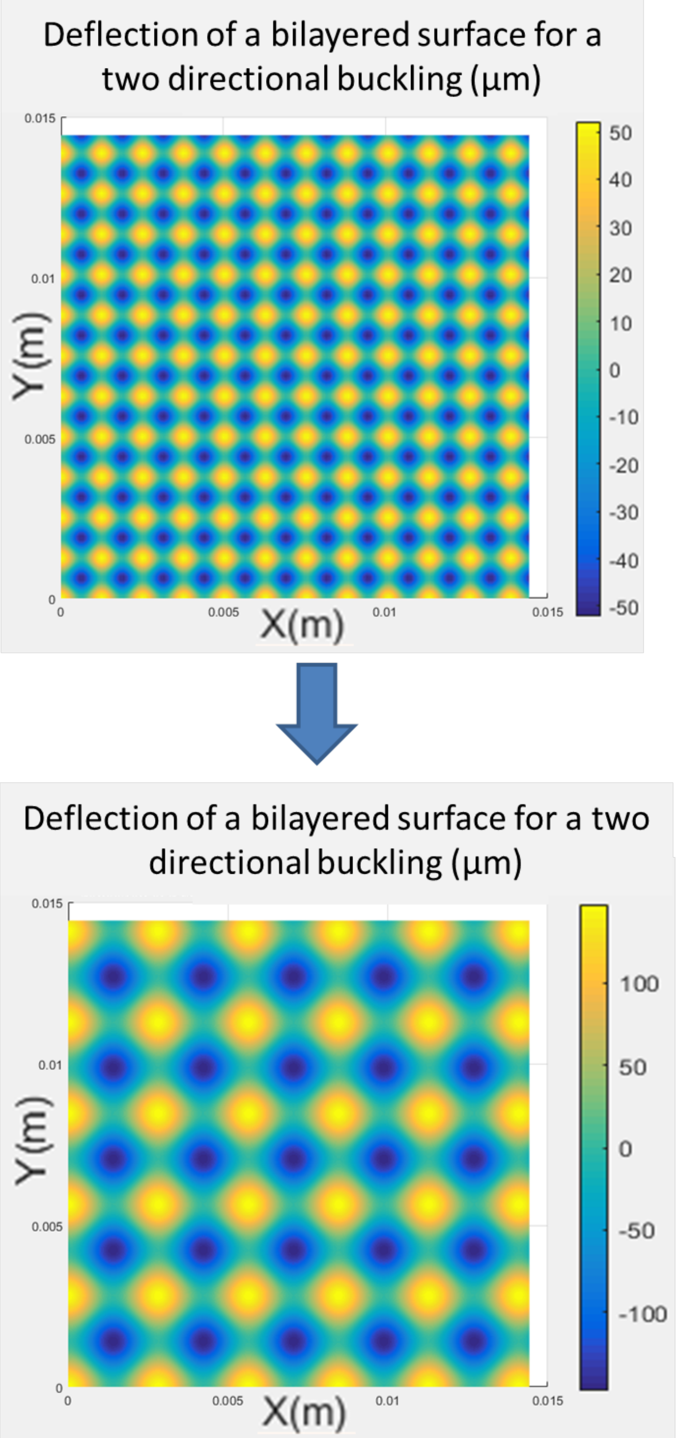
Deflection of a bilayered surface for a two directional buckling (µm)

Deflection of a bilayered surface for a two directional buckling (µm)

Figure 4.4: Illustration of the influence of the electric field on wrinkles: from initial state on the upper half part, the application of external voltage will result in higher amplitude and smaller number of wrinkles in the final state on the lower half part.

Chapter 5

WRINKLING CONTROL BY ELECTRIC FIELD: FINITE DEFORMATION SIMULATIONS

In this chapter we continue the investigation of potential control of wrinkles using an electric field in a finite deformation setting using the commercial finite element package ABAQUS [1]. We limit the study to a two-dimensional setting of plane strain.

5.1 Strain mismatch-induced wrinkles

We begin with the purely mechanical problem where a strain mismatch between the film and the substrate induces wrinkles.

5.1.1 Computational setting

We use the material parameters shown in Table 5.2. These parameters are chosen consistent with the choice of PDMS as the substrate and metal as the film.

It is important to choose the computation domain and element size appropriately to capture the desired phenomena. Following Cao and Hutchinson [18] we choose the element size to be approximately $1/100$ of the expected wrinkle size. A typical mesh is shown in Figure 5.1.

Finally, we use the following boundary conditions, also shown in Figure 5.1. The top is traction-free to be consistent with cases described in Chapter 2 while the bottom is placed on rollers to mimic stress-free conditions at infinity. The displacements are assumed to be periodic on the lateral surface, mimicking an infinite body. The method chosen for those periodic displacements was inspired by Wu et al. [82]. Note however that the lateral size has to be large for the wrinkle to be independent of the domain size. The size chosen is indicated in Table 5.2

Regarding the units of our system, we just have to keep in mind that ABAQUS is unitless. This allows us to pick the most convenient set of units adapted to the scale of our system. Our choice is indicated in Table 5.1.

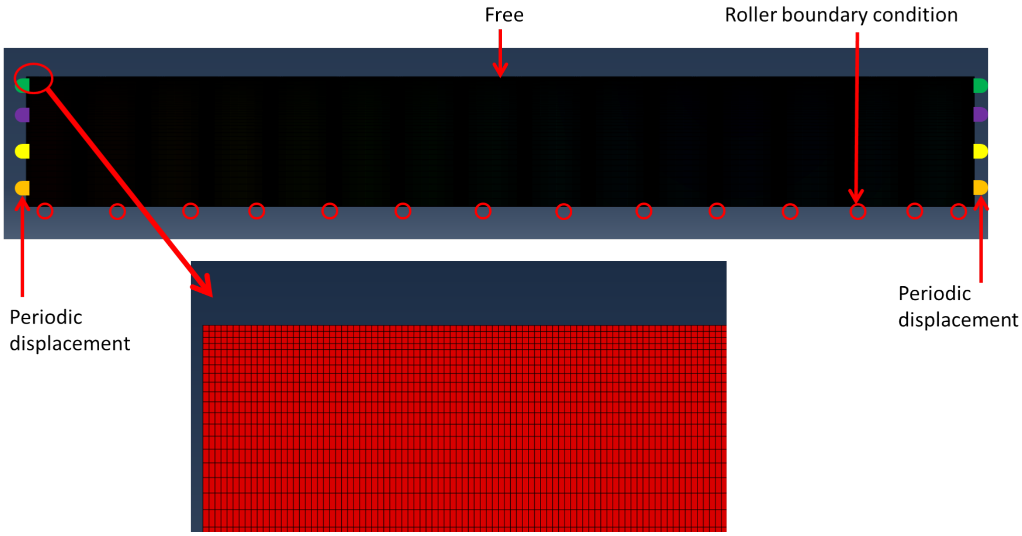
Free
Roller boundary condition
Periodic displacement
Periodic displacement

Figure 5.1: ABAQUS mesh illustration.

physical parameter	***unit system used in our case***
Length	0.1 mm
Force	N
Stress	100 MPa
Mass	10^4kg
Energy	10^{-4}J
Time	s

Table 5.1: Possible sets of units in ABAQUS.

physical parameter	***film***	***substrate***
Width	2.2 cm	2.2 cm
Thickness	$30\mu m$	3 mm
Young's modulus	10 GPa	10 MPa
Poisson coefficient	0.3	0.4
Relative permittivity	0	6.7
coefficient of thermal expansion	$0.0001K^{-1}$	$0.000001K^{-1}$

Table 5.2: Physical parameters of the film and the substrate in ABAQUS.

5.1.2 Buckling method

General strategy

The buckling strategy follows the approach of Wong and Pellegrino [80, 79] in 2002, followed by Cao and Hutchinson [18], Zang et al [83], Song et al [65], Zheng [84], and Cai et al [17]. It consists of two steps: the first one is to find the critical buckling load and potential instability modes by solving an eigenvalue problem; the second one is to introduce a small perturbation associated with the identified instability modes as an initial imperfection to find the post-buckled shape.

More precisely, the first step falls into two parts: initially, it is necessary to generate an equilibrium state represented by the stiffness matrix K_0 by applying an initial load P on the entire bilayered system. Then, based on this equilibrium state, an incremental load Q is applied in addition to the initial load to generate an associated stiffness matrix K_Δ. Then, we find the potential instabilities by solving the generalized eigenvalue problem

$$(K_0 + \lambda_i K_\Delta) v_i = 0. \tag{5.1}$$

Here the indice i refers to the i^{th} buckling mode. The resulting instability modes v_i represent the possible shapes resulting from buckling.

Once obtained, the most representative instability modes v_i are then linearly combined to obtain a state of initial imperfection δz. This initial imperfection helps generate the buckling deformation in a continuous way as ABAQUS has difficulties dealing with a discontinuous response. The most representative modes are associated with the smallest eigenvalues λ_i, and the initial imperfection is obtained by

$$\delta z = \sum_i \phi_i v_i. \tag{5.2}$$

Here the coefficients ϕ_i are taken with values around 1% of the thickness of the film in order to minimize the influence of the imperfection on the final amplitude of the wrinkles and in order to have the formation of wrinkles as smooth and continuous as possible.

Strategy adapted to our particular case

We introduce a strain mismatch between the substrate and the film by subjecting it to a temperature, since the thermal expansion coefficients are taken to be different

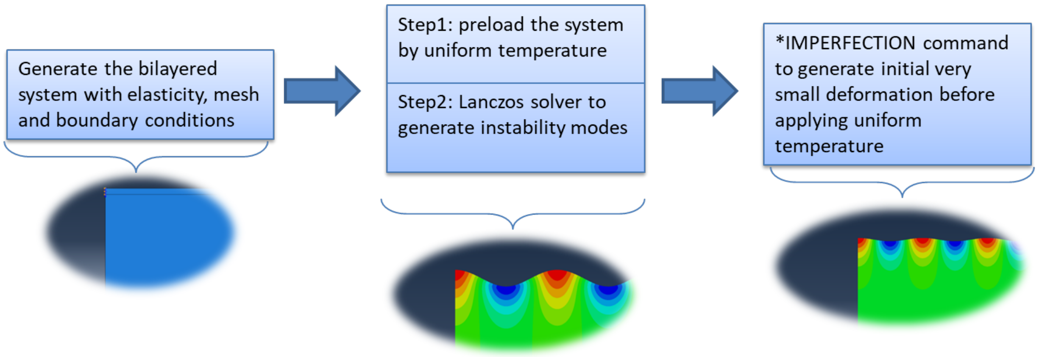
Generate the bilayered system with elasticity, mesh and boundary conditions
Step1: preload the system by uniform temperature
Step2: Lanczos solver to generate instability modes
*IMPERFECTION command to generate initial very small deformation before applying uniform temperature

Figure 5.2: Steps used to generate wrinkles in ABAQUS.

(Table 5.2).

According to the linear theory, the buckling strain η satisfies

$$\eta(1+\nu)\frac{4}{(\frac{E_s^*}{D})^{2/3}} - h^2 > 0 \;\Rightarrow\; \eta > \frac{h^2(\frac{E_s^*}{D})^{2/3}}{4(1+\nu)}. \tag{5.3}$$

If we use the numerical values of h, E_s, E, ν_s, ν given in Table 5.2, Equation 5.3 becomes $\eta > 0.0043$. As the coefficient of thermal expansion of the film is 0.0001 K^{-1}, then taking an initial temperature of 20 K will give $\eta = 0.002$ which is under the buckling threshold. Afterwards, the step *BUCKLE with the Lanczos method is selected to generate an eigenvalue problem. It is noted that the resulting eigenvalues are not very well-spaced from each other.

It means that there is not one particular buckling mode that is preferred when the system buckles. It would then require that all the first buckling modes within a certain range would be used in the definition of imperfection (5.2) with the same coefficient ϕ in order to reflect properly the sensitivity of the bilayered system to several neighboring modes.

But something allows us to deal with the imperfection differently: we have done a post-buckling analysis performed with initial imperfection composed of 6 different modes. We have then made a Fourier analysis of the deflection at the surface of our model. We did this analysis for different cases associated with different elasticity moduli for the film and the substrate. The Fourier analysis of the deflection of the three cases is shown in Figure 5.3.

We see that in each case, the post-buckling behavior, even if showing several wavelengths, has one wavelength associated with an amplitude far more important than all other wavelengths. This results in the deflection always taking an almost sinusoidal form. Most importantly, in each case, the dominant wavelength of those wrinkles is the one closest to the theoretical value and is also the one associated with the first buckling mode obtained from the buckling step in ABAQUS. We can conclude that regardless of what the stiffness of the materials is and what the number of modes we consider in our initial geometrical imperfection is, the post-buckling behavior converges towards wrinkles with one dominant frequency. As a consequence, we can simply reduce the expression of the initial small deformation (5.2) to a single term corresponding to this dominant mode instead of considering 6 different ones.

Using the *IMPERFECTION command, this deformation is injected into the initial shape of the bilayered system associated with coefficient ϕ=0.002, which corresponds to 0.67 % of the thickness of the film. The wrinkle deformations are then progressively generated by using thermal expansions with the same coefficients as in the previous step. All those steps are illustrated in Figure 5.2.

5.1.3 Results

The influence of the temperature T generating the strain mismatch and the wrinkles is illustrated in Figure 5.4. This figure shows the case with $E_s = 7\,MPa$, and the rest of the parameters are indicated in Table 5.2. The parameter $U2$ corresponds to the out-of-plane displacement. We can see the formation of periodic sinusoidal wrinkles in Figure 5.4.

Figure 5.5 shows the von Mises stress distribution for five different stiffness ratios for the parameters in Table 5.2. We see that the stress in the substrate is negligible compared to the stress in the film. This is due to the strain mismatch and also to the elasticity ratio between the two materials.

We repeat these simulations for various parameters shown in Table 5.3. We extract the deformation and use MATLAB to find the wrinkle frequency. The results are shown in Figure 5.6 and Table 5.3 and are compared to those of the linear theory. Here the stiffness ratio corresponds to the following expression:

$$stiffness\ ratio \ = \ \frac{E_f}{12(1-\nu_f^2)}\frac{(1+\nu_s)(3-4\nu_s)}{(1-\nu_s)E_s}. \tag{5.4}$$

Table 5.3 shows that for each case study, the relative difference between the theoretical and numerical values remains under 3.5%.

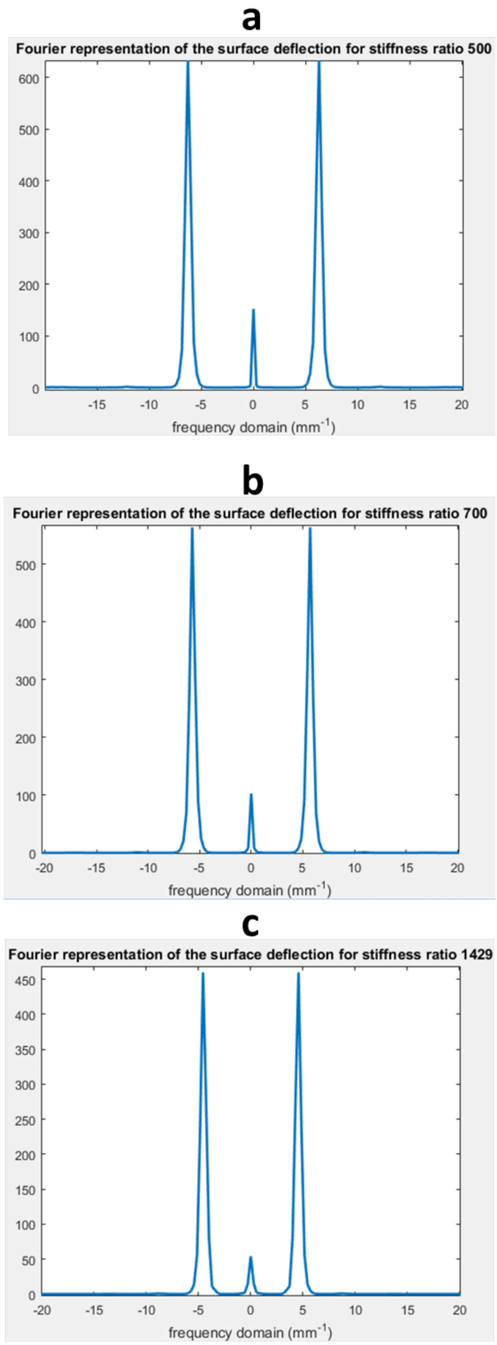

Figure 5.3: Fourier representation of the wrinkles in 3 different cases: a) the Young's modulus of the film is 5 GPa and the Young's modulus of the substrate is 10 MPa ; b)the Young's modulus of the film is 7 GPa and the Young's modulus of the substrate is 10 MPa ; c) the Young's modulus of the film is 10 GPa and the Young's modulus of the substrate is 7 MPa.

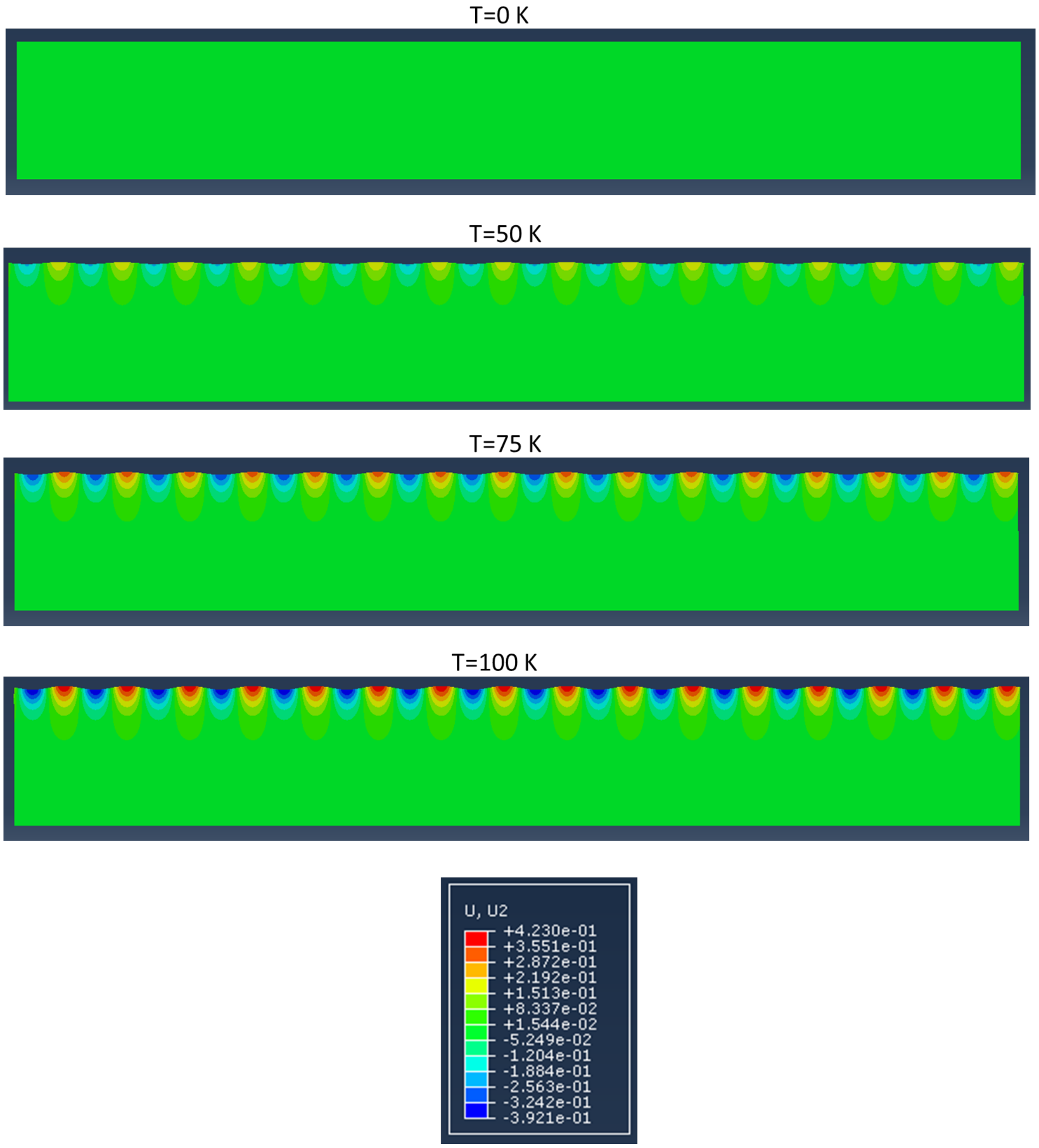

Figure 5.4: ABAQUS wrinkle behavior influenced by increasing temperature T.

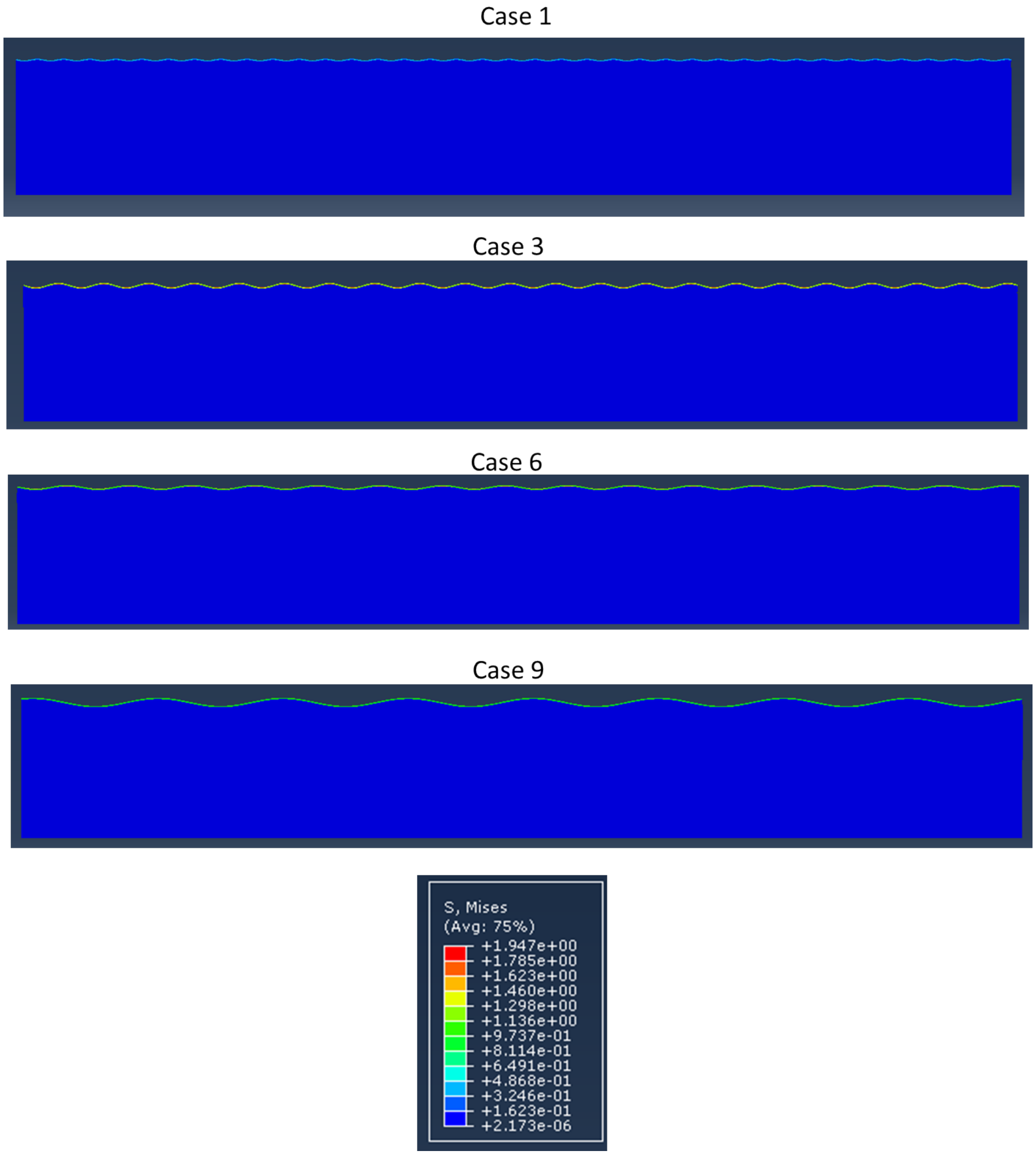
Case 1
Case 3
Case 6
Case 9
S, Mises
(Avg: 75%)
+1.947e+00
+1.785e+00
+1.623e+00
+1.460e+00
+1.298e+00
+1.136e+00
+9.737e-01
+8.114e-01
+6.491e-01
+4.868e-01
+3.246e-01
+1.623e-01
+2.173e-06

Figure 5.5: ABAQUS wrinkles for four different stiffness ratios. The physical parameters are all indicated in Table 5.3.

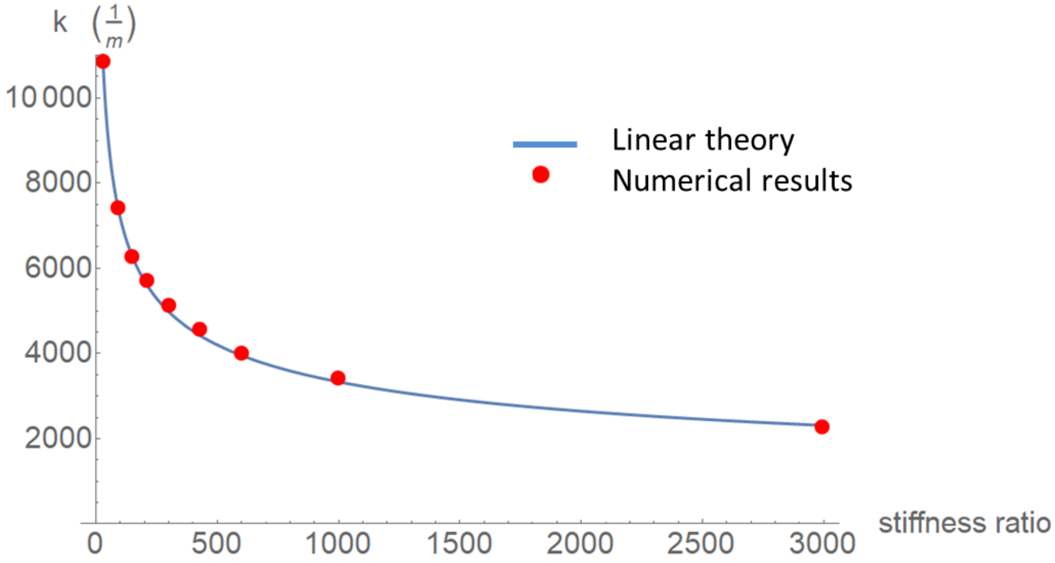

Figure 5.6: Comparison of numerical and theoretical results in the case of a wavelength vs stiffness ratio plot.

	Case 1	***Case 2***	***Case 3***	***Case 4***	***Case 5***	***Case 6***	***Case 7***	***Case 8***	***Case 9***
E_f (GPa)	1	3	5	7	10	10	10	10	10
E_s (MPa)	10	10	10	10	10	7	5	3	1
strain	0.03	0.03	0.024	0.025	0.01	0.01	0.009	0.009	0.009
numerical wavelength (m^{-1})	10850	7425	6283	5712	5140	4570	3998	3427	2285
theoretical wavelength (m^{-1})	10738	7445	6280	5613	4984	4425	3955.86	3337	2313
relative difference (%)	1.04	0.26	0.06	1.76	3.13	3.27	1.06	2.71	1.22
theoretical amplitude (μm)	21.28	43.75	47.59	56.80	34.54	41.90	45.72	57.48	88.57
numerical amplitude (μm)	20.67	44.4	48.04	56.55	34.55	40.59	45.28	56.1	90.09

Table 5.3: Comparison between numerical values and theoretical values of wrinkles'wavelengths.

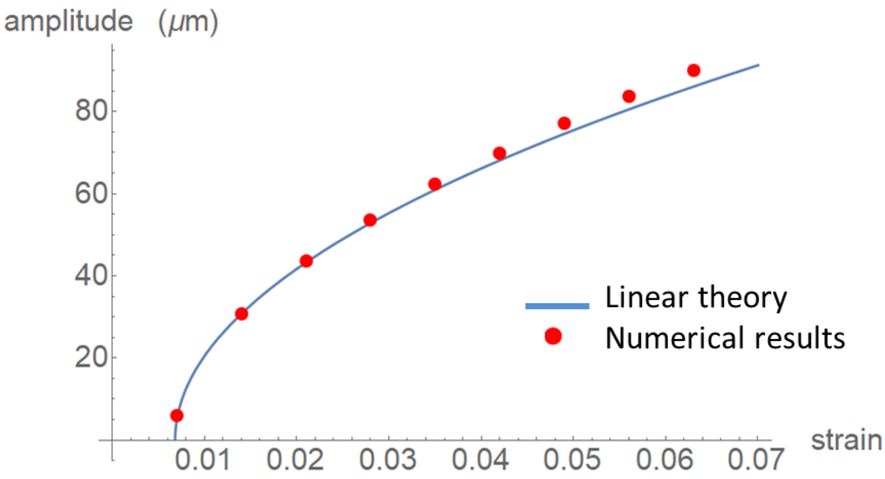

Figure 5.7: Comparison of numerical and theoretical results in the case of a amplitude vs strain plot.

	Case A	***Case B***	***Case C***	***Case D***	***Case E***	***Case F***	***Case G***	***Case H***	***Case I***
strain	0.007	0.014	0.021	0.028	0.035	0.042	0.049	0.056	0.063
numerical amplitude (μm)	5.932	30.66	43.51	53.56	62.23	69.94	77.07	83.75	90.05
theoretical amplitude (μm)	4.805	30.76	43.24	52.84	60.95	68.11	74.58	80.53	86.07
relative difference (%)	23.4	3.25	0.624	1.36	2.1	2.69	3.34	4.0	4.62

Table 5.4: Comparison between numerical values and theoretical values of wrinkle amplitudes.

A second comparison concerns the effect of differential strain on the post-buckling amplitude. For a fixed stiffness ratio, a similar study for different values of strain was conducted corresponding to the moduli in case 3.

The results are shown in Figure 5.7 and Table 5.4. Again the results agree with those of the linear theory.

We conclude that the numerical model built in ABAQUS is remarkably consistent with the linear theory described in Chapter 2 in the chosen range of stiffness ratio and buckling strain.

One particular case we can also present is the case with materials' properties close to experimental studies. The values used in Table 5.5 show the case of a very thin film made of gold attached to a PDMS substrate. For both materials, the Young

physical parameter	*film*	*substrate*
Thickness	30 nm	3 μm
Young's modulus	82 GPa	20 MPa
Poisson coefficient	0.33	0.48

Table 5.5: Datas used to model gold film attached to PDMS substrate.

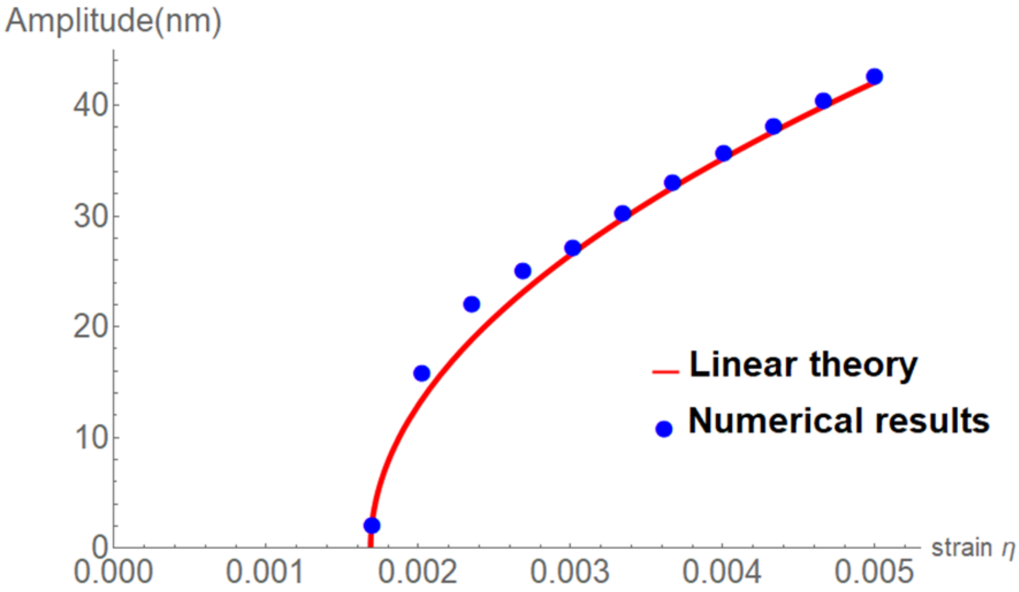

Figure 5.8: Amplitude of wrinkles vs homogeneous strain in case of gold film attached to PDMS substrate.

modulus and the Poisson ratio are taken from the study made by Bowden et al. [10]

The results for varying strain biaxial strain ($\eta_x = \eta_y$) is shown in Figure 5.8. The results are not matching accurately for strain smaller than 0.0028 but correspond to theoretical results beyond that value. This can be explained by the fact that the convergence of ABAQUS might lack accuracy when the strain is close to the buckling threshold. In addition to the amplitude results, the wavelength of the wrinkles was $3.142 \times 10^6 m^{-1}$ and the expected theoretical value was $3.156 \times 10^6 m^{-1}$ making the relative error being 0.44 %.

5.2 Dielectric material modeling

A subroutine can be used to generate electromechanical coupling in an ABAQUS model: the element subroutine UEL allows us to introduce new behaviors based on nonstandard degrees of freedom. Instead of defining explicitly only the stress, the user is asked to define all residuals, stiffness matrices, and energies associated with the Galerkin method in finite element modeling. In our case, this subroutine allows us to generate an electric potential gradient between elements, and as a consequence, to generate an electric field distribution within the entire dielectric elastomer.

The formulation of the electromechanical problem in a dielectric undergoing finite deformation is rather tricky [73, 29, 72]. We follow Henann et al. [38], used a standard Galerkin approach to define a new element level system of equations, residuals, and corresponding tangents. Based on the discretization of both the displacement u and the electric potential ϕ using shape functions N^A :

$$u = \sum u^A N^A \tag{5.5}$$

$$\phi = \sum \phi^A N^A \tag{5.6}$$

They[38] implemented the formulation in a user-element subroutine that was used to describe the behavior of bending and twisting actuators as well as a barrel-type energy harvesting device. We adapt the formulation to our problem: we turn the Gent model into a neo-hookean model by setting the Gent coefficient I_0 to be 10^{15}. We compute the Lame parameters and the bulk moduli from the Young's moduli and Poisson's ratios of each material and assign those parameters to each corresponding material.

Before we use this model to study the influence of the electric field on wrinkles, we checked that the electromechanical coupling had the expected effect for the linear deformation of a dielectric substrate. We simply applied the electric field on top of the substrate and calculated the resulting Cauchy stress along the out-of-plane direction σ_z. This was compared with the expected Maxwell stress resulting from the applied electric field σ_{el}:

$$\sigma_{el} = \frac{1}{2}\varepsilon_0\varepsilon_r E^2 \quad \textit{and} \quad \sigma_z = \mu\frac{1}{J^{5/3}}(F_{zz} - \frac{I_1}{3}) + \kappa(J-1). \tag{5.7}$$

In this case $J = det(F)$, $I_1 = F_{xx}^2 + F_{yy}^2 + F_{zz}^2$, $\mu = \frac{E_s}{2(1+\nu_s)}$, $\kappa = \lambda + \frac{2}{3}\mu$, $\lambda = \frac{\nu_s E_s}{(1+\nu_s)(1-2\nu_s)}$ and

$$F = \begin{pmatrix} 1 & 0 & 0 \\ 0 & 1 & 0 \\ 0 & 0 & \sqrt{1 + 2\frac{H_{deformed} - H_{initial}}{H_{initial}}} \end{pmatrix}. \tag{5.8}$$

with $H_{initial}$ and $H_{deformed}$ being the depth of the substrate before and after the electric field is applied.

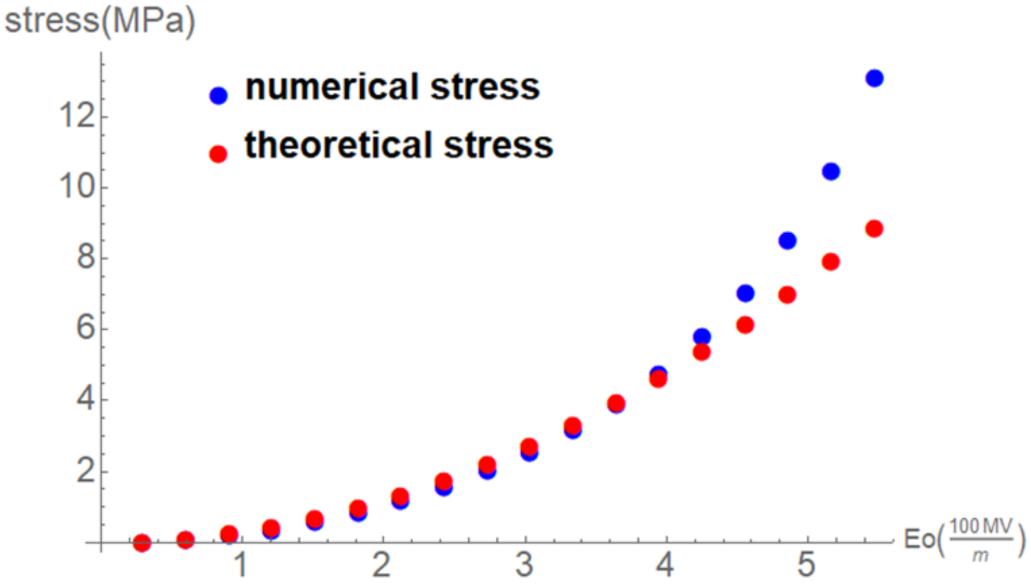

Figure 5.9: Comparison of the numerical and theoretical stress within the substrate for different electric fields. The substrate Young modulus is 30 MPa.

We compare the two stresses for different values of applied voltage and Young modulus of the substrate. At first we study the case of the Young modulus being 30 MPa illustrated in Figure 5.9.

This figure shows that this comparison is reliable only for electric fields up to 400 MV/m. A similar study can be done for different values of the Young modulus of the substrate as illustrated in Figure 5.10. We can see that there is still a difference between the theoretical stress and the numerical stress, although this difference is less important for lower values of the Young modulus. As a consequence we will study the influence of the electric field only for values of E_s less than or equal to 30 MPa.

One point with this method is that it uses the temperature variable as the degree of freedom to represent the electric potential: the imposed electric potential at the top and bottom of the bilayered system is actually an imposed temperature. As a consequence, we cannot use thermal expansion to create the differential strain within the bilayered system to generate the initial buckling before applying the electric field.

We overcome this by generating the mismatch directly within the subroutine by implementing a change of reference: if we suppose that we want to impose a strain with value 0.03 to trigger the buckling, then the gradient deformation tensor would be modified as:

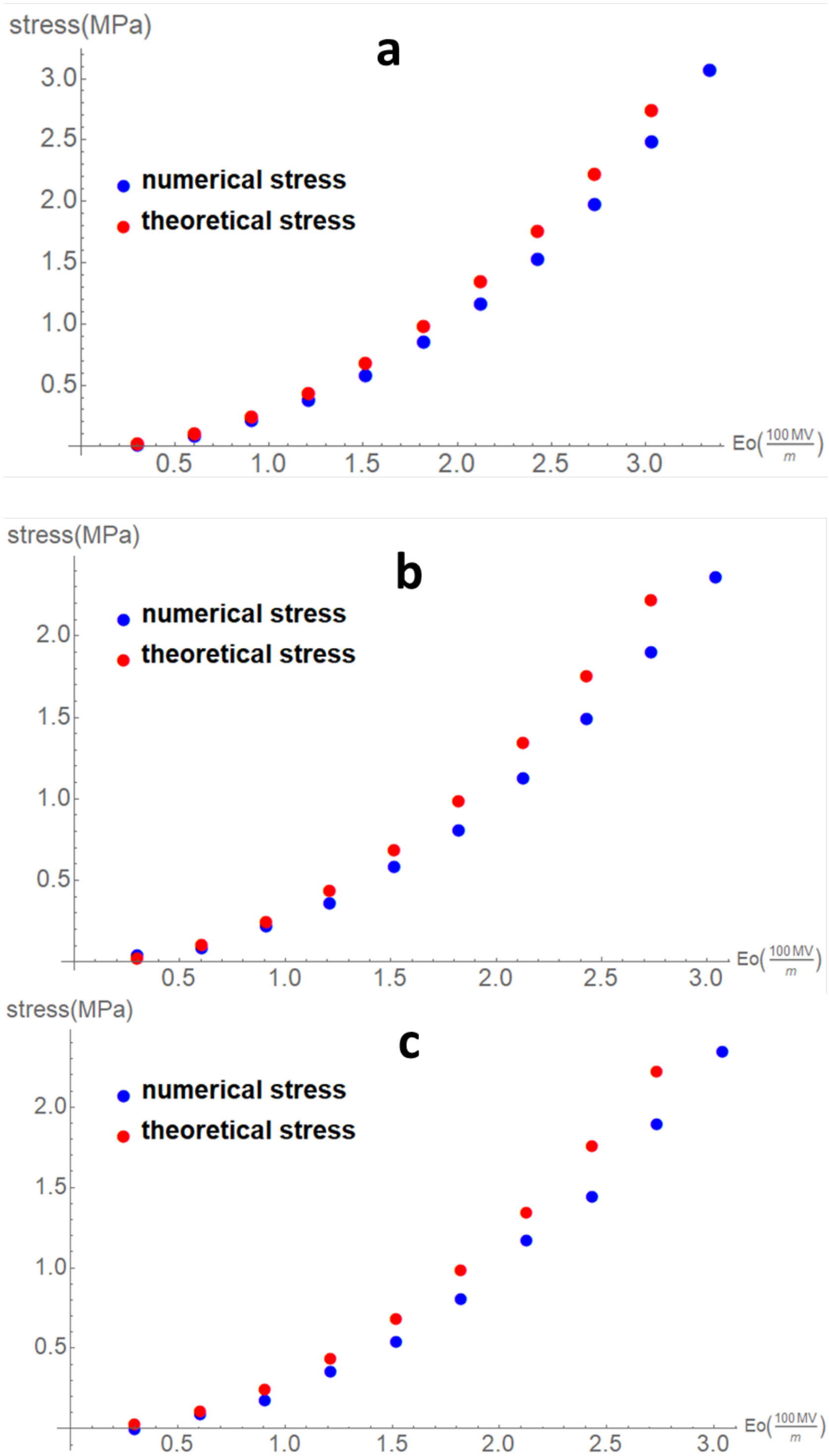

Figure 5.10: Comparison of the numerical and theoretical stress within the substrate for different Young moduli. Case a : E_s = 100 MPa; case b: E_s = 40 MPa; case c: E_s = 200 MPa.

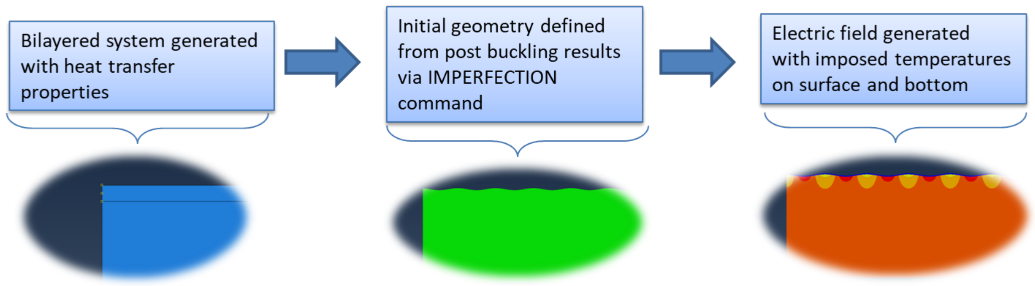
Bilayered system generated with heat transfer properties
Initial geometry defined from post buckling results via IMPERFECTION command
Electric field generated with imposed temperatures on surface and bottom

Figure 5.11: Steps used to generate electric field in ABAQUS.

$$F = F.U_{buckling} \tag{5.9}$$

with

$$U_{buckling} = \begin{pmatrix} \frac{1}{1.03} & 0 & 0 \\ 0 & 1.03 & 0 \\ 0 & 0 & 1 \end{pmatrix}. \tag{5.10}$$

The process is illustrated in Figure 5.11.

More details about the input file used to generate the bilayered system with wrinkles and apply the external electric field are in Appendix B.

5.3 Results

As different values for external voltage were applied, we observed that the wavelength did not change with the variation of the electric field distribution. There are two possibilities to explain this: the total energy of the system stays in a local minimum associated with the specific wavelength obtained during the linear perturbation process, creating a high energy barrier to prevent the transfer to a different wavelength. The second possibility is that the choice of periodic boundary condition imposed at the edges constrains the wavelength of the wrinkles and prevents any change for that variable.

This observation forces us to reconsider the expression of the amplitude in the linear theory. Restarting from equation

$$\begin{aligned}\mathscr{E}_{total} = \frac{Eh}{2(1-\nu^2)}(\eta_x^2 + \eta_y^2 + 2\nu\eta_x\eta_y - \frac{\eta_x + \nu\eta_y}{2}k^2A^2 + \frac{1}{16}k^4A^4) \\ + \frac{1}{4}Dk^4A^2 + \frac{1}{2}(E_s^* - \frac{1}{2}\epsilon_0\epsilon_r E_0^2)kA^2 - \frac{1}{2}\epsilon_0\epsilon_r E_0^2 H,\end{aligned} \tag{5.11}$$

physical parameter	***film***	***substrate***
Thickness	$30\mu m$	∞
Young's modulus	10 GPa	30 MPa
Poisson coefficient	0.3	0.4
Relative permittivity	0	6.7

Table 5.6: Physical parameters of the film and the substrate for amplitude comparison.

it is possible to express the amplitude minimizing the energy at a constant wavelength by solving

$$\frac{d\mathscr{E}_{total}}{dA} = 0 \tag{5.12}$$

which gives

$$A = \sqrt{(\eta_x + \nu\eta_y)\frac{4}{k^2} - \frac{4D(1-\nu^2)}{Eh} - E_s^*\frac{8(1-\nu^2)}{Ehk^3} + \frac{4(1-\nu^2)}{Ehk^3}\epsilon_0\epsilon_r E_0^2}. \tag{5.13}$$

In this equation, we cannot use the expression of k involving the electric field given in Equation (4.47). But in order to see which parameters influence the coefficient associated with the electric field, it is necessary to develop a simplification using Equation (2.36), defining k independently of the electric field. At the end we obtain

$$A = \sqrt{(\eta_x + \nu\eta_y)\frac{4}{k^2} - \frac{4D(1-\nu^2)}{Eh} - E_s^*\frac{8(1-\nu^2)}{Ehk^3} + \frac{h^2}{3E_s^*}\epsilon_0\epsilon_r E_0^2} = \sqrt{c_1 + c_2 E_0^2} \tag{5.14}$$

To illustrate the difference between the amplitude depending on a varying k and the amplitude only depending on the electric field with a constant k, Figure 5.12 is plotted using the parameters of Table 5.6 and taking the differential strain in the main directions η_x and η_y to be 0.03. We find that those two amplitudes are similar for small electric fields.

The result for the parameters given in Table 5.6 is illustrated in Figure 5.13, and we can observe both the linear deformation of the large depth of the substrate and the deformation of the wrinkles on top of the bilayered system.

5.3.1 Results with varying elasticity of the substrate

We make different models with varying value for E_{sub}. The final deformation for each case is illustrated in Figure 5.14. In this figure, the parameter $NT11$ represents the electric potential distribution.

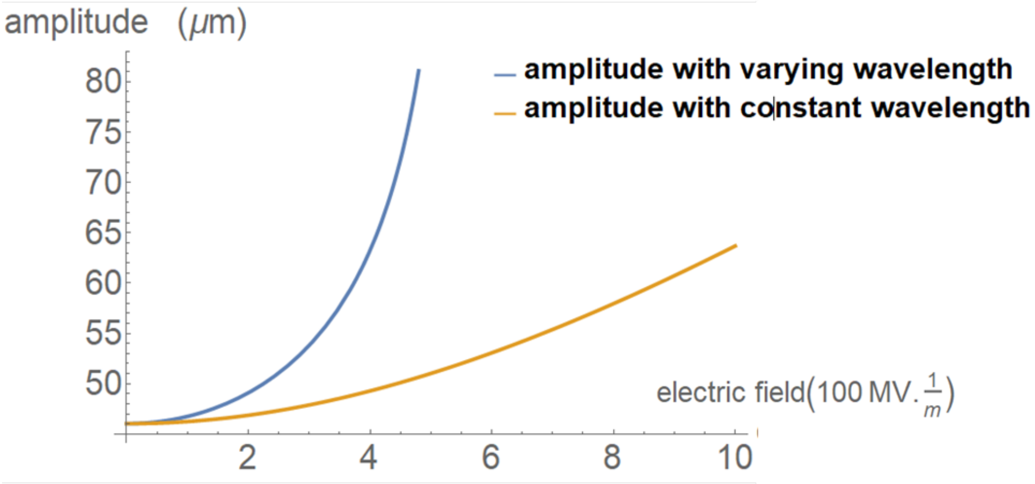

Figure 5.12: Comparison of amplitude of wrinkles for constant and varying wavelengths as a function of applied electric field.

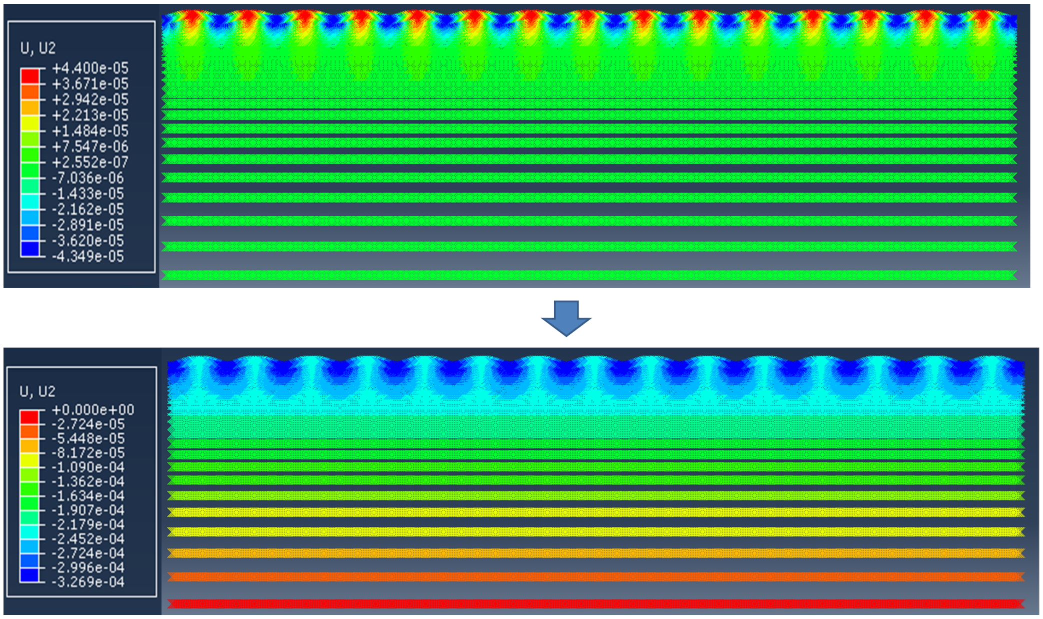
U, U2
+4.400e-05
+3.671e-05
+2.942e-05
+2.213e-05
+1.484e-05
+7.547e-06
+2.552e-07
-7.036e-06
-1.433e-05
-2.162e-05
-2.891e-05
-3.620e-05
-4.349e-05
U, U2
+0.000e+00
-2.724e-05
-5.448e-05
-8.172e-05
-1.090e-04
-1.362e-04
-1.634e-04
-1.907e-04
-2.179e-04
-2.452e-04
-2.724e-04
-2.996e-04
-3.269e-04

Figure 5.13: Evolution of out-of-plane displacement between initial state with no electric field and state with electric field equal to 362.4 MV/m.

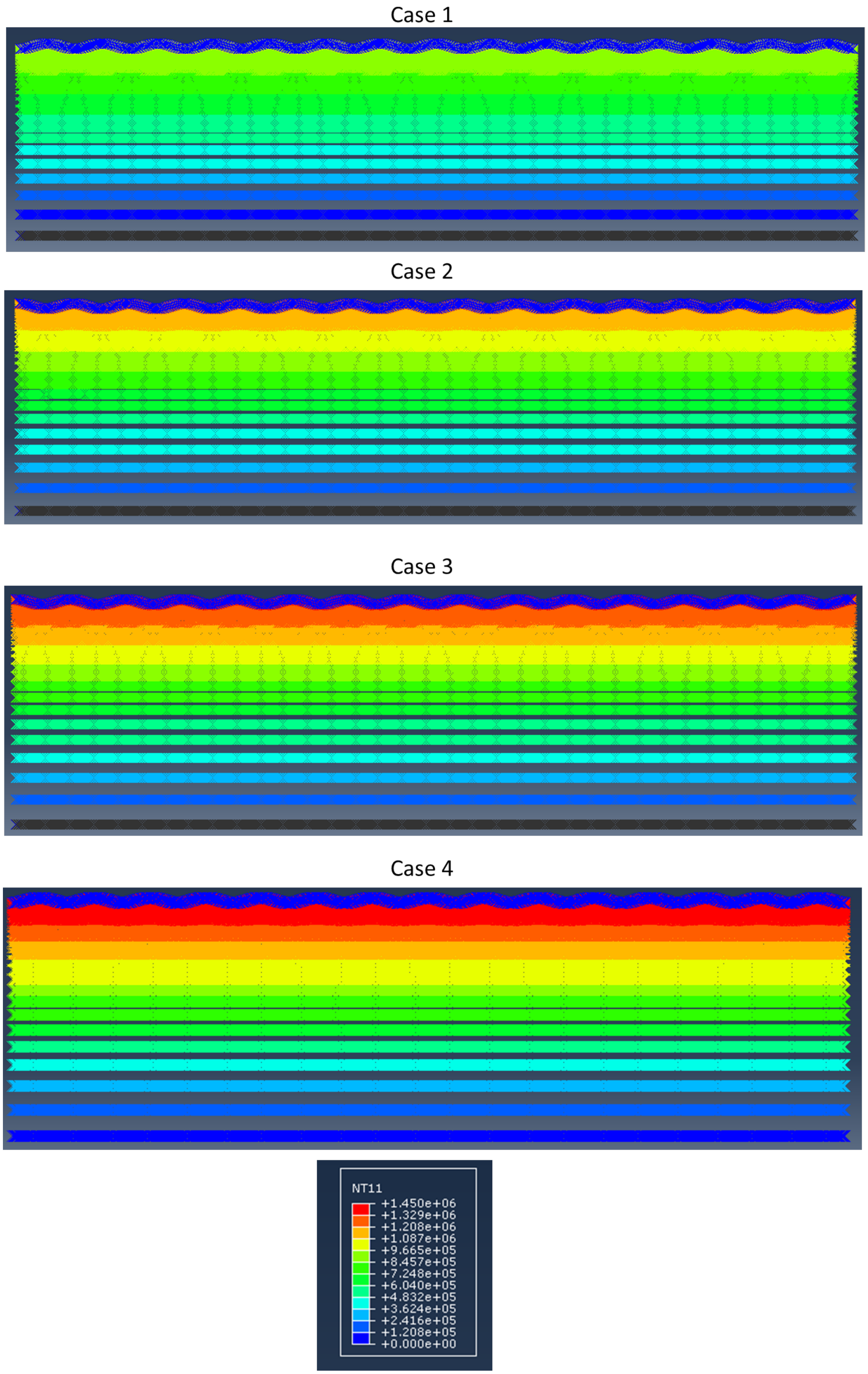

Figure 5.14: Final deformation with electric potential distribution for each case described in Table 5.7.

	Case 1	***Case 2***	***Case 3***	***Case 4***
E_s (MPa)	30	25	20	15
theoretical coefficient c_2 ($10^{-4}\mu m^4/V^2$)	19.37	23.24	29.05	38.74
numerical coefficient c_2 ($10^{-4}\mu m^4/V^2$)	19.61	23.56	29.58	38.93

Table 5.7: Comparison of linear approximation of amplitude with theory coefficients for varying substrate elasticity.

It is now possible to compare the theoretical results and the results obtained with ABAQUS. We keep in mind that in this section, the Poisson coefficient of the two materials is taken from Table 5.2, and the deformation gradient tensor generating wrinkles is given by Equation (5.10).

As illustrated in Figure 5.15, the numerical results and the theoretical results present a good matching. We note that the value of the substrate elasticity is taken as the varying parameter because, as indicated in Equation (5.14), changing this elasticity parameter will influence the coefficient associated with the electric field.

To illustrate the results further, Table 5.7 compares the coefficient c_2 illustrated in Equation 5.14

Width of the system

As mentioned in Section 5.1, we use periodic boundary conditions on the edges. This choice, combined with a fixed length for all cases with varying parameters for the bilayered system, actually prevents the model from reaching perfect accuracy regarding the wavelength of the wrinkles. The buckling command of ABAQUS will have to deal with the fact that the displacements at the extremities must be equal. As a consequence, the resulting wavelength will still give an integer number of wrinkles over the width of the bilayered system. In the case of a very large number of wrinkles, the error will be small, but still can be corrected by adapting the width of the materials. Instead of using the value given by Table 5.2, assigning the width to the value L given below will make the deformation produce exactly n wrinkles, and the resulting wavelength will be exactly k_{theory} calculated with Equation (2.36)

$$L = \frac{2\pi}{k_{theory}} n. \tag{5.15}$$

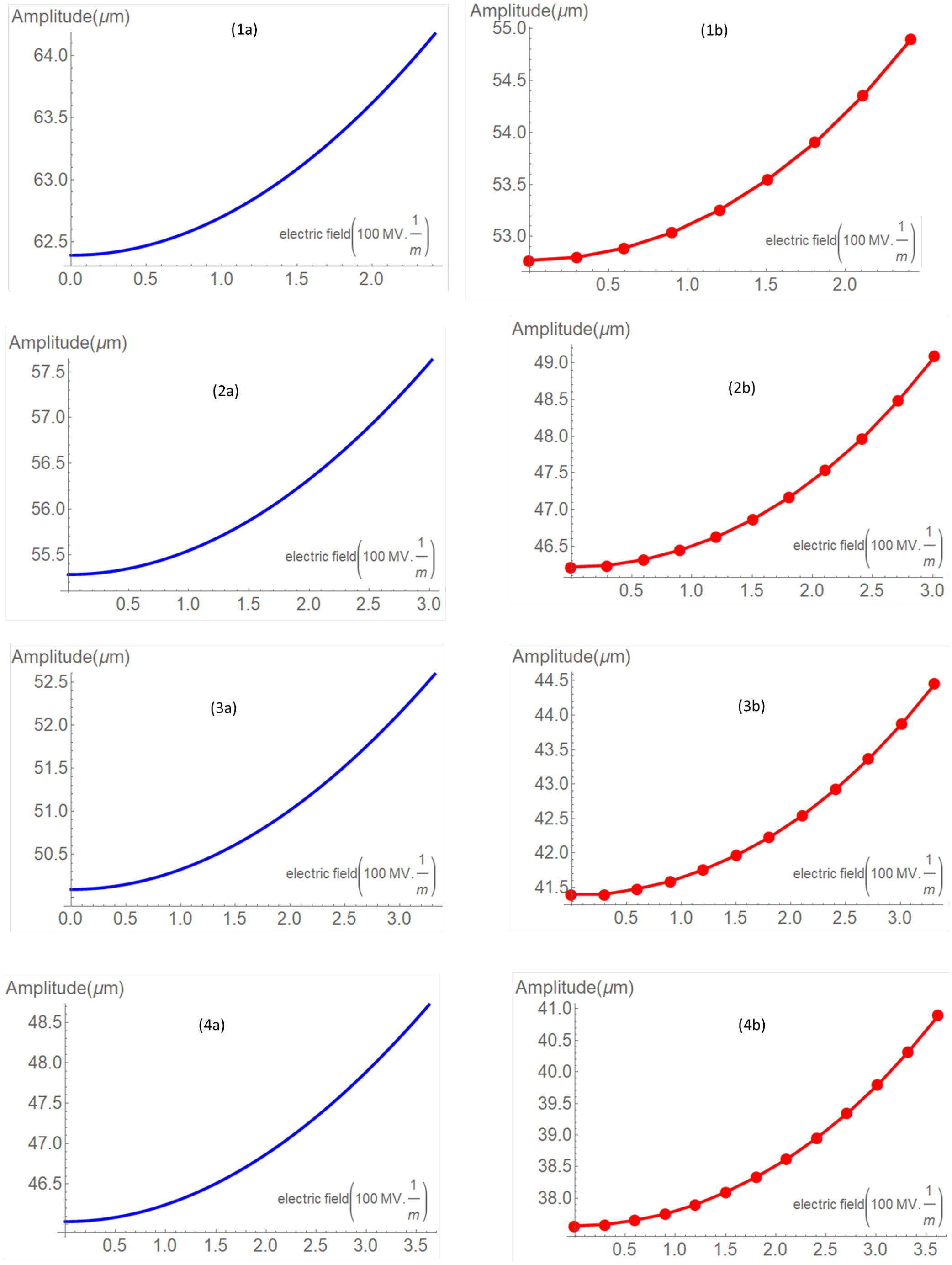

Figure 5.15: Amplitude vs external applied electric field for different elasticity modulus in both theoretical (blue) and numerical results (red): Case (1a), (1b): E_{sub}=15 MPa; Case (2a), (2b): E_{sub}=20 MPa; Case (3a), (3b): E_{sub}=25 MPa; Case (4a), (4b): E_{sub}=30 MPa.

5.3.2 Different options for deformation gradient tensor and mesh size

Deformation gradient tensor

The plot shown in Figure 5.15 shows that there is an important shift in the initial amplitude between theory and subroutine results. This brings us to consider the possibility that the gradient deformation tensor depicted in Equations (5.9) and (5.10) might not correctly represent the applied uniform strain. One correction to be made is to consider the third spatial direction along z to be different from 1. If that is the case, then the expression (5.10) must also be modified to conserve incompressibility:

$$U_{buckling} = \begin{pmatrix} \frac{1}{1.03^2} & 0 & 0 \\ 0 & 1.03 & 0 \\ 0 & 0 & 1.03 \end{pmatrix} \tag{5.16}$$

The influence of this new form is illustrated in Figure 5.16. In this figure, the blue curve represents the theoretical evolution of the amplitude vs the external applied electric field when considering the data of Table 5.6 and a strain of 0.03 applied to generate wrinkles. The green curve represents the ABAQUS evolution of the amplitude when the gradient deformation tensor of the element user subroutine corresponds to Equation (5.10), with the red curve representing the same results for a gradient deformation tensor corresponding to (5.16). It appears that the green curve is significantly closer to the theoretical results. As a consequence, this format of deformation tensor should be preferred to generate a more accurate initial wrinkle generation.

Influence of mesh density

In the results of the previous sections, the mesh was taken to be 1000 nodes along the width and 30 nodes along the depth of the bilayered system. The distribution of the nodes along the depth was not linear, so that more nodes would be located on the top of the bilayered system where the most interesting deformations happen. Given that we observed 15 wrinkles in our model every time due to the choice of length described in the previous section, the number of nodes per wrinkle from a horizontal perspective was 67. A more dense mesh would result in higher calculation cost.

We still made models with a higher mesh density. We made a model with mesh density of 1500×45 nodes with 15 wrinkles so that the horizontal number of nodes

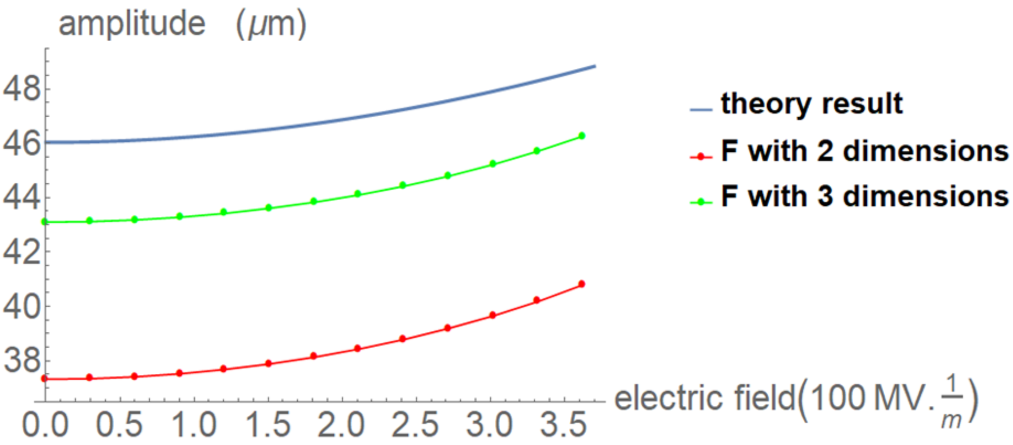

Figure 5.16: Amplitude vs external applied electric field for different gradient deformation tensor formats.

per wrinkle would be 100. We also made a model with a mesh density of 1600 × 30 with 16 wrinkles to reduce the computational cost and still maintain the same horizontal number of nodes per wrinkle. We also made a model with a mesh of size 1800 × 30 with 16 wrinkles to see the influence of a larger number of nodes per wrinkle period.The results of those three models are represented alongside the results for a model with 1000 × 30 nodes in Figure 5.17. We see that the results from the meshes with 1500 × 45 nodes and 1800 × 30 nodes differ from the two other results. It indicates that the solution ABAQUS computes increment after increment is very sensitive to the mesh density. A higher mesh density does not necessarily result in a more accurate solution. In fact, we can think that a higher mesh density adds more equations to a problem that is already made unstable by the presence of the periodic boundary conditions, making it more sensitive to edge effects or local minima.

5.3.3 Results with varying thickness of film

Taking into account this different deformation gradient tensor and the mesh of size 1000x30 nodes, Equation (5.14) also indicates that the linear coefficient associated with the external electric field also depends on the thickness h of the film.

The influence of the thickness is even more important since the coefficient depends on h^2. Simulations have been conducted with varying thickness to observe if the numerical results match the theory in that case. Those simulations have been performed with a gradient deformation tensor given by Equation (5.16), the width of

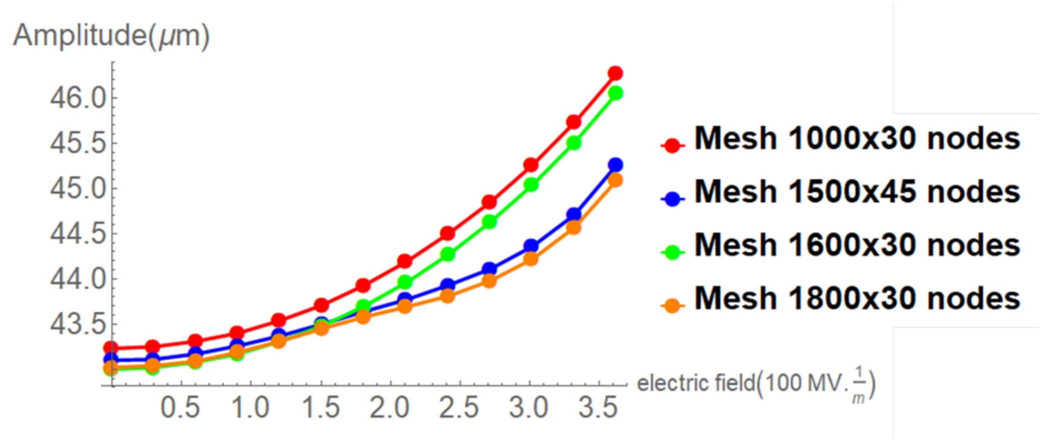

Figure 5.17: Amplitude vs external applied electric field for mesh sizes.

	Case A	***Case B***	***Case C***	***Case D***
film thickness (μm)	10	20	30	40
theoretical coefficient c_2 ($10^{-4}\mu m^4/V^2$)	2.15	8.64	19.37	34.44
numerical coefficient c_2 ($10^{-4}\mu m^4/V^2$)	2.25	8.95	20.35	36.42

Table 5.8: Comparison of linear approximation of amplitude with theoretical coefficients for varying thickness.

the materials given by Equation (5.15), and the elasticity parameters of the materials given by Table 5.6.

Figure 5.18 shows all final deformations with deflection $U2$ distribution. We observe that 15 wrinkles in each case, the thicker the film is, the smaller the width necessary to observe 15 wrinkles becomes. This is due to the relation between the thickness and the wavelength of the wrinkles.

The comparison with theoretical results is illustrated in Figure 5.19 and in Table 5.8. Again, the linear coefficients c_2 are quite similar between theoretical and numerical results.

In both cases of varying substrate elasticity and varying film thickness, the ABAQUS results match the theoretical expectations regarding the evolution of the amplitude when the external electric field increases. This match is still limited to an electric field under 360 MV/m. For higher electric fields, the ABAQUS model cannot converge and we cannot obtain further data. Still, those results confirm the initial influence developed in Chapter 4: the amplitude increases as a square root function

Case A

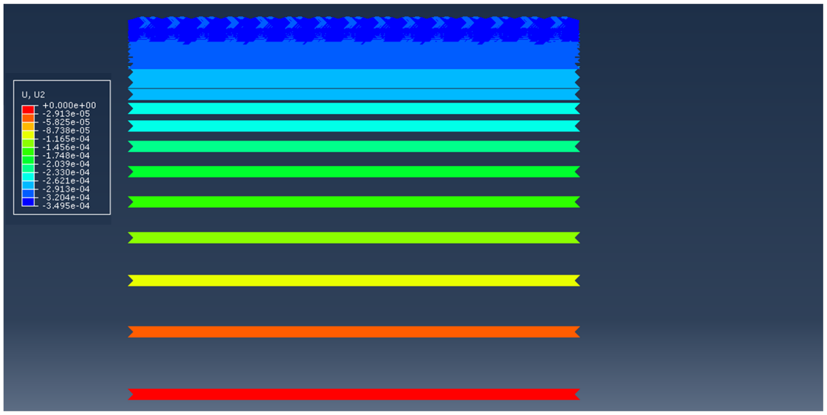

Case B

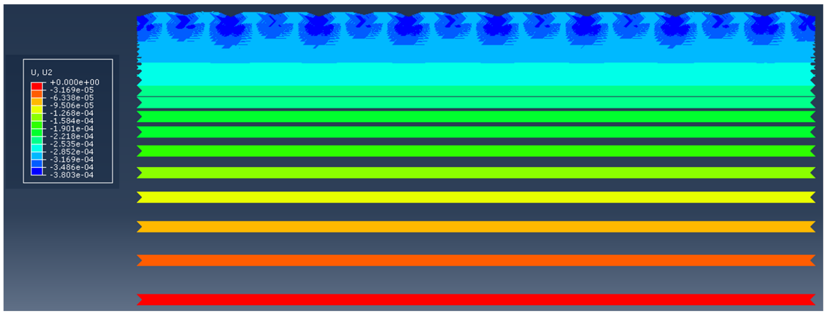

Case C

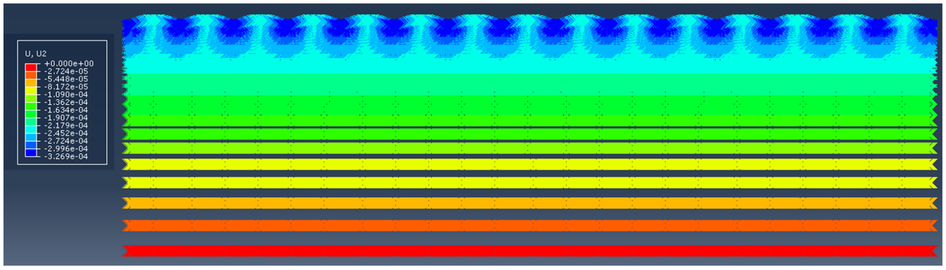

Case D

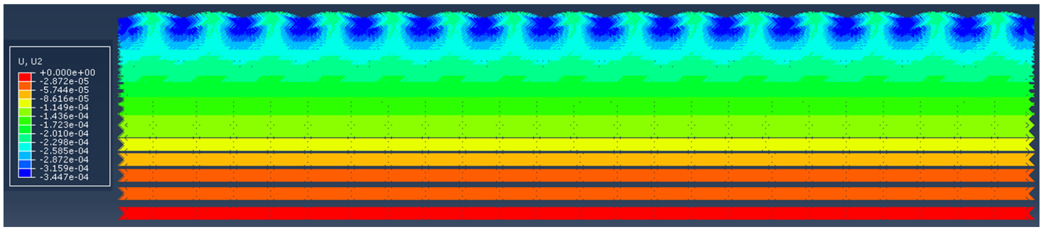

Figure 5.18: Final deformation with deflection distribution for each case described in Table 5.8.

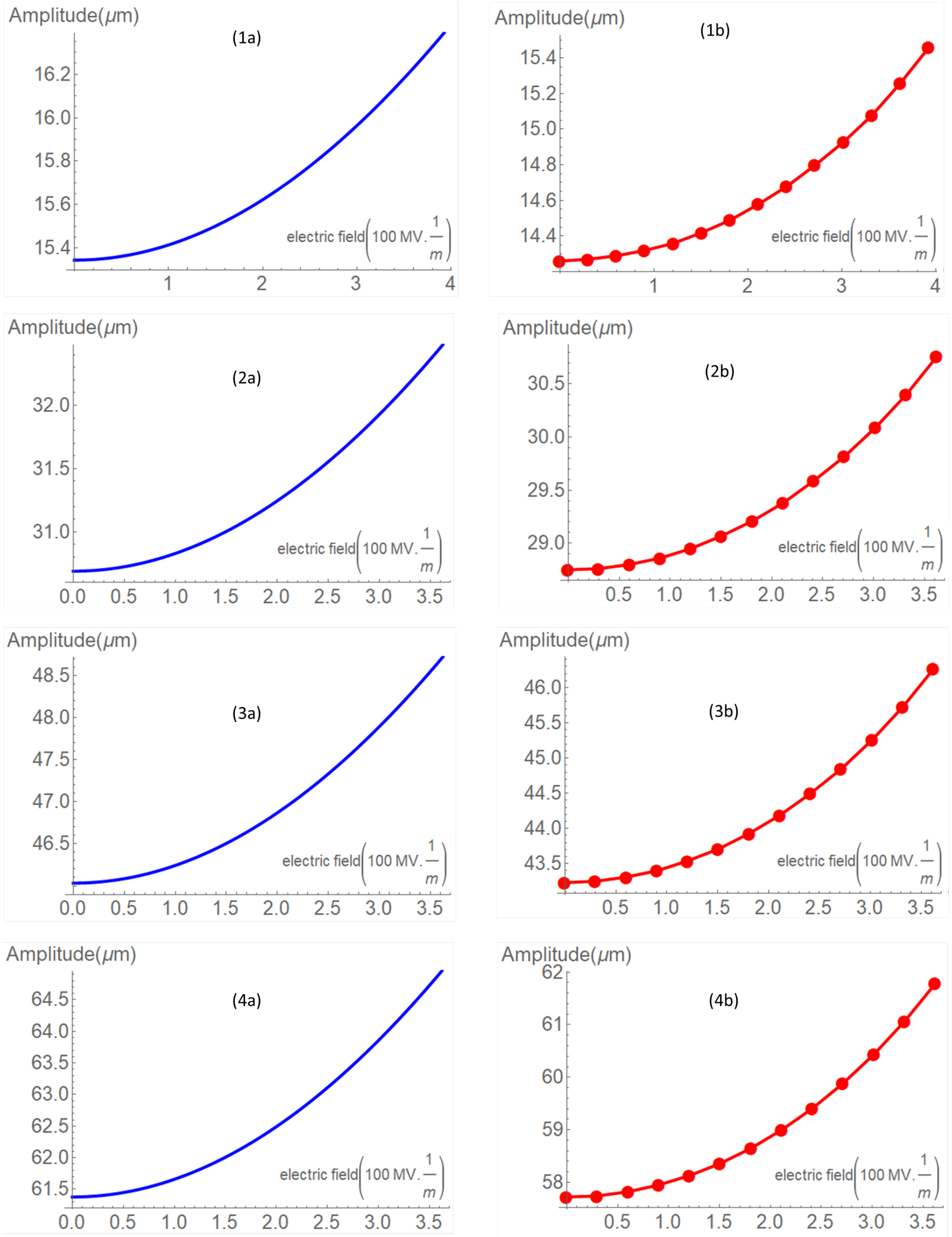

Figure 5.19: Amplitude vs external applied electric field for different film thickness in both theoretical (blue) and numerical results (red): Case (1a), (1b): h=10 μm; Case (2a), (2b): h=20 μm; Case (3a), (3b): h=30 μm; Case (4a), (4b): h=40 μm.

physical parameter	***unit system used in gold film case***
Length	cm
Force	N
Stress	10 kPa
Mass	100 kg
Voltage	V

Table 5.9: Set of units in the case of a film made of gold.

of the quadratic electric field.

5.3.4 Results for gold film and PDMS substrate

In the previous sections, the values taken for the elasticity and the thickness of the film are not exactly the ones that can be found in experimental studies. We can perform a study with values corresponding to the experimental values given in Table 5.5 with the thickness of the film being 50 nm and the thickness of the substrate being 0.3 mm. Because those dimensions are very small, we had to rescale everything to ease the convergence within ABAQUS. The dimensions used in this particular case are depicted in Table 5.9. We chose to apply a differential strain of 0.005 within the film to generate the initial wrinkles. We made this choice so that the amplitude of initial wrinkles would be in the range of the thickness of the film. The comparison between theoretical results and numerical results is illustrated in Figure 5.20. When we make an approximation of the linear coefficient c_2, we obtain a value of 7615 nm^4/V^2 for the red curve and 7594 nm^4/V^2 for the blue curve. We can conclude that the model is still coherent for elasticity and thickness of the film close to the values taken in experimental studies.

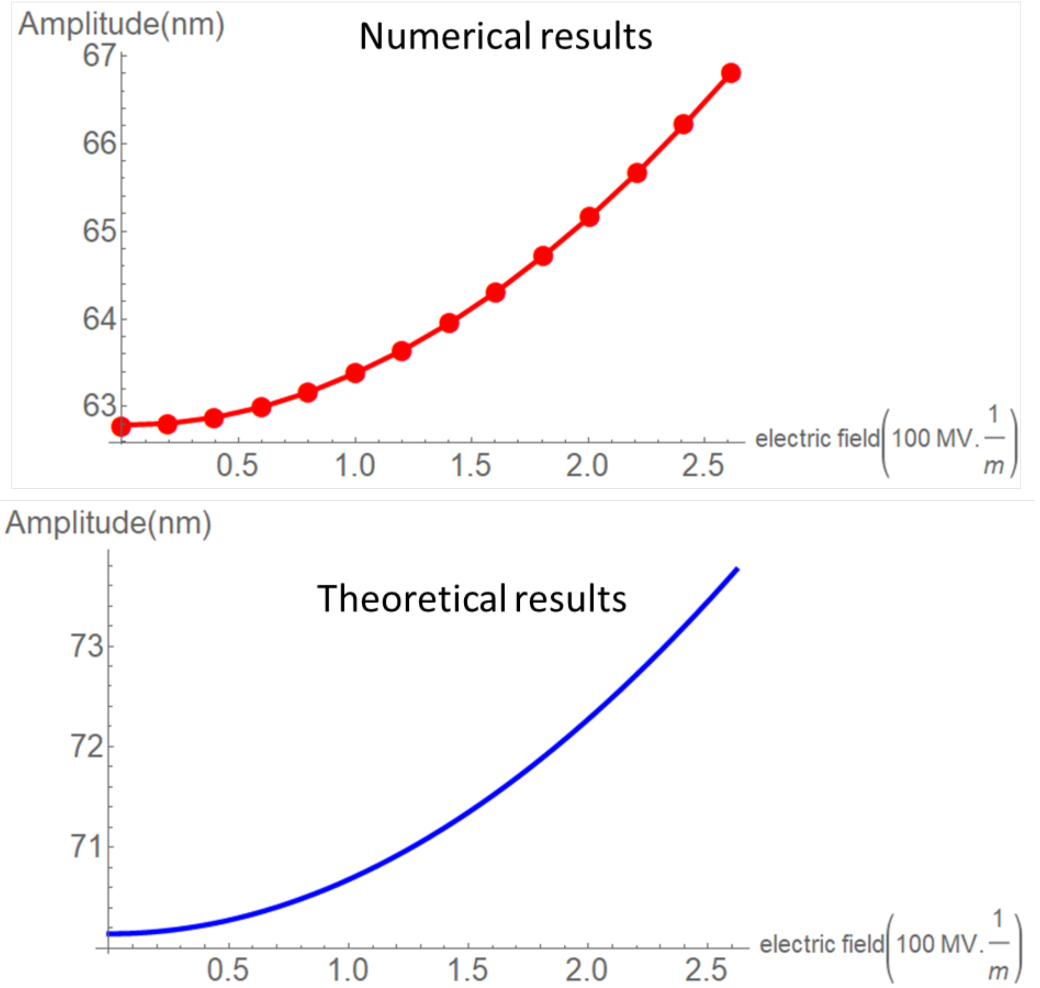

Figure 5.20: Amplitude vs external applied electric field for gold film attached to PDMS substrate.

Chapter 6

CONCLUSION

6.1 General conclusion

This thesis studied several aspects of surface deformation of bilayered systems. The perspectives of those investigations were motivated by the potential uses of bilayered systems. Our specific focus concerned heterogeneity and tunability.

First we revisited the theory of deformation for bilayered systems. It was necessary to establish which models were used for each material component and the consequences of those models on the final nonlinear behavior. This work focused essentially on the elastic energy of the bilayered system. Indeed, the entire study of deformation rests on the principle that deformation, linear and nonlinear will serve only one objective: the minimization of the energy of the system. Once this state of minimal energy is reached, the bilayered system has reached its equilibrium in terms of displacement field. The energy study of such systems brought us to split the total energy into different terms where each term represented a contribution from a specific order of derivative of the displacement field. Each contribution imposed a specific pattern for the equilibrium state of displacement, and the relative importance of each term depended on the dimensions and elasticity of the materials. Most of this work was based on literature review of previous work done on bilayered systems. We then proceeded to give a detailed and well-explained theory regarding the elastic energy of the substrate: by solving the Navier equation, taking into account specific boundary conditions associated with properties of bilayered systems, we gave a complete formulation of the energy, taking into account the contribution of the in-plane displacement. All previous work in this field did not consider this contribution, as its value was negligible compared to the contribution of the deflection. But, the average value requirements of numerical methods made it necessary to consider in-plane displacements in the final expression of the energy. To result in nonlinear displacements, the energy minimization must be associated with a differential strain between the two materials. The pattern observed at the surface and the possible evolution of this pattern will depend on the value of this differential strain. The type of pattern that is studied in this thesis is called the wrinkling pattern and is the first one to appear when the surface of a bilayered system buckles. The study of wrinkles is done by determining the value of their amplitude and their wavelength.

Not only did the pattern depend on the amplitude of this differential strain, but it also depended on the orientation of this strain. In the second part, we demonstrated the influence of this orientation by implementing all the theory and expressions of the first part into a numerical loop. We showed that from a starting point with any random distribution of in-plane displacements and deflection at the surface of a bilayered system, it was possible to recover the nonlinear pattern that would minimize the total energy. The implementation of such a numerical method was challenging due to the coexistence of energy terms related to different orders of derivatives of the displacements: more specifically, order 0, order 1, and order 2 of deflection derivatives were making the minimization too difficult in the space domain. Thus, we developed a form of the energy expressed in the Fourier domain. This transfer was made possible by considering a semi-infinite domain for the system and then using the Plancherel theorem to generate an infinite integral over the frequency domain to express the energy. This Fourier transfer only partially solved the problem, as some derivative terms were not simplified by the Plancherel theorem. It was then necessary to replace those terms by extra variables associated with constraints, creating then an Augmented Lagrangian loop system to converge from an initial random distribution to a set of displacements minimizing the energy.

The method was first tested on a simple 1D model with unidirectional differential strain generating wrinkles. The results in this case were very satisfying since the amplitude and the wavelength predicted by theory were exactly recovered with no relative mistake after completing approximately 40,000 iterations of the simulation. In comparison to the one-dimensional case, implementation of a two-dimensional model was more difficult, as it was computationally far more expensive to take into account two components of the in-plane displacement and two spatial coordinates. More importantly, in order to maintain the convergence of the model, it was necessary to consider the contribution of the in-plane displacements in the substrate energy. Eventually, the convergence of unidirectional wrinkles was still achieved and the wavelength and amplitude of the wrinkles converged towards the expected theoretical values. We were then able to revisit the initial objective for a heterogeneous strain distribution with an interface for the orientation of the strain at an arbitrary, predefined position on the surface. This interface would define the border for a discontinuous angle of orientation of the strain. We showed with the Augmented Lagrangian loop applied on the two-dimensional model that such a discontinuity in the strain would result in a discontinuity in the direction of the wrinkles. This discontinuity could be observed in two ways: a change of spatial angle of wrinkles between each side of the interface, and in non-symmetric cases, a change in the number of wrinkles between each side of the interface. One interesting point from this discontinuity was that it would affect neither the global amplitude or the wavelength away from the interface.

The next part of this thesis was about another aspect of the instabilities of a bilayered system: the possibility of actively influencing those instabilities by an external constraint that would not be a mechanical load. We were particularly interested in electromechanical coupling by using dielectric elastomers as the substrate of the bilayered system. The goal was to predictably control the wrinkles with an external applied voltage at the top and bottom of the bilayered system. To begin our study of this electromechanical coupling, we focused on the theory of electric elastomers to determine how the Maxwell equations and the Maxwell stress tensor would influence the nonlinear deformations at the top surface of the bilayered system. Considering a Taylor expansion of the electric potential at the top surface, it was possible to inject the correct contribution of the nonlinear electric field into the expression of the electric energy. From energy minimization, it was then possible to prove that the electric field was actually influencing the value of the wavelength and the amplitude of the wrinkles at the minimum energy state. More precisely, our study proved that the electric field had the effect of counteracting the influence of the substrate on the nonlinear deformation. As a consequence, the higher the applied voltage on top of the substrate, the more the bilayered system behaved like a single plate at the top surface. Another interesting feature from this chapter is the range of the electric field required for significantly modifying the amplitude and wavelength. This range depends on the relative permittivity of the dielectric material, and in the case of a dielectric elastomer, this permittivity lies within a range of 1 to 10. In this case, we notice that the variation in the amplitude of electric field to observe a 10% variation in the amplitude of the wrinkles is 300 MV/m. When considering the size of the materials involved here, a bilayered system with a depth of 1 mm would require an external field of 300,000 V to obtain this variation. Such a high value is due to the fact that the dielectric permittivity of those materials is quite small, and consequently, high voltages are required to deform dielectric elastomers.

After establishing the theory of nonlinear deformation by electromechanical coupling, it was necessary to create a method to confirm this theory. Finite element modeling can allow for the building of sufficiently small models and sufficiently refined mesh to observe the desired deformations. ABAQUS was used to build a bilayered system with a dimensional scale of millimeters for the substrate and a dimensional scale of micrometers for the film. The main advantage of ABAQUS was its capacity to reproduce the initial buckling phenomena described in Chapter 2. All the results regarding the buckling behavior and associated nonlinear deformations could be reproduced with high accuracy, confirming that ABAQUS was representing the studied phenomena well. As ABAQUS does not provide a pre-existing dielectric model, we implemented a user-defined element capable of performing electromechanical coupling through the implementation of a material model that added the Maxwell stress to the initial Cauchy stress tensor. One limitation compared to the theoretical model is that it was impossible to build a semi-infinite model. More specifically, regarding the in-plane dimensions, to compensate the finite length of the bilayered system, periodic boundary conditions were imposed on the model at the edges. Even though it would be equivalent to having an infinite model, it would also prevent the wavelength of the wrinkles from being modified by an imposed electric field. We then developed a different angle of comparison, as it was possible to consider an optimal amplitude, minimizing the energy independently of the wavelength. This new form would be less impacted by the influence of the electromechanical coupling than by the form with varying wavelengths, but would still give a clear comparison support. The simulation provided deformation for values of electric field up to 360 MV/m, for different values of thickness of the film and elasticity of the substrate. The comparative results were accurate enough to confirm the validity of the theory.

In a more general view, this thesis has managed to show that nonlinear wrinkles on top of a bilayered surface are not the end of a buckling process, but instead can be seen as a first step of a more complex behavior. The evolution of the amplitude and the wavelength of wrinkles can lead to a significantly different pattern, and this evolution can then be used to serve the different purposes described in the introduction of this thesis. Also it is important to note that those wrinkles do not necessarily require a uniformly distributed strain on the whole surface to remain stable. It is now confirmed that discontinuous wrinkles can coexist within the same surface, thus opening the path to more applications and behavioral phenomena.

6.2 Future work

This thesis opens the door for more studies on both the part associated with the Augmented Lagrangian loop and the part associated with the ABAQUS numerical studies. The numerical methods used to observe the formation of wrinkles with a sudden change of main orientation offers the ideal support for an experimental comparison. As mentioned in Chapter 3, several experimental studies have been using liquid crystal elastomers to generate discontinuous wrinkles. It would be very interesting to realize an experimental process based on those results that would yield wrinkles with measurable amplitude and wavelength with a controlled change of angle for wrinkles. This way, all measured values could be compared in both areas away from the discontinuity interface and on this interface. Based on those methods, the next potential step would be to study what energy minimization tools are involved in the interface and more specifically, in the merging process at this very interface. Even though the energy minimization method introduced in this thesis was used to study the specific case of wrinkles, it would be natural to consider extending this method to other buckling phenomena. We showed that a checkerboard pattern scenario was achievable through this numerical method for higher values of imposed strain. It is possible to consider applying this method to even more complex buckling, such as the creasing or folding of the surface. Another very interesting buckling pattern that could become accessible numerically with this method is the herringbone pattern described by Audoly and Boudaoud [6], which is present in many engineering applications.

The influence of dielectric elastomers on the surface wrinkles of a bilayered system is also a first step for even more interesting studies. As mentioned previously, the values of the electric field necessary for this model are very high, but the dielectric elastomer is not the only option for achieving our initial goal. Even though the electromechanical coupling laws of this material make it convenient to work with, more materials like ferroelectric materials, liquid crystal elastomers or ionic polymers could be considered for providing the extra electric energy. Exploring such materials could uncover better relative permittivity options, leading to smaller values of voltage required to obtain the desired deformations. Another aspect to explore is extending the study of the influence of the electric field to more complex buckling patterns. Even though we studied this influence for a two-directional case at the end of Chapter 4, there are more possible buckling patterns still left to study with the Maxwell stress.

With regards to the finite element modeling problem that we solved, we can envision that the next step would be to find a way to unconstrain the value of the buckling wavelength. For example, one could explore the attempt to use very powerful finite element software in order to model a very high number of wrinkles to approximate a model equivalent to an infinite model with an appropriately refined mesh. If this option is not possible, the entire focus would shift to the edge boundary conditions. Finding conditions that would enable the frequency of wrinkles to evolve without a significantly high energy cost would solve this local minimum problem. We can also consider other improvements to the model used here: for example, it would be more convenient to use another degree of freedom than the temperature to represent the electric field, since the temperature cannot be used anymore to generate the initial differential strain necessary to trigger the buckling. Although a predefined deformation gradient tensor was an acceptable replacement option, it is not capable of fully recovering the initial amplitude of wrinkles. The use of thermal strain remains much more appreciated for that purpose.

This thesis has also established a complete basis to be compared with experimental results regarding the influence of electromechanical coupling on bilayered systems. One could think about creating an experimental setup involving a dielectric elastomer attached to a rigid, thin electrode and measuring the influence of an applied electric field on the surface. One aspect that requires careful investigation is the selection of measurement tools, since the small scale of the materials requires equipment with a very high resolution to capture the evolution of the amplitude and the wavelength of the wrinkles. Other aspects include the choice of materials and the attachment method in order to generate the initial wrinkles. In case the problem of imposed wavelength in the numerical method cannot be fixed, it would be interesting to see if the experimental results of such a system would match the theoretical results or the numerical results regarding the evolution of the wavelength. Even though one could initially expect the experimental results to match the numerical solutions because of the edge effects that would come with an experimental process, it could be possible to observe a varying wavelength if the plane is taken to be so large that hundreds of wrinkles could be observed. In that case, local variation could occur, as the side effects would become negligible in areas very far from the edges. This discussion is, of course, based on hypotheses, and it is possible to think that experimental results could uncover a new, completely different cause to the wavelength problem encountered in the numerical case. If the theoretical and numerical results can be matched experimentally, such bilayered systems could be practically implemented as actuators in more complex engineering systems.

Finally, one last idea of investigation for the future could be to explore the possibilities of all the results in this thesis applied to different dimensional scales. All scales here were chosen to fit in the necessary assumption of the Föppl-von Kármán theory, but it could be interesting to calculate the critical size of the film and the substrate, at which the small deformation theory would no longer hold and then find the maximum size of wrinkles that could be created while this theory would still hold. As a matter of fact, the initial assumptions did not impose the range of value for the thickness to be within the μm range, but that deformation size is limited with respect to the thickness of the film. As a consequence, it is possible to increase this size as long as the substrate remains sufficiently larger than the film and the in-plane dimensions also remain far larger than the thickness of the film.

BIBLIOGRAPHY

[1] *Abaqus 6.13 User's Guide*. URL: `http://130.149.89.49:2080/v6.13/`. Accessed: 2018-07-05.

[2] Aditya Agrawal et al. "Surface wrinkling in liquid crystal elastomers". In: *Soft Matter* 8.27 (2012), pp. 7138–7142.

[3] Howard G Allen. *Analysis and design of structural sandwich panels*. Pergamon Press, New York, 1969.

[4] Basile Audoly and Arezki Boudaoud. "Buckling of a stiff film bound to a compliant substrate—Part I:: Formulation, linear stability of cylindrical patterns, secondary bifurcations". In: *Journal of the Mechanics and Physics of Solids* 56.7 (2008), pp. 2401–2421.

[5] Basile Audoly and Arezki Boudaoud. "Buckling of a stiff film bound to a compliant substrate—Part II:: A global scenario for the formation of herringbone pattern". In: *Journal of the Mechanics and Physics of Solids* 56.7 (2008), pp. 2422–2443.

[6] Basile Audoly and Arezki Boudaoud. "Buckling of a stiff film bound to a compliant substrate—Part III:: Herringbone solutions at large buckling parameter". In: *Journal of the Mechanics and Physics of Solids* 56.7 (2008), pp. 2444–2458.

[7] Anesia Auguste et al. "The role of substrate pre-stretch in post-wrinkling bifurcations". In: *Soft Matter* 10.34 (2014), pp. 6520–6529.

[8] *Bending actuator input file*. URL: `http://brown.edu/Research/Henann/Codes_-_David_Henann_files/Beam_DE.inp`. Accessed: 2018-09-25.

[9] MA Biot. "Bending of an infinite beam on an elastic foundation". In: *Journal of Applied Mechanics* 59 (1937), A1–A7.

[10] Ned Bowden et al. "Spontaneous formation of ordered structures in thin films of metals supported on an elastomeric polymer". In: *Nature* 393.6681 (1998), pp. 146–149.

[11] Ned Bowden et al. "The controlled formation of ordered, sinusoidal structures by plasma oxidation of an elastomeric polymer". In: *Applied Physics Letters* 75.17 (1999), pp. 2557–2559.

[12] Fabian Brau et al. "Multiple-length-scale elastic instability mimics parametric resonance of nonlinear oscillators". In: *Nature Physics* 7.1 (2011), pp. 56–60.

[13] Derek Breid and Alfred J Crosby. "Surface wrinkling behavior of finite circular plates". In: *Soft Matter* 5.2 (2009), pp. 425–431.

[14] Silvia Budday, Ellen Kuhl, and John W Hutchinson. “Period-doubling and period-tripling in growing bilayered systems”. In: *Philosophical Magazine* 95.28-30 (2015), pp. 3208–3224.

[15] Silvia Budday, Paul Steinmann, and Ellen Kuhl. “The role of mechanics during brain development”. In: *Journal of the Mechanics and Physics of Solids* 72 (2014), pp. 75–92.

[16] Shengqiang Cai et al. “Creasing instability of elastomer films”. In: *Soft Matter* 8.5 (2012), pp. 1301–1304.

[17] Shengqiang Cai et al. “Periodic patterns and energy states of buckled films on compliant substrates”. In: *Journal of the Mechanics and Physics of Solids* 59.5 (2011), pp. 1094–1114.

[18] Yanping Cao and John W Hutchinson. “Wrinkling phenomena in neo-Hookean film/substrate bilayers”. In: *Journal of applied mechanics* 79.3 (2012), p. 031019.

[19] Peter W Carpenter. “Status of transition delay using compliant walls”. In: *Viscous drag reduction in boundary layers* 123 (1990), pp. 79–113.

[20] PW Carpenter. “The optimization of compliant surfaces for transition delay”. In: *Turbulence management and relaminarisation*. Springer, 1988, pp. 305–313.

[21] Edwin P Chan and Alfred J Crosby. “Fabricating microlens arrays by surface wrinkling”. In: *Advanced Materials* 18.24 (2006), pp. 3238–3242.

[22] Dinesh Chandra, Shu Yang, and Pei-Chun Lin. “Strain responsive concave and convex microlens arrays”. In: *Applied Physics Letters* 91.25 (2007), p. 251912.

[23] ShiYi Chen et al. “Constrained large-eddy simulation and detached eddy simulation of flow past a commercial aircraft at 14 degrees angle of attack”. In: *Science China Physics, Mechanics and Astronomy* 56.2 (2013), pp. 270–276.

[24] Xi Chen and John W Hutchinson. “Herringbone buckling patterns of compressed thin films on compliant substrates”. In: *Journal of applied mechanics* 71.5 (2004), pp. 597–603.

[25] Yu-Cheng Chen and Alfred J Crosby. “High aspect ratio wrinkles via substrate prestretch”. In: *Advanced Materials* 26.32 (2014), pp. 5626–5631.

[26] Haecheon Choi, Jungil Lee, and Hyungmin Park. “Aerodynamics of heavy vehicles”. In: *Annual Review of Fluid Mechanics* 46 (2014), pp. 441–468.

[27] Jun Young Chung, Adam J Nolte, and Christopher M Stafford. “Surface wrinkling: a versatile platform for measuring thin-film properties”. In: *Advanced Materials* 23.3 (2011), pp. 349–368.

[28] D Destarac and J Van Der Vooren. “Drag/thrust analysis of jet-propelled transonic transport aircraft; definition of physical drag components”. In: *Aerospace science and technology* 8.6 (2004), pp. 545–556.

[29] A Dorfmann and RW Ogden. “Nonlinear electroelasticity”. In: *Acta Mechanica* 174.3-4 (2005), pp. 167–183.

[30] Luis Dorfmann and Ray W Ogden. *Nonlinear theory of electroelastic and magnetoelastic interactions*. Springer Science & Business Media, 2014.

[31] August Föppl. *Vorlesungen uber technische Mechanik*. Vol. 5. 1907.

[32] Jan Genzer and Jan Groenewold. “Soft matter with hard skin: From skin wrinkles to templating and material characterization”. In: *Soft Matter* 2.4 (2006), pp. 310–323.

[33] Philip E.. Gill, Walter Murray, and Margaret H.. Wright. *Practical optimization*. Academic Press, 1981.

[34] Laurens T de Haan et al. “On-Demand Wrinkling Patterns in Thin Metal Films Generated from Self-Assembling Liquid Crystals”. In: *Advanced Functional Materials* 25.9 (2015), pp. 1360–1365.

[35] Mohamed Gad-el Hak. “Compliant coatings for drag reduction”. In: *Progress in Aerospace Sciences* 38.1 (2002), pp. 77–99.

[36] Christopher Harrison et al. “Sinusoidal phase grating created by a tunably buckled surface”. In: *Applied Physics Letters* 85.18 (2004), pp. 4016–4018.

[37] A. M. A. van der Heijden. *W. T. Koiter’s Elastic stability of solids and structures*. Cambridge (UK): Cambridge University Press, 2008.

[38] David L Henann, Shawn A Chester, and Katia Bertoldi. “Modeling of dielectric elastomers: Design of actuators and energy harvesting devices”. In: *Journal of the Mechanics and Physics of Solids* 61.10 (2013), pp. 2047–2066.

[39] Magnus R Hestenes. “Multiplier and gradient methods”. In: *Journal of optimization theory and applications* 4.5 (1969), pp. 303–320.

[40] MA Holland et al. “Instabilities of soft films on compliant substrates”. In: *Journal of the Mechanics and Physics of Solids* 98 (2017), pp. 350–365.

[41] Wei Hong, Xuanhe Zhao, and Zhigang Suo. “Formation of creases on the surfaces of elastomers and gels”. In: *Applied Physics Letters* 95.11 (2009), p. 111901.

[42] R Huang. “Kinetic wrinkling of an elastic film on a viscoelastic substrate”. In: *Journal of the Mechanics and Physics of Solids* 53.1 (2005), pp. 63–89.

[43] ZY Huang, W Hong, and Z Suo. “Nonlinear analyses of wrinkles in a film bonded to a compliant substrate”. In: *Journal of the Mechanics and Physics of Solids* 53.9 (2005), pp. 2101–2118.

[44] John W Hutchinson. “The role of nonlinear substrate elasticity in the wrinkling of thin films”. In: *Phil. Trans. R. Soc. A* 371.1993 (2013), p. 20120422.

[45] Francesca Iacopi, SH Brongersma, and Karen Maex. “Compressive stress relaxation through buckling of a low-k polymer-thin cap layer system”. In: *Applied physics letters* 82.9 (2003), pp. 1380–1382.

[46] Hanqing Jiang et al. “Finite deformation mechanics in buckled thin films on compliant supports”. In: *Proceedings of the National Academy of Sciences* 104.40 (2007), pp. 15607–15612.

[47] Hanqing Jiang et al. “Finite width effect of thin-films buckling on compliant substrate: experimental and theoretical studies”. In: *Journal of the Mechanics and Physics of Solids* 56.8 (2008), pp. 2585–2598.

[48] Lihua Jin et al. “Bifurcation diagrams for the formation of wrinkles or creases in soft bilayers”. In: *Journal of Applied Mechanics* 82.6 (2015), p. 061008.

[49] Seock Hwan Kang et al. “Self-organized anisotropic wrinkling of molecularly aligned liquid crystalline polymer”. In: *Langmuir* 28.7 (2012), pp. 3576–3582.

[50] Max O Kramer. “Boundary layer stabilization by distributed damping”. In: *Naval Engineers Journal* 72.1 (1960), pp. 25–34.

[51] Stephanie P Lacour et al. “Stretchable interconnects for elastic electronic surfaces”. In: *Proceedings of the IEEE* 93.8 (2005), pp. 1459–1467.

[52] Bo Li, Yan-Ping Cao, and Xi-Qiao Feng. “Growth and surface folding of esophageal mucosa: a biomechanical model”. In: *Journal of biomechanics* 44.1 (2011), pp. 182–188.

[53] Bo Li, Shi-Qing Huang, and Xi-Qiao Feng. “Buckling and postbuckling of a compressed thin film bonded on a soft elastic layer: a three-dimensional analysis”. In: *Archive of Applied Mechanics* 80.2 (2010), p. 175.

[54] Bo Li et al. “Mechanics of morphological instabilities and surface wrinkling in soft materials: a review”. In: *Soft Matter* 8.21 (2012), pp. 5728–5745.

[55] M Luhar, AS Sharma, and BJ McKeon. “On the design of optimal compliant walls for turbulence control”. In: *Journal of Turbulence* 17.8 (2016), pp. 787–806.

[56] Mitul Luhar, Ati S Sharma, and BJ McKeon. “A framework for studying the effect of compliant surfaces on wall turbulence”. In: *Journal of Fluid Mechanics* 768 (2015), pp. 415–441.

[57] Vladimir Lumelsky, Michael S Shur, and Sigurd Wagner. *Sensitive skin*. World Scientific, 2000.

[58] Stephen J Ma et al. “Photodirected Formation and Control of Wrinkles on a Thiol–ene Elastomer”. In: *ACS Macro Letters* 2.6 (2013), pp. 474–477.

[59] Teng Ma et al. “Micro-strain sensing using wrinkled stiff thin films on soft substrates as tunable optical grating”. In: *Optics express* 21.10 (2013), pp. 11994–12001.

[60] Meghies. *Mutlilayered composite material*. 2018. URL: `http://www.mehgies.com/mta/Wiki-Textile-Architecture/The-Fabric.php` (visited on 05/10/2018).

[61] Jorge Nocedal and Stephen J Wright. *Numerical optimization 2nd*. 2006.

[62] Ron Pelrine et al. “High-field deformation of elastomeric dielectrics for actuators”. In: *Materials Science and Engineering: C* 11.2 (2000), pp. 89–100.

[63] Ronald E Pelrine, Roy D Kornbluh, and Jose P Joseph. “Electrostriction of polymer dielectrics with compliant electrodes as a means of actuation”. In: *Sensors and Actuators A: Physical* 64.1 (1998), pp. 77–85.

[64] David P Richman et al. “Mechanical model of brain convolutional development”. In: *Science* 189.4196 (1975), pp. 18–21.

[65] J Song et al. “Buckling of a stiff thin film on a compliant substrate in large deformation”. In: *International Journal of Solids and Structures* 45.10 (2008), pp. 3107–3121.

[66] Christopher M Stafford et al. “Combinatorial and high-throughput measurements of the modulus of thin polymer films”. In: *Review of Scientific Instruments* 76.6 (2005), p. 062207.

[67] Eric Sultan and Arezki Boudaoud. “The buckling of a swollen thin gel layer bound to a compliant substrate”. In: *Journal of applied mechanics* 75.5 (2008), p. 051002.

[68] Jeong-Yun Sun et al. “Folding wrinkles of a thin stiff layer on a soft substrate”. In: *Proc. R. Soc. A*. Vol. 468. 2140. The Royal Society. 2012, pp. 932–953.

[69] Yugang Sun et al. “Controlled buckling of semiconductor nanoribbons for stretchable electronics”. In: *Nature nanotechnology* 1.3 (2006), pp. 201–207.

[70] Tuomas Tallinen and John S Biggins. “Mechanics of invagination and folding: Hybridized instabilities when one soft tissue grows on another”. In: *Physical Review E* 92.2 (2015), p. 022720.

[71] Tuomas Tallinen et al. “Gyrification from constrained cortical expansion”. In: *Proceedings of the National Academy of Sciences* 111.35 (2014), pp. 12667–12672.

[72] Lixiu Tian. “Effective behavior of dielectric elastomer composites”. PhD thesis. California Institute of Technology, 2008.

[73] Richard A Toupin. “The elastic dielectric”. In: *Journal of Rational Mechanics and Analysis* 5.6 (1956), pp. 849–915.

[74] Rafael Verduzco et al. “Buckling instability in liquid crystalline physical gels”. In: *Physical review letters* 96.14 (2006), p. 147802.

[75] Theodore Von Kármán. *Festigkeitsprobleme im maschinenbau*. Vol. 4. Teubner, 1910, pp. 311–385.

[76] Sigurd Wagner et al. “Electronic skin: architecture and components”. In: *Physica E: Low-dimensional Systems and Nanostructures* 25.2 (2004), pp. 326–334.

[77] Qiming Wang and Xuanhe Zhao. “Phase diagrams of instabilities in compressed film-substrate systems”. In: *Journal of applied mechanics* 81.5 (2014), p. 051004.

[78] Mark Warner and Eugene Michael Terentjev. *Liquid crystal elastomers*. Vol. 120. OUP Oxford, 2003.

[79] Wesley Wong and Sergio Pellegrino. “Wrinkled membranes III: numerical simulations”. In: *Journal of Mechanics of Materials and Structures* 1.1 (2006), pp. 63–95.

[80] YW Wong and Sergio Pellegrino. “Computation of wrinkle amplitudes in thin membrane”. In: *43rd AIAA/ASME/ASCE/AHS/ASC Structures, Structural Dynamics, and Materials Conference*, p. 1369.

[81] Richard M Wood. *Impact of advanced aerodynamic technology on transportation energy consumption*. Tech. rep. SAE Technical Paper, 2004.

[82] Weidong Wu et al. “Applying periodic boundary conditions in finite element analysis”. In: *SIMULIA Community Conference, Providence*. 2014, pp. 707–719.

[83] Jianfeng Zang et al. “Localized ridge wrinkling of stiff films on compliant substrates”. In: *Journal of the Mechanics and Physics of Solids* 60.7 (2012), pp. 1265–1279.

[84] Ling Zheng. *Wrinkling of dielectric elastomer membranes*. California Institute of Technology, 2009.

Appendix A

AUGMENTED LAGRANGIAN CODE

This is the Matlab code implemented for the Augmented Lagragian method described in Chapter 3.

Matlab Code

```
clear all
close all
clc

options = optimset('TolFun',1e-15,'Display','off');

%define the Poisson coeff for the root program
coeff = 0.3;
POISSON = 1-coeff;

%physical paramters
thickness=30*10^-6;
Efilm = 10*10^9;
Esub = 10*10^6;
nufilm=0.3;
nusub=0.4;
epsilon0=8.85*10^-12;
epsilonr=7;
electric_field=0*10^8;
bendingModulus = Efilm*thickness^3/(12*(1-nufilm^2));
SubstrateModulus = (1-nusub)/((1+nusub)*(3-4*nusub))*
    Esub;
eta=0.01;
ktheory=(SubstrateModulus/bendingModulus)^(1/3);
Atheory=sqrt(eta*(1+nufilm)*4/ktheory^2-thickness^2);
ktheory2=((SubstrateModulus-1/2*epsilon0*epsilonr*
    electric_field^2)/bendingModulus)^(1/3);
```

```
%define space and frequency domain
N = 128;
a = 0;
b = 300*pi;
dx = (b-a)/N;
spaceDomain = a + dx*(0:N-1);

[X,Y] = meshgrid(spaceDomain);

kDomain = (-N/2)*2*pi/(b-a) + 2*pi/(b-a)*(0:N-1) ;

[KX,KY] = meshgrid(kDomain);

%define a coeff of balance of energies
  balancebend = 1100;     %bending coefficient

balancesubs = 2*balancebend*(2*pi*12/b)^3;     %
    substrate energy coefficient
balancestretch = 2;      %stretching energy coefficient



% define the quadratic penalty coefficient
beta = 1200;

% define undimensionalized parameters
x0=(balancesubs/balancebend*bendingModulus/(2*
    SubstrateModulus))^(1/3);
w0=sqrt(balancestretch/balancebend*thickness^2/12);
u0=sqrt(balancestretch/balancebend*thickness^2/12*w0^2/
    x0^2);
eta0=sqrt(balancestretch/balancebend*thickness^2/12*(w0
    ^2)/(x0^4));
energy0=balancebend*2/bendingModulus*x0^2/w0^2;
```

```
elec0=sqrt(1/epsilon0/epsilonr*2*SubstrateModulus/
   balancesubs);


% define the scales coefficients for space and
   frequency
 Xcorrect = x0*X;
    Ycorrect = x0*Y;
    KXcorrect=(1/x0)*KX;
    KYcorrect=(1/x0)*KY;

%define the size of the loop
sizeloop = 40000;

%define the angle of orientation of the wrinkles
teta = -pi/4*ones(N);
  for y = 1:N/2
      for x = 1:N
          teta(x,y)= pi/4;

      end
  end

%define the undimensionalized electric field
elecbar = electric_field/elec0;
%define the undimensionalized strain magnitude
etabar=eta/eta0;

%define the strain in each of the main direction and
   the shear strain
etaxyTensor = etabar*cos(teta).*sin(teta);   %
   undimensionalized shear strain
etaxTensor = etabar*cos(teta).*cos(teta);    %
   undimensionalized strain in x-direction
etayTensor = etabar*sin(teta).*sin(teta);    %
   undimensionalized strain in y-direction
```

```
%strain distributions are now transferred into the Fourier domain
  etaxFou = fftshift(fft2(etaxTensor));
  etayFou = fftshift(fft2(etayTensor));
  etaxyFou = fftshift(fft2(etaxyTensor));

  %define initial guess for w

wTensor =-Atheory/w0/2+Atheory/w0*rand(N);
uTensor = -2.5+5*rand(N);
vTensor = -2.5+5*rand(N);

%create an empty box for xi
xi1Tensor = zeros(N,N);
xi2Tensor = zeros(N,N);

%initial Lagrange multiplier lambda is set to be 0
lambda1=zeros(N);
lambda2=zeros(N);

%create the quadratic coefficient
 quad1 = 2*(balancestretch/(1))*(KX.*KX+POISSON/2*(KY.*KY))+2*balancesubs*(KX.*KX)./((KX.*KX+KY.*KY).^0.5);
 quad2 = 2*(balancestretch/(1))*(KY.*KY+POISSON/2*(KX.*KX))+2*balancesubs*(KY.*KY)./((KX.*KX+KY.*KY).^0.5);
 quad12 = 2*(balancestretch/(1))*((1+coeff)/2*KX.*KY);
quad3 = 2*(balancebend/(1))*(KX.*KX+KY.*KY).^2+(beta/(1))*(KX.*KX+KY.*KY)+2*balancesubs*(KX.*KX+KY.*KY).^0.5-elecbar^2*(KX.*KX+KY.*KY).^0.5;


%create a quadratic matrix for the shear components of the substrate
```

```
quadsub11 =    2*balancesubs*(KX.*KX./(KX.*KX+KY.*KY).^0.5+(3-4*nusub)/(1-nusub)/4*KY.*KY./(KX.*KX+KY.*KY).^0.5);
quadsub12 =    2*balancesubs*(1/(1-nusub)/4*KX.*KY./(KX.*KX+KY.*KY).^0.5);
quadsub13 =    2*balancesubs*(-1/2*1i*KX*(1-2*nusub)/(1-nusub));
quadsub21 =    quadsub12;
quadsub22 =    2*balancesubs*(KY.*KY./(KX.*KX+KY.*KY).^0.5+(3-4*nusub)/(1-nusub)/4*KX.*KX./(KX.*KX+KY.*KY).^0.5);
quadsub23 =    2*balancesubs*(-1/2*1i*KY*(1-2*nusub)/(1-nusub));
quadsub31=     -quadsub13;
quadsub32=     -quadsub23;
quadsub33=    0*quadsub11;

%add the two matrices
quad1=quad1+quadsub11;
quad2=quad2+quadsub22;
quad3=quad3+quadsub33;
quad12=quad12+quadsub12;
quad13=quadsub13;
quad31=quadsub31;
quad23=quadsub23;
quad32=quadsub32;

%compute the intermediary coefficients to build the inverse of the quadratic matrix
bigA=quad2.*quad3-quad23.*quad32;
bigB=-(quad12.*quad3-quad23.*quad31);
bigC=quad12.*quad32-quad2.*quad31;
bigD=-(quad12.*quad3-quad1.*quad32);
bigE=quad1.*quad3-quad13.*quad31;
bigF=-(quad1.*quad32-quad12.*quad31);
```

```
bigG=quad12.*quad23-quad13.*quad2;
bigH=-(quad1.*quad23-quad13.*quad12);
bigI=quad1.*quad2-quad12.*quad12;
determi=quad1.*bigA+quad12.*bigB+quad13.*bigC;

%compute the coefficients of the inverse of the
    quadratic matrix
invquad11=bigA./determi;
invquad12=bigD./determi;
invquad13=bigG./determi;
invquad21=bigB./determi;
invquad22=bigE./determi;
invquad23=bigH./determi;
invquad31=bigC./determi;
invquad32=bigF./determi;
invquad33=bigI./determi;

%build a waitbar to indicate the progress of the loop
h = waitbar(0,'Please␣wait...');

% build a box to stock the number of mistakes (cases
    where the polynomial for xi can't be solved)
numberofMistakes = 0;
xi1check = zeros(N);
xi2check = zeros(N);
residue = ones(N,N);

%transfer all displacements u, v , w into the Fourier
    domain and creating their derivatives using f'= ik f
wFou = fftshift(fft2(wTensor));
wxFou = (1i*KX).*wFou;
wxTensor = real(ifft2(ifftshift(wxFou)));
wyFou = (1i*KY).*wFou;
 wyTensor = real(ifft2(ifftshift(wyFou)));
 uFou = fftshift(fft2(uTensor));
uxFou = (1i*KX).*uFou;
 uxTensor = real(ifft2(ifftshift(uxFou)));
uyFou = (1i*KY).*uFou;
uyTensor = real(ifft2(ifftshift(uyFou)));


vFou = fftshift(fft2(vTensor));
vxFou = (1i*KX).*vFou;
vxTensor = real(ifft2(ifftshift(vxFou)));
vyFou = (1i*KY).*vFou;
vyTensor = real(ifft2(ifftshift(vyFou)));

%transfer Lagrange parameters lambdas into the Fourier
   domain
        lambda1Fou = fftshift(fft2(lambda1));
        lambda2Fou = fftshift(fft2(lambda2));

 %start the loop
 for loo=1:sizeloop

    %solve for xi

    parfor i=1:N
        for j=1:N
            guess = [wxTensor(i,j),wyTensor(i,j)];
            fun = @(y)xiRoot2Duvxy(y,etaxTensor,
               etayTensor,etaxyTensor,lambda1,lambda2,
               beta,wxTensor,wyTensor,uxTensor,vyTensor
               ,uyTensor,vxTensor,i,j,POISSON,
               balancestretch);
[solution,fval,exitflag,output]=fsolve(fun,guess,
   options);

if exitflag <1 && exitflag >1
   numberofMistakes = numberofMistakes+1 ;
```

```
end
xi1Tensor(i,j) = solution(1);
xi2Tensor(i,j) = solution(2);
%we make a check that every value of the xi
  distributions is satisfaying the polynomial
xi1check(i,j) = (2*solution(1)*balancestretch*(-
  etaxTensor(i,j)+uxTensor(i,j)+0.5*solution(1)^2-
  etayTensor(i,j)+vyTensor(i,j)+0.5*solution(2)^2-
  POISSON*(-etayTensor(i,j)+vyTensor(i,j)+0.5*solution
  (2)^2))+2*balancestretch*POISSON*solution(2)*(-
  etaxyTensor(i,j)+0.5*(uyTensor(i,j)+vxTensor(i,j))
  +0.5*solution(1)*solution(2))+lambda1(i,j)-beta*(
  wxTensor(i,j)-solution(1));
xi2check(i,j) = (2*solution(2)*balancestretch*(-
  etaxTensor(i,j)+uxTensor(i,j)+0.5*solution(1)^2-
  etayTensor(i,j)+vyTensor(i,j)+0.5*solution(2)^2-
  POISSON*(-etaxTensor(i,j)+uxTensor(i,j)+0.5*solution
  (1)^2))+2*balancestretch*POISSON*solution(1)*(-
  etaxyTensor(i,j)+0.5*(uyTensor(i,j)+vxTensor(i,j))
  +0.5*solution(1)*solution(2))+lambda2(i,j)-beta*(
  wyTensor(i,j)-solution(2));

      end
   end
   %this is to stop the loop if there is one value of
     xi not satisfying the xi equation
  if max(max(xi1check))>0.000001
     msg = 'Error␣occurred␣with␣xi1';
error(msg)
  end
  if max(max(xi2check))>0.000001
     msg = 'Error␣occurred␣with␣xi2';
error(msg)
  end
```

```
    %create xi^2 and transfer everything into the
       Fourier Domain
    xi1Square = xi1Tensor.*xi1Tensor;
    xi1Fou = fftshift(fft2(xi1Tensor));
    xi1SquareFou = fftshift(fft2(xi1Square));

    xi2Square = xi2Tensor.*xi2Tensor;
    xi2Fou = fftshift(fft2(xi2Tensor));
    xi2SquareFou = fftshift(fft2(xi2Square));
%create xi1*xi2 and transfer it into the Fourier domain
    xi1xi2 = xi1Tensor.*xi2Tensor;
     xi1xi2Fou = fftshift(fft2(xi1xi2));


    %create B term by the intermediary of its conjugate
Bstar1=(balancestretch/(1))*(2*(1i)*KX.*conj(-etaxFou
   +1/2*xi1SquareFou-etayFou+1/2*xi2SquareFou)-2*
   POISSON*(1i)*KX.*conj(-etayFou+1/2*xi2SquareFou)+2*
   POISSON*(1i)*KY.*conj(-etaxyFou+1/2*xi1xi2Fou));
Bstar2=(balancestretch/(1))*(2*(1i)*KY.*conj(-etaxFou
   +1/2*xi1SquareFou-etayFou+1/2*xi2SquareFou)-2*
   POISSON*(1i)*KY.*conj(-etaxFou+1/2*xi1SquareFou)+2*
   POISSON*(1i)*KX.*conj(-etaxyFou+1/2*xi1xi2Fou));
Bstar3=(1i*KX.*conj((-lambda1Fou)+(beta)*(-xi1Fou))+1i*
   KY.*conj((-lambda2Fou)+beta*(-xi2Fou)));

Bterm1=conj(Bstar1);
Bterm2=conj(Bstar2);
Bterm=conj(Bstar3);
    %update w, w' and lambda

    wFouNext = -invquad31.*Bterm1-invquad32.*Bterm2-
       invquad33.*Bterm;
    % because one of the quadratic matrix terms is 0,
       its inverse will be infinite. It represents the
   mean value of the distribution w and must be set
    to 0
wFouNext(N/2+1,N/2+1)=0;

% compute the derivatives and the Laplacian of
   delfection w using the method f'=ik*f
wxFou = (1i*KX).*wFouNext;
wyFou = (1i*KY).*wFouNext;
wFou = wFouNext;
LaplacianFou = (1i*KX).*wxFou + (1i*KY).*wyFou;



%update u
 %uFouNext = -(inversequad1).*Bterm1 -(
    inversequad12).*Bterm2;
 uFouNext = -invquad11.*Bterm1-invquad12.*Bterm2-
    invquad13.*Bterm;
 %set the average value of u to be 0
 uFouNext(N/2+1,N/2+1) = 0;

 %compute derivative of in plane displacement u
uxFou = (1i*KX).*uFouNext;
uyFou = (1i*KY).*uFouNext;
uFou = uFouNext;

%update v
 vFouNext = -invquad21.*Bterm1-invquad22.*Bterm2-
    invquad23.*Bterm;
 %set the average value of v to be 0
vFouNext(N/2+1,N/2+1) = 0;

%compute derivative of in plane displacement v
vxFou = (1i*KX).*vFouNext;
vyFou = (1i*KY).*vFouNext;
vFou = vFouNext;
```

```
    %update the Lagrange multiplier lambda
    lambda1Fou = lambda1Fou-beta*(wxFou-xi1Fou);
    lambda2Fou = lambda2Fou-beta*(wyFou-xi2Fou);

    %transfer all displacements fields and derivatives
       back to the space domain
    wNext = ifft2(ifftshift(wFouNext));
    wTensor = real(wNext);


wxTensor = (ifft2(ifftshift(wxFou)));
wxTensor = real(wxTensor);
wyTensor = (ifft2(ifftshift(wyFou)));
wyTensor = real(wyTensor);
Laplacian = real(ifft2(ifftshift(LaplacianFou)));


uTensor = real(ifft2(ifftshift(uFouNext)));
uxTensor = (ifft2(ifftshift(uxFou)));
uxTensor = real(uxTensor);
uyTensor = (ifft2(ifftshift(uyFou)));
uyTensor = real(uyTensor);


vTensor = real(ifft2(ifftshift(vFouNext)));
vxTensor = (ifft2(ifftshift(vxFou)));
vxTensor = real(vxTensor);
vyTensor = (ifft2(ifftshift(vyFou)));
vyTensor = real(vyTensor);

%transfer the Lagrange multipliers lambda back to the
   space domain
lambda1 = (ifft2(ifftshift(lambda1Fou)));
lambda1 = real(lambda1);
lambda2 = (ifft2(ifftshift(lambda2Fou)));
```

```
lambda2 = real(lambda2);


  %create a residue tensor to check the convergence
  residue1Fou = wxFou-xi1Fou;
  residue2Fou = wyFou-xi2Fou;
  residue1 = real(ifft2(ifftshift(wxFou-xi1Fou)));
  residue2 = real(ifft2(ifftshift(wyFou-xi2Fou)));

 %compute stretching energy and bending energy
  stretching_energy = Efilm*thickness*(0.5/(1-nufilm
     ^2)*(-eta0*etaxTensor+x0/u0*uxTensor+(x0/w0)
     ^2*1/2*wxTensor.^2-eta0*etayTensor+x0/u0*
     vyTensor+(x0/w0)^2*1/2*wyTensor.^2).^2-1/(1+
     nufilm)*(-eta0*etaxTensor+x0/u0*uxTensor+(x0/w0)
     ^2*1/2*wxTensor.^2).*(-eta0*etayTensor+x0/u0*
     vyTensor+(x0/w0)^2*1/2*wyTensor.^2)+1/(1+nufilm)
     *(-eta0*etaxyTensor+x0/u0*0.5*(vxTensor+uyTensor
     )+(x0/w0)^2*1/2*wyTensor.*wxTensor));
  bending_energy = 1/2*bendingModulus*x0^4/w0^2*
     Laplacian.^2;

  %compute deflection at the correct scale thanks to
     the dimensional coefficient
  wcorrect=w0*wTensor;

  %plot the distribution of deflection w at the
     correct scale with indication of loop
     advancement
 figure(8)
 surf(Xcorrect,Ycorrect,wcorrect)
 colorbar
  view(2)
shading interp
  title(['w␣Tensor',num2str(loo)])
```

```
    %plot the Fourier distribution of deflection w with
        indication of loop advancement
    wobs=abs(wFou);
    figure(67)
    surf(KXcorrect,KYcorrect,wobs)
    colorbar
    view(2)
shading interp
    title(['Fourier␣representation␣of␣w',num2str(loo)])

    %plot the relative error between xi and grad(w)
       distribution with indication of loop advancement
     figure(111)
    surf(X,Y,residue1./wxTensor)
    colorbar
    view(2)
shading interp
    title(['residue1',num2str(loo)])

  %in case convergence is prevented by local minima
     after high number of iterations, it is still
     possible to try to get rid of those local minima
     either
  %with a filter or with a noise disturbation
    % try to kill default by adding noise every 5000
       iterations
    if loo == 100000 || loo==55000 || loo == 41000

        choice=input('Do␣you␣want␣to␣filter␣or␣noise␣or
           ␣change␣beta␣or␣continue,␣F/N/B/C␣','s');
        if choice=='N'

        wxTensor = max(max(wxTensor))/1*rand(N)+
           wxTensor;
        wyTensor = max(max(wyTensor))/1*rand(N)+
           wyTensor;
        uxTensor = max(max(uxTensor))/1*rand(N)+
           uxTensor;
        uyTensor = max(max(uyTensor))/1*rand(N)+
           uyTensor;
        vxTensor = max(max(vxTensor))/1*rand(N)+
           vxTensor;
        vyTensor = max(max(vyTensor))/1*rand(N)+
           vyTensor;
        lambda1 = max(max(lambda1))/1*rand(N)+lambda1;
        lambda2 = max(max(lambda2))/1*rand(N)+lambda2;
        xi1Tensor = max(max(xi1Tensor))/1*rand(N)+
           xi1Tensor;
        xi2Tensor = max(max(xi2Tensor))/1*rand(N)+
           xi2Tensor;
        wxFou = fftshift(fft2(wxTensor));
        wyFou = fftshift(fft2(wyTensor));
        uxFou = fftshift(fft2(uxTensor));
        uyFou = fftshift(fft2(uyTensor));
        vxFou = fftshift(fft2(uxTensor));
        vyFou = fftshift(fft2(uyTensor));
        lambda1Fou = fftshift(fft2(lambda1));
        lambda2Fou = fftshift(fft2(lambda2));
        xi1Fou = fftshift(fft2(xi1Tensor));
        xi2Fou = fftshift(fft2(xi2Tensor));


    % try to kill default by using a filter
        elseif choice=='F'
        powerfilter='What␣value␣do␣you␣want␣for␣filter?
           ␣';
            filt=input(powerfilter);
       [M,I] = max(abs(wFou(:)));
[I_row, I_col] = ind2sub(size(abs(wFou)),I);
w2=wFou;
w2(abs(wFou)<filt*M*ones(N))=0;
wFou = 1.0*w2;
```

```
wxFou = (1i*KX).*wFou;
    wyFou = (1i*KY).*wFou;
        wxTensor=real(ifft2(ifftshift(wxFou)));
        wyTensor=real(ifft2(ifftshift(wyFou)));



[M,I] = max(abs(lambda1Fou(:)));
[I_row, I_col] = ind2sub(size(abs(lambda1Fou)),I);
lambda12=lambda1Fou;
lambda12(abs(lambda1Fou)<filt*M*ones(N))=0;
lambda1Fou = 1.0*lambda12;
        lambda1=real(ifft2(ifftshift(lambda1Fou)));

[M,I] = max(abs(lambda2Fou(:)));
[I_row, I_col] = ind2sub(size(abs(lambda2Fou)),I);
lambda22=lambda2Fou;
lambda22(abs(lambda2Fou)<filt*M*ones(N))=0;
lambda2Fou = 1.0*lambda22;
        lambda2=real(ifft2(ifftshift(lambda2Fou)));

  [M,I] = max(abs(uxFou(:)));
[I_row, I_col] = ind2sub(size(abs(uxFou)),I);
ux2=uxFou;
ux2(abs(uxFou)<filt*M*ones(N))=0;
uxFou = 1.0*ux2;
        uxTensor=real(ifft2(ifftshift(uxFou)));

   [M,I] = max(abs(uyFou(:)));
[I_row, I_col] = ind2sub(size(abs(uyFou)),I);
uy2=uyFou;
uy2(abs(uyFou)<filt*M*ones(N))=0;
uyFou = 1.0*uy2;
        uyTensor=real(ifft2(ifftshift(uyFou)));

         [M,I] = max(abs(vxFou(:)));
```

```
[I_row, I_col] = ind2sub(size(abs(vxFou)),I);
vx2=vxFou;
vx2(abs(vxFou)<filt*M*ones(N))=0;
vxFou = 1.0*vx2;
        vxTensor=real(ifft2(ifftshift(vxFou)));

    [M,I] = max(abs(vyFou(:)));
[I_row, I_col] = ind2sub(size(abs(vyFou)),I);
vy2=vyFou;
vy2(abs(vyFou)<filt*M*ones(N))=0;
vyFou = 1.0*vy2;
        vyTensor=real(ifft2(ifftshift(vyFou)));

        elseif choice=='B'
            newbeta='What␣value␣do␣you␣want␣for␣beta?␣'
               ;
            beta=input(newbeta);

        end
    end


    %terminate the loop if the residue becomes small
    if norm(real(residue1))/norm(real(wxTensor))
       <0.00000001
        break
    end
     [M,I] = max(wobs(:));
[I_row, I_col] = ind2sub(size(wobs),I);
Kinterest=KYcorrect(I_row,I_col);
    waitbar(loo / sizeloop,h,sprintf('%12.9f',Kinterest
       ))


    %save the data every 2000 iterations
    if mod(loo,5000)<1
```

```
            save('C:\Users\Paul␣Mazur\Documents\MATLAB\
               dimensionalized␣results\better␣sampling\
               opposite-angles.mat')
        end
    end
    close(h)

    %convert everything obtained in the space domain
    wTensor = ifft2(ifftshift(wFouNext));
    wxTensor = ifft2(ifftshift(wxFou));
    wyTensor = ifft2(ifftshift(wyFou));
    lambda1 = ifft2(ifftshift(lambda1Fou));
    lambda2 = ifft2(ifftshift(lambda2Fou));
    xi1Tensor = ifft2(ifftshift(xi1Fou));
    xi2Tensor = ifft2(ifftshift(xi2Fou));
```

Appendix B

ABAQUS BILAYERED SYSTEM CODE

This is the ABAQUS inp file used for generating wrinkles on a bilayered system and then applying an external electric field on top of the bilayered system. The results of this file are presented in Chapter 5. This code is a modification of the code realized by Henann et al. [38] available at [8].

```
*Heading
2D plane-strain, bilayered system
**
**************************************************
**                    PARAMETERS
**************************************************
*Parameter
**
** size of specimen (m)
total_thickness=4.0e-3
t0_top = 0.03e-3
t0_bot = total_thickness-t0_top
**
**Young Modulus (Pa)
Efilm = 10.0e9
Esub = 30.0e6
NuFilm = 0.3
NuSub = 0.4
ratio = (12.0*(1 - NuFilm*NuFilm)*Esub/Efilm*(1.0 -
   NuSub)/((1.0 + NuSub)*(3.0 - 4.0*NuSub)))
ktheory = 1/t0_top*pow(ratio,0.333333)
** length of the specimen allowing to observe 15
   wrinkles
L0 = 2.0*16.0*3.1416/ktheory
** Shear moduli
G = Efilm/(2.0*(1.0+NuFilm))
Gsub = Esub/(2.0*(1.0+NuSub))
```

```
**
** Bulk modulus (Pa)
K = Efilm/(3.0*(1.0-2.0*NuFilm))
Ksub = 1.0*Esub/(3.0*(1.0-2.0*NuSub))
**
** Gent parameter
Imax = 7.0e15
**
** Permittivity (arbitrary units)
permit = 6.7*8.85e-12
permitfilm = 0.0
**
** number of elements in the x and y directions
ex = 1600
ey_top = 4
ey_bot = 30-ey_top
**
** Final time (s)
tf = 1.0
**
*****************************************************
** calculations for geometry, node numbering, loads,
   etc., don't change
**
** Geometry
t_tot = t0_bot + t0_top
**
** node/element numbering
ey = ey_bot + ey_top
nlayer = ex + 1
**
n1 = 1
n2 = n1 + ex
n3 = ey*nlayer + 1
n4 = n3 + ex
e1 = 1
```

```
e2 = e1 − 1 + ex
e3 = 1 + (ey − 1)*ex + (e1 − 1)
e4 = e3 + ex − 1
**
nmidbottom=n1+ex/2
nmid1 = ey_bot*nlayer + 1
nmid2 = nmid1 + ex
**
left2=n2+1
right2=left2+ex
left3=right2+1
right3=left3+ex
left4=right3+1
right4=left4+ex
left5=right4+1
right5=left5+ex
left6=right5+1
right6=left6+ex
left7=right6+1
right7=left7+ex
left8=right7+1
right8=left8+ex
left9=right8+1
right9=left9+ex
left10=right9+1
right10=left10+ex
left11=right10+1
right11=left11+ex
left12=right11+1
right12=left12+ex
left13=right12+1
right13=left13+ex
left14=right13+1
right14=left14+ex
left15=right14+1
right15=left15+ex
```

```
left16=right15+1
right16=left16+ex
left17=right16+1
right17=left17+ex
left18=right17+1
right18=left18+ex
left19=right18+1
right19=left19+ex
left20=right19+1
right20=left20+ex
left21=right20+1
right21=left21+ex
left22=right21+1
right22=left22+ex
left23=right22+1
right23=left23+ex
left24=right23+1
right24=left24+ex
left25=right24+1
right25=left25+ex
left26=right25+1
right26=left26+ex
left27=right26+1
right27=left27+ex
left28=right27+1
right28=left28+ex
left29=right28+1
right29=left29+ex
left30=right29+1
right30=left30+ex
left31=right30+1
right31=left31+ex
left32=right31+1
right32=left32+ex
left33=right32+1
right33=left33+ex
```

```
left34=right33+1
right34=left34+ex
left35=right34+1
right35=left35+ex
left36=right35+1
right36=left36+ex
left37=right36+1
right37=left37+ex
left38=right37+1
right38=left38+ex
left39=right38+1
right39=left39+ex
left40=right39+1
right40=left40+ex
left41=right40+1
right41=left41+ex
left42=right41+1
right42=left42+ex
left43=right42+1
right43=left43+ex
left44=right43+1
right44=left44+ex
left45=right44+1
right45=left45+ex
left46=right45+1
right46=left46+ex
left47=right46+1
right47=left47+ex
left48=right47+1
right48=left48+ex
left49=right48+1
right49=left49+ex
left50=right49+1
right50=left50+ex
left51=right50+1
right51=left51+ex
```

```
left52=right51+1
right52=left52+ex
left53=right52+1
right53=left53+ex
left54=right53+1
right54=left54+ex
left55=right54+1
right55=left55+ex
left56=right55+1
right56=left56+ex
left57=right56+1
right57=left57+ex
left58=right57+1
right58=left58+ex
left59=right58+1
right59=left59+ex
left60=right59+1
right60=left60+ex
**
elbot_mas1 = n1
elbot_mas2 = n1 + 1
elbot_mas3 = n1 + 1 + nlayer
elbot_mas4 = n1 + nlayer
**
eltop_mas1 = nmid1
eltop_mas2 = nmid1 + 1
eltop_mas3 = nmid1 + 1 + nlayer
eltop_mas4 = nmid1 + nlayer
**
e1dum = ex*ey + 1
e2dum = e1dum - 1 + ex
e3dum = 1 + (ey - 1)*ex + (e1dum - 1)
e4dum = e3dum + ex - 1
emid1dum = 1 + (ey - ey_top)*ex + (e1dum - 1)
emid2dum = emid1dum + ex - 1
emid3dum = 1 + (ey - ey_top-1)*ex + (e1dum - 1)
```

```
emid4dum = emid3dum + ex − 1
**
etop_master = ex*ey_bot + 1
**
** Final potential
phi = 2.0*1208079.59
**
**
**************************************************
**                    MODEL DEFINITION
**************************************************
*Node
<n1>,   0.0,   0.0
<n2>,   <L0>,   0.0
<n3>,   0.0,   <t_tot>
<n4>,   <L0>, <t_tot>
<nmid1>,   0.0,   <t0_bot>
<nmid2>,   <L0>,   <t0_bot>
**
** Nodes
**
*Nset, nset=n1
<n1>
*Nset, nset=n2
<n2>
*Nset, nset=n3
<n3>
*Nset, nset=n4
<n4>
*Nset, nset=nmidbottom
<nmidbottom>
*Nset, nset=nmid1
<nmid1>
*Nset, nset=nmid2
<nmid2>
*Nset, nset=left2
```

```
<left2>
*Nset, nset=left3
<left3>
*Nset, nset=left4
<left4>
*Nset, nset=left5
<left5>
*Nset, nset=left6
<left6>
*Nset, nset=left7
<left7>
*Nset, nset=left8
<left8>
*Nset, nset=left9
<left9>
*Nset, nset=left10
<left10>
*Nset, nset=right2
<right2>
*Nset, nset=right3
<right3>
*Nset, nset=right4
<right4>
*Nset, nset=right5
<right5>
*Nset, nset=right6
<right6>
*Nset, nset=right7
<right7>
*Nset, nset=right8
<right8>
*Nset, nset=right9
<right9>
*Nset, nset=right10
<right10>
*Nset, nset=left11
```

```
<left11>
*Nset, nset=left12
<left12>
*Nset, nset=left13
<left13>
*Nset, nset=left14
<left14>
*Nset, nset=left15
<left15>
*Nset, nset=left16
<left16>
*Nset, nset=left17
<left17>
*Nset, nset=left18
<left18>
*Nset, nset=left19
<left19>
*Nset, nset=left20
<left20>
*Nset, nset=right11
<right11>
*Nset, nset=right12
<right12>
*Nset, nset=right13
<right13>
*Nset, nset=right14
<right14>
*Nset, nset=right15
<right15>
*Nset, nset=right16
<right16>
*Nset, nset=right17
<right17>
*Nset, nset=right18
<right18>
*Nset, nset=right19
```

```
<right19>
*Nset, nset=right20
<right20>
*Nset, nset=left21
<left21>
*Nset, nset=right21
<right21>
*Nset, nset=left22
<left22>
*Nset, nset=left23
<left23>
*Nset, nset=left24
<left24>
*Nset, nset=left25
<left25>
*Nset, nset=left26
<left26>
*Nset, nset=left27
<left27>
*Nset, nset=left28
<left28>
*Nset, nset=left29
<left29>
*Nset, nset=left30
<left30>
*Nset, nset=right22
<right22>
*Nset, nset=right23
<right23>
*Nset, nset=right24
<right24>
*Nset, nset=right25
<right25>
*Nset, nset=right26
<right26>
*Nset, nset=right27
```

```
<right27>
*Nset, nset=right28
<right28>
*Nset, nset=right29
<right29>
*Nset, nset=right30
<right30>
*Nset, nset=left31
<left31>
*Nset, nset=left32
<left32>
*Nset, nset=left33
<left33>
*Nset, nset=left34
<left34>
*Nset, nset=left35
<left35>
*Nset, nset=left36
<left36>
*Nset, nset=left37
<left37>
*Nset, nset=left38
<left38>
*Nset, nset=left39
<left39>
*Nset, nset=left40
<left40>
*Nset, nset=right31
<right31>
*Nset, nset=right32
<right32>
*Nset, nset=right33
<right33>
*Nset, nset=right34
<right34>
*Nset, nset=right35
```

```
<right35>
*Nset, nset=right36
<right36>
*Nset, nset=right37
<right37>
*Nset, nset=right38
<right38>
*Nset, nset=right39
<right39>
*Nset, nset=right40
<right40>
*Nset, nset=left41
<left41>
*Nset, nset=left42
<left42>
*Nset, nset=left43
<left43>
*Nset, nset=left44
<left44>
*Nset, nset=left45
<left45>
*Nset, nset=left46
<left46>
*Nset, nset=left47
<left47>
*Nset, nset=left48
<left48>
*Nset, nset=left49
<left49>
*Nset, nset=left50
<left50>
*Nset, nset=right41
<right41>
*Nset, nset=right42
<right42>
*Nset, nset=right43
```

```
<right43>
*Nset, nset=right44
<right44>
*Nset, nset=right45
<right45>
*Nset, nset=right46
<right46>
*Nset, nset=right47
<right47>
*Nset, nset=right48
<right48>
*Nset, nset=right49
<right49>
*Nset, nset=right50
<right50>
*Nset, nset=left51
<left51>
*Nset, nset=left52
<left52>
*Nset, nset=left53
<left53>
*Nset, nset=left54
<left54>
*Nset, nset=left55
<left55>
*Nset, nset=left56
<left56>
*Nset, nset=left57
<left57>
*Nset, nset=left58
<left58>
*Nset, nset=left59
<left59>
*Nset, nset=left60
<left60>
*Nset, nset=right51
```

```
<right51>
*Nset, nset=right52
<right52>
*Nset, nset=right53
<right53>
*Nset, nset=right54
<right54>
*Nset, nset=right55
<right55>
*Nset, nset=right56
<right56>
*Nset, nset=right57
<right57>
*Nset, nset=right58
<right58>
*Nset, nset=right59
<right59>
*Nset, nset=right60
<right60>
**
*Nfill, nset=left_sub, bias = 1.20
n1, nmid1, <ey_bot>, <nlayer>
*Nfill, nset=left_film
nmid1, n3, <ey_top>, <nlayer>
*Nfill, nset=right_sub, bias = 1.20
n2, nmid2, <ey_bot>, <nlayer>
*Nfill, nset=right_film
nmid2, n4, <ey_top>, <nlayer>
*Nfill, nset=Nall_sub
left_sub, right_sub, <ex>,1
*Nfill, nset=Nall_film
left_film, right_film, <ex>,1
*Nset, nset=top, gen
<n3>, <n4>, 1
*Nset, nset=bottom, gen
<n1>, <n2>, 1
```

```
*Nset, nset=midplane, gen
<nmid1>,<nmid2>,1
**
** Elements
**
*User Element,Nodes=4,Type=U1,Iproperties=1,Properties
   =4,Coordinates=2,Variables=1,Unsymm
1,2,11
**
*Element, type=U1
<e1>, <elbot_mas1>,<elbot_mas2>,<elbot_mas3>,<
   elbot_mas4>
*Elset, elset=first_element
<e1>
*Elgen, elset=elbot
<e1>,<ex>,1,1,<ey_bot>,<nlayer>,<ex>
*Element, type=U1
<etop_master>, <eltop_mas1>,<eltop_mas2>,<eltop_mas3>,<
   eltop_mas4>
*Elgen, elset=eltop
<etop_master>,<ex>,1,1,<ey_top>,<nlayer>,<ex>
*Elset, elset=Elall
elbot,eltop
*Elset, elset=elrightside, gen
<e2>, <e4>, <ex>
*Elset, elset=elleftside, gen
<e1>, <e3>, <ex>
**
** Constraint: Constraint-1
*Equation
2
n1, 1, 1.
n2, 1, -1.
** Constraint: Constraint-1-Copy
*Equation
2
```

```
n1, 2, 1.
n2, 2, -1.
** Constraint: Constraint-1
*Equation
2
n3, 1, 1.
n4, 1, -1.
** Constraint: Constraint-1-Copy
*Equation
2
n3, 2, 1.
n4, 2, -1.
** Constraint: Constraint-2
*Equation
2
left2, 1, 1.
right2, 1, -1.
** Constraint: Constraint-2-Copy
*Equation
2
left2, 2, 1.
right2, 2, -1.
** Constraint: Constraint-3
*Equation
2
left3, 1, 1.
right3, 1, -1.
** Constraint: Constraint-3-Copy
*Equation
2
left3, 2, 1.
right3, 2, -1.
** Constraint: Constraint-4
*Equation
2
left4, 1, 1.
```

```
right4, 1, -1.
** Constraint: Constraint-4-Copy
*Equation
2
left4, 2, 1.
right4, 2, -1.
** Constraint: Constraint-5
*Equation
2
left5, 1, 1.
right5, 1, -1.
** Constraint: Constraint-5-Copy
*Equation
2
left5, 2, 1.
right5, 2, -1.
** Constraint: Constraint-6
*Equation
2
left6, 1, 1.
right6, 1, -1.
** Constraint: Constraint-6-Copy
*Equation
2
left6, 2, 1.
right6, 2, -1.
** Constraint: Constraint-7
*Equation
2
left7, 1, 1.
right7, 1, -1.
** Constraint: Constraint-7-Copy
*Equation
2
left7, 2, 1.
right7, 2, -1.
```

```
** Constraint: Constraint-8
*Equation
2
left8, 1, 1.
right8, 1, -1.
** Constraint: Constraint-8-Copy
*Equation
2
left8, 2, 1.
right8, 2, -1.
** Constraint: Constraint-9
*Equation
2
left9, 1, 1.
right9, 1, -1.
** Constraint: Constraint-9-Copy
*Equation
2
left9, 2, 1.
right9, 2, -1.
** Constraint: Constraint-10
*Equation
2
left10, 1, 1.
right10, 1, -1.
** Constraint: Constraint-10-Copy
*Equation
2
left10, 2, 1.
right10, 2, -1.
** Constraint: Constraint-11
*Equation
2
left11, 1, 1.
right11, 1, -1.
** Constraint: Constraint-11-Copy
```

```
*Equation
2
left11, 2, 1.
right11, 2, -1.
** Constraint: Constraint-12
*Equation
2
left12, 1, 1.
right12, 1, -1.
** Constraint: Constraint-12-Copy
*Equation
2
left12, 2, 1.
right12, 2, -1.
** Constraint: Constraint-13
*Equation
2
left13, 1, 1.
right13, 1, -1.
** Constraint: Constraint-13-Copy
*Equation
2
left13, 2, 1.
right13, 2, -1.
** Constraint: Constraint-14
*Equation
2
left14, 1, 1.
right14, 1, -1.
** Constraint: Constraint-14-Copy
*Equation
2
left14, 2, 1.
right14, 2, -1.
** Constraint: Constraint-15
*Equation
```

```
2
left15 , 1, 1.
right15 , 1, −1.
** Constraint: Constraint −15−Copy
*Equation
2
left15 , 2, 1.
right15 , 2, −1.
** Constraint: Constraint −16
*Equation
2
left16 , 1, 1.
right16 , 1, −1.
** Constraint: Constraint −16−Copy
*Equation
2
left16 , 2, 1.
right16 , 2, −1.
** Constraint: Constraint −17
*Equation
2
left17 , 1, 1.
right17 , 1, −1.
** Constraint: Constraint −17−Copy
*Equation
2
left17 , 2, 1.
right17 , 2, −1.
** Constraint: Constraint −18
*Equation
2
left18 , 1, 1.
right18 , 1, −1.
** Constraint: Constraint −18−Copy
*Equation
2
```

```
left18, 2, 1.
right18, 2, -1.
** Constraint: Constraint-19
*Equation
2
left19, 1, 1.
right19, 1, -1.
** Constraint: Constraint-19-Copy
*Equation
2
left19, 2, 1.
right19, 2, -1.
** Constraint: Constraint-20
*Equation
2
left20, 1, 1.
right20, 1, -1.
** Constraint: Constraint-20-Copy
*Equation
2
left20, 2, 1.
right20, 2, -1.
** Constraint: Constraint-21
*Equation
2
left21, 1, 1.
right21, 1, -1.
** Constraint: Constraint-21-Copy
*Equation
2
left21, 2, 1.
right21, 2, -1.
** Constraint: Constraint-22
*Equation
2
left22, 1, 1.
```

```
right22, 1, −1.
** Constraint: Constraint−22−Copy
*Equation
2
left22, 2, 1.
right22, 2, −1.
** Constraint: Constraint−23
*Equation
2
left23, 1, 1.
right23, 1, −1.
** Constraint: Constraint−23−Copy
*Equation
2
left23, 2, 1.
right23, 2, −1.
** Constraint: Constraint−24
*Equation
2
left24, 1, 1.
right24, 1, −1.
** Constraint: Constraint−24−Copy
*Equation
2
left24, 2, 1.
right24, 2, −1.
** Constraint: Constraint−25
*Equation
2
left25, 1, 1.
right25, 1, −1.
** Constraint: Constraint−25−Copy
*Equation
2
left25, 2, 1.
right25, 2, −1.
```

```
** Constraint: Constraint-26
*Equation
2
left26, 1, 1.
right26, 1, -1.
** Constraint: Constraint-26-Copy
*Equation
2
left26, 2, 1.
right26, 2, -1.
** Constraint: Constraint-27
*Equation
2
left27, 1, 1.
right27, 1, -1.
** Constraint: Constraint-27-Copy
*Equation
2
left27, 2, 1.
right27, 2, -1.
** Constraint: Constraint-28
*Equation
2
left28, 1, 1.
right28, 1, -1.
** Constraint: Constraint-28-Copy
*Equation
2
left28, 2, 1.
right28, 2, -1.
** Constraint: Constraint-29
*Equation
2
left29, 1, 1.
right29, 1, -1.
** Constraint: Constraint-29-Copy
```

```
*Equation
2
left29, 2, 1.
right29, 2, -1.
** Constraint: Constraint-30
*Equation
2
left30, 1, 1.
right30, 1, -1.
** Constraint: Constraint-30-Copy
*Equation
2
left30, 2, 1.
right30, 2, -1.
**
*IMPERFECTION,FILE=Job-buckling-henann-1600x30,STEP=2
1,0.0000003
**************************************************
**                      MATERIAL DEFINITION
**************************************************
**
** Material properties for the real material
**
*uel property,elset=eltop
**************************************************
**G      Kbulk    Imax     permitfilm               pe
<G>,     <K>,     <Imax>,  <permitfilm>,    1
**
**************************************************
*uel property,elset=elbot
**************************************************
**G      Kbulk    Imax     permit           pe
<Gsub>,  <Ksub>,  <Imax>,  <permit>,        1
**
**************************************************
**
```

```
**************************************************
**                     INITIAL CONDITIONS
**************************************************
*Initial conditions, type=temperature
nall_sub, 0.0
nall_film, 0.0
**************************************************
**                        AMPLITUDE
**************************************************
*Amplitude, name=Amp-1
0.0,0.0,<tf>,1.0
**************************************************
**                     STEP DEFINITION
**************************************************
*Step, Name=Load, nlgeom=yes, inc=50000
*Coupled temperature-displacement, deltmx=100.0
0.05,<tf>,1.e-8,0.05
*controls, parameters=line search
10,1.0,0.0001,0.25,0.10
*controls, parameters=time incrementation
,,,,,,,10,,,,,,
**
*Boundary
<nmid1>,2,2
bottom,11,11,0.0
*Boundary
bottom,YSYMM
*Boundary
nmidbottom,XSYMM
*Output, field, time interval=0.05
*node output, nset=nall_film
u,nt,coord
*node output, nset=nall_sub
u,nt,coord
*Element Output, elset=Elall, directions=YES
BF, FV, LE, PE, PEEQ, PEMAG, S, SDV
```

```
**
*Output, history, time interval=0.05
*node output, nset=right_film
u1,u2
*node output, nset=top
nt11
*node output, nset=midplane
rfl11
**
*End Step
**************************************************
*Step, Name=Electricity, nlgeom=yes, inc=50000
*Coupled temperature-displacement, deltmx=100.0
0.05,<tf>,1.e-8,0.05
*controls, parameters=line search
10,1.0,0.0001,0.25,0.10
*controls, parameters=time incrementation
,,,,,,,10,,,,,,
**
*Boundary, amplitude=Amp-1
midplane,11,11,<phi>
**
*Output, field, time interval=0.05
*node output, nset=nall_film
u,nt,coord
*node output, nset=nall_sub
u,nt,coord
**
*Output, history, time interval=0.05
*node output, nset=right_sub
u1,u2
*node output, nset=right_film
u1,u2
*node output, nset=top
nt11
*node output, nset=midplane
```

```
rf111
**
*End Step
```

Appendix C

SUBSTRATE ENERGY CODE

This is the Mathematica notebook written to solve the exact expression of the substrate energy in the Fourier domain described in Chapter 2.

Substrate energy

First we write down the differential operator A :

```
A = {{0, 0, 0, 1, 0, 0}, {0, 0, 0, 0, 1, 0}, {0, 0, 0, 0, 0, 1},
    {kx^2 * (λ + 2 * μ) / μ + ky^2, (λ + μ) / μ * kx * ky, 0, 0, 0, -I * kx * (λ + μ) / μ},
    {(λ + μ) / μ * kx * ky, ky^2 * (λ + 2 * μ) / μ + kx^2, 0, 0, 0, -I * ky * (λ + μ) / μ},
    {0, 0, μ / (λ + 2 * μ) * (kx^2 + ky^2),
     -I * kx * (λ + μ) / (λ + 2 * μ), -I * ky * (λ + μ) / (λ + 2 * μ), 0}};
```

Then we evaluate the eigenvalues and eigenvectors of this differential operator:

```
Eigensystem[A]
```

$$\Big\{\Big\{-\sqrt{kx^2+ky^2},\ -\sqrt{kx^2+ky^2},\ -\sqrt{kx^2+ky^2},\ \sqrt{kx^2+ky^2},\ \sqrt{kx^2+ky^2},\ \sqrt{kx^2+ky^2}\Big\},$$

$$\Big\{\Big\{\frac{i}{kx},\ 0,\ -\frac{1}{\sqrt{kx^2+ky^2}},\ -\frac{i\sqrt{kx^2+ky^2}}{kx},\ 0,\ 1\Big\},$$

$$\Big\{\frac{ky}{kx\sqrt{kx^2+ky^2}},\ -\frac{1}{\sqrt{kx^2+ky^2}},\ 0,\ -\frac{ky}{kx},\ 1,\ 0\Big\},$$

$$\{0,\ 0,\ 0,\ 0,\ 0,\ 0\},\ \Big\{\frac{i}{kx},\ 0,\ \frac{1}{\sqrt{kx^2+ky^2}},\ \frac{i\sqrt{kx^2+ky^2}}{kx},\ 0,\ 1\Big\},$$

$$\Big\{-\frac{ky}{kx\sqrt{kx^2+ky^2}},\ \frac{1}{\sqrt{kx^2+ky^2}},\ 0,\ -\frac{ky}{kx},\ 1,\ 0\Big\},\ \{0,\ 0,\ 0,\ 0,\ 0,\ 0\}\Big\}\Big\}$$

We see that we have two different eigenvalues, each one having a multiplicity 3. The two eigenspace each have dimension 2. It is possible to ask Mathematica to solve the differential system on its own, but the result is not favorable to the boundary conditions we want to apply.

```
DSolve[{(λ + μ) * (-kx^2 * u[z] - kx * ky * v[z] + I * kx * w'[z]) +
      μ * (-kx^2 * u[z] - ky^2 * u[z] + u''[z]) == 0 &&
    (λ + μ) * (-kx * ky * u[z] - ky^2 * v[z] + I * ky * w'[z]) +
      μ * (-kx^2 * v[z] - ky^2 * v[z] + v''[z]) == 0 &&
    (λ + μ) * (I * kx * u'[z] + I * ky * v'[z] + w''[z]) +
      μ * (-kx^2 * w[z] - ky^2 * w[z] + w''[z]) == 0}, {u[z], v[z], w[z]}, z]
```

This result gives us the form that must be investigated for u ,v, and w. We determine the independent constants of functions u,v,w by solving the following systems:

```
Solve[μ (kx^2 + ky^2) u2 + I kx (λ + μ) (-Sqrt[(kx^2 + ky^2)] w2) -
    u2 (kx^2 (λ + 2 μ) + μ ky^2) - v2 (λ + μ) kx ky == 0 &&
  μ (kx^2 + ky^2) v2 + I ky (λ + μ) (-Sqrt[(kx^2 + ky^2)] w2) -
    v2 (ky^2 (λ + 2 μ) + μ kx^2) - u2 (λ + μ) kx ky == 0 &&
  (λ + 2 μ) (kx^2 + ky^2) w2 + I kx (λ + μ) (-Sqrt[(kx^2 + ky^2)] u2) +
    I ky (λ + μ) (-Sqrt[(kx^2 + ky^2)] v2) - μ (kx^2 + ky^2) w2 == 0 &&
  μ ((kx^2 + ky^2) u1 - 2 Sqrt[(kx^2 + ky^2)] u2) + I kx (λ + μ)
      (-Sqrt[(kx^2 + ky^2)] w1 + w2) - u1 (kx^2 (λ + 2 μ) + μ ky^2) - v1 (λ + μ) kx ky == 0 &&
  μ ((kx^2 + ky^2) v1 - 2 Sqrt[(kx^2 + ky^2)] v2) + I ky (λ + μ)
      (-Sqrt[(kx^2 + ky^2)] w1 + w2) - v1 (ky^2 (λ + 2 μ) + μ kx^2) - u1 (λ + μ) kx ky == 0 &&
  (λ + 2 μ) ((kx^2 + ky^2) w1 - 2 Sqrt[(kx^2 + ky^2)] w2) +
    I kx (λ + μ) (-Sqrt[(kx^2 + ky^2)] u1 + u2) + I ky (λ + μ)
      (-Sqrt[(kx^2 + ky^2)] v1 + v2) - μ w1 (kx^2 + ky^2) == 0, {u1, u2, v1, v2, w1, w2}]
```

```
Solve::svars : Equations may not give solutions for all "solve" variables. >>
```

$$\left\{\left\{\mathrm{v1}\to-\frac{\mathrm{kx}\,\mathrm{u1}}{\mathrm{ky}}-\frac{\mathrm{i}\,\sqrt{\mathrm{kx}^2+\mathrm{ky}^2}\,\mathrm{w1}}{\mathrm{ky}}-\frac{\mathrm{u2}\,\left(\mathrm{kx}^2\,\lambda+\mathrm{ky}^2\,\lambda+3\,\mathrm{kx}^2\,\mu+3\,\mathrm{ky}^2\,\mu\right)}{\mathrm{kx}\,\mathrm{ky}\,\sqrt{\mathrm{kx}^2+\mathrm{ky}^2}\,(\lambda+\mu)},\right.\right.$$
$$\left.\left.\mathrm{v2}\to\frac{\mathrm{ky}\,\mathrm{u2}}{\mathrm{kx}},\ \mathrm{w2}\to\frac{\mathrm{i}\,\sqrt{\mathrm{kx}^2+\mathrm{ky}^2}\,\mathrm{u2}}{\mathrm{kx}}\right\}\right\}$$

```
Solve[
 μ (kx^2 + ky^2) u4 + I kx (λ + μ) (Sqrt[(kx^2 + ky^2)] w4) - u4 (kx^2 (λ + 2 μ) + μ ky^2) -
    v4 (λ + μ) kx ky == 0 && μ (kx^2 + ky^2) v4 + I ky (λ + μ) (Sqrt[(kx^2 + ky^2)] w4) -
    v4 (ky^2 (λ + 2 μ) + μ kx^2) - u4 (λ + μ) kx ky == 0 &&
  (λ + 2 μ) (kx^2 + ky^2) w4 + I kx (λ + μ) (Sqrt[(kx^2 + ky^2)] u4) +
    I ky (λ + μ) (Sqrt[(kx^2 + ky^2)] v4) - μ (kx^2 + ky^2) w4 == 0 &&
  μ ((kx^2 + ky^2) u3 + 2 Sqrt[(kx^2 + ky^2)] u4) + I kx (λ + μ)
      (Sqrt[(kx^2 + ky^2)] w3 + w4) - u3 (kx^2 (λ + 2 μ) + μ ky^2) - v3 (λ + μ) kx ky == 0 &&
  μ ((kx^2 + ky^2) v3 + 2 Sqrt[(kx^2 + ky^2)] v4) + I ky (λ + μ)
      (Sqrt[(kx^2 + ky^2)] w3 + w4) - v3 (ky^2 (λ + 2 μ) + μ kx^2) - u3 (λ + μ) kx ky == 0 &&
  (λ + 2 μ) ((kx^2 + ky^2) w3 + 2 Sqrt[(kx^2 + ky^2)] w4) +
    I kx (λ + μ) (Sqrt[(kx^2 + ky^2)] u3 + u4) + I ky (λ + μ) (Sqrt[(kx^2 + ky^2)] v3 + v4) -
    μ w3 (kx^2 + ky^2) == 0, {u3, u4, v3, v4, w3, w4}]
```

```
Solve::svars : Equations may not give solutions for all "solve" variables. >>
```

$$\left\{\left\{\mathrm{v3}\to-\frac{\mathrm{kx}\,\mathrm{u3}}{\mathrm{ky}}+\frac{\mathrm{i}\,\sqrt{\mathrm{kx}^2+\mathrm{ky}^2}\,\mathrm{w3}}{\mathrm{ky}}-\frac{\mathrm{u4}\,\left(-\mathrm{kx}^2\,\lambda-\mathrm{ky}^2\,\lambda-3\,\mathrm{kx}^2\,\mu-3\,\mathrm{ky}^2\,\mu\right)}{\mathrm{kx}\,\mathrm{ky}\,\sqrt{\mathrm{kx}^2+\mathrm{ky}^2}\,(\lambda+\mu)},\right.\right.$$
$$\left.\left.\mathrm{v4}\to\frac{\mathrm{ky}\,\mathrm{u4}}{\mathrm{kx}},\ \mathrm{w4}\to-\frac{\mathrm{i}\,\sqrt{\mathrm{kx}^2+\mathrm{ky}^2}\,\mathrm{u4}}{\mathrm{kx}}\right\}\right\}$$

From here we only consider the terms associated with exp[-k*z] since the boundary conditions make the others terms to be zero. We first check that our result satisfies the set of coupled differential equations:

```
u[z_] = (c4 * ky + c6 * kx * z) * Exp[Sqrt[kx^2 + ky^2] * z];
v[z_] = (-c4 * kx + c5 * I * Sqrt[kx^2 + ky^2] + c6 *
        (Sqrt[kx^2 + ky^2] / ky * (λ + 3 * μ) / (λ + μ) + ky * z)) * Exp[Sqrt[kx^2 + ky^2] * z];
w[z_] = (c5 * ky + c6 * I * (-Sqrt[kx^2 + ky^2]) * z) * Exp[Sqrt[kx^2 + ky^2] * z];
uconj[z_] = (Conjugate[c4] * ky + Conjugate[c6] * kx * z) * Exp[Sqrt[kx^2 + ky^2] * z];
vconj[z_] = (-Conjugate[c4] * kx - Conjugate[c5] * I * Sqrt[kx^2 + ky^2] + Conjugate[c6] *
        (Sqrt[kx^2 + ky^2] / ky * (λ + 3 * μ) / (λ + μ) + ky * z)) * Exp[Sqrt[kx^2 + ky^2] * z];
wconj[z_] = (Conjugate[c5] * ky + Conjugate[c6] * I * Sqrt[kx^2 + ky^2] * z) *
    Exp[Sqrt[kx^2 + ky^2] * z];
```

```
(λ + μ) * (-kx^2 * u[z] - kx * ky * v[z] + I * kx * w'[z]) +
   μ * (-kx^2 * u[z] - ky^2 * u[z] + u''[z]) // Simplify
(λ + μ) * (-kx * ky * u[z] - ky^2 * v[z] + I * ky * w'[z]) +
   μ * (-kx^2 * v[z] - ky^2 * v[z] + v''[z]) // Simplify
(λ + μ) * (I * kx * u'[z] + I * ky * v'[z] + w''[z]) +
   μ * (-kx^2 * w[z] - ky^2 * w[z] + w''[z]) // Simplify
```

```
0

0

0
```

Now, we inject those functions into the expression of the energy of the substrate:

```
energy = 1 / 2 * Integrate[
      (2 * μ + λ) * (kx^2 * u[z] * uconj[z] + ky^2 * v[z] * vconj[z] + wconj'[z] * w'[z]) +
       λ * (ky * kx * u[z] * vconj[z] + kx * ky * uconj[z] * v[z] + I * kx * u[z] * wconj'[z] -
           I * kx * uconj[z] * w'[z] + I * ky * v[z] * wconj'[z] - I * ky * vconj[z] * w'[z]) +
       μ * ((I * ky * u[z] + I * kx * v[z]) * (-I * ky * uconj[z] - I * kx * vconj[z]) +
           (I * kx * w[z] + u'[z]) * (-I * kx * wconj[z] + uconj'[z]) + (I * ky * w[z] + v'[z]) *
            (-I * ky * wconj[z] + vconj'[z])), {z, -Infinity, 0}] // Simplify
```

$$
\begin{aligned}
&\text{ConditionalExpression}\Big[\\
&\frac{1}{2\,ky^2\sqrt{kx^2+ky^2}\,(\lambda+\mu)^2}\,\mu\,\Big(ky\,(kx^2+ky^2)\,(\lambda+\mu)\,\Big(c4\,ky\,(kx^2+ky^2)\,(\lambda+\mu)-\\
&\qquad \mathrm{i}\,kx\sqrt{kx^2+ky^2}\,\big(c5\,ky\,(\lambda+\mu)-\mathrm{i}\,c6\,(\lambda+3\,\mu)\big)\Big)\,\text{Conjugate}[c4]+\\
&\quad ky\,(kx^2+ky^2)\,(\lambda+\mu)\,\Big(ky\,\Big(\mathrm{i}\,c4\,kx\sqrt{kx^2+ky^2}+c5\,(kx^2+4\,ky^2)\Big)\,(\lambda+\mu)-\\
&\qquad \mathrm{i}\,c6\,(kx^2+2\,ky^2)\,(\lambda+3\,\mu)\Big)\,\text{Conjugate}[c5]+\\
&\quad (\lambda+3\,\mu)\,\Big(\mathrm{i}\,ky\sqrt{kx^2+ky^2}\,\Big(\mathrm{i}\,c4\,kx\,(kx^2+ky^2)+c5\sqrt{kx^2+ky^2}\,(kx^2+2\,ky^2)\Big)\,(\lambda+\mu)+\\
&\qquad c6\,(kx^2+ky^2)\,\big(2\,ky^2\,(\lambda+2\,\mu)+kx^2\,(\lambda+3\,\mu)\big)\Big)\,\text{Conjugate}[c6]\Big),\ \text{Re}\Big[\sqrt{kx^2+ky^2}\Big]>0\Big]
\end{aligned}
$$

$$
ky\Big/\sqrt{kx^2+ky^2} * (\lambda+\mu) \,/\, (\lambda + 3 * \mu) * \Big(vint + kx \,/\, ky * uint - I * \sqrt{kx^2+ky^2}\Big/ ky * wint\Big)
$$

Now, we replace the constants c4 c5 c6 with their expressions as functions of the displacements at the interface between film and substrate (at z=0):

energybis =

$$\begin{aligned}
&\mathbf{Simplify}\Big[\frac{1}{2\,\mathbf{ky}^2\sqrt{\mathbf{kx}^2+\mathbf{ky}^2}\;(\lambda+\mu)^2}\,\mu\,\Big(\mathbf{ky}\,\left(\mathbf{kx}^2+\mathbf{ky}^2\right)\,(\lambda+\mu)\,\Big(\mathbf{uint}\,/\,\mathbf{ky}\;\mathbf{ky}\,\left(\mathbf{kx}^2+\mathbf{ky}^2\right)\,(\lambda+\mu)\,-\\
&\quad\mathbb{i}\,\mathbf{kx}\,\sqrt{\mathbf{kx}^2+\mathbf{ky}^2}\,\Big(\mathbf{wint}\,/\,\mathbf{ky}\;\mathbf{ky}\,(\lambda+\mu)\,-\,\mathbb{i}\,\mathbf{ky}\Big/\sqrt{\mathbf{kx}^2+\mathbf{ky}^2}\,*\,(\lambda+\mu)\,\Big/\,\left(\lambda+3*\mu\right)\,*\\
&\qquad\Big(\mathbf{vint}+\mathbf{kx}\,/\,\mathbf{ky}*\mathbf{uint}-\mathbf{I}*\sqrt{\mathbf{kx}^2+\mathbf{ky}^2}\Big/\mathbf{ky}*\mathbf{wint}\Big)\,\left(\lambda+3\,\mu\right)\Big)\Big)\\
&\quad\mathbf{Conjugate[uint]}\,/\,\mathbf{ky}+\mathbf{ky}\,\left(\mathbf{kx}^2+\mathbf{ky}^2\right)\,(\lambda+\mu)\\
&\quad\Big(\mathbf{ky}\,\Big(\mathbb{i}\,\mathbf{uint}\,/\,\mathbf{ky}\;\mathbf{kx}\,\sqrt{\mathbf{kx}^2+\mathbf{ky}^2}+\mathbf{wint}\,/\,\mathbf{ky}\,\left(\mathbf{kx}^2+4\,\mathbf{ky}^2\right)\Big)\,(\lambda+\mu)\,-\,\mathbb{i}\,\mathbf{ky}\Big/\sqrt{\mathbf{kx}^2+\mathbf{ky}^2}\,*\\
&\qquad(\lambda+\mu)\,\Big/\,\left(\lambda+3*\mu\right)\,*\,\Big(\mathbf{vint}+\mathbf{kx}\,/\,\mathbf{ky}*\mathbf{uint}-\mathbf{I}*\sqrt{\mathbf{kx}^2+\mathbf{ky}^2}\Big/\mathbf{ky}*\mathbf{wint}\Big)\\
&\qquad\left(\mathbf{kx}^2+2\,\mathbf{ky}^2\right)\,\left(\lambda+3\,\mu\right)\Big)\,\mathbf{Conjugate[wint]}\,/\,\mathbf{ky}+\left(\lambda+3\,\mu\right)\\
&\quad\Big(\mathbb{i}\,\mathbf{ky}\,\sqrt{\mathbf{kx}^2+\mathbf{ky}^2}\,\Big(\mathbb{i}\,\mathbf{uint}\,/\,\mathbf{ky}\;\mathbf{kx}\,\left(\mathbf{kx}^2+\mathbf{ky}^2\right)+\mathbf{wint}\,/\,\mathbf{ky}\,\sqrt{\mathbf{kx}^2+\mathbf{ky}^2}\,\left(\mathbf{kx}^2+2\,\mathbf{ky}^2\right)\Big)\\
&\qquad(\lambda+\mu)+\mathbf{ky}\Big/\sqrt{\mathbf{kx}^2+\mathbf{ky}^2}\,*\,(\lambda+\mu)\,\Big/\,\left(\lambda+3*\mu\right)\,*\,\Big(\mathbf{vint}+\mathbf{kx}\,/\,\mathbf{ky}*\mathbf{uint}-\\
&\qquad\mathbf{I}*\sqrt{\mathbf{kx}^2+\mathbf{ky}^2}\Big/\mathbf{ky}*\mathbf{wint}\Big)\,\left(\mathbf{kx}^2+\mathbf{ky}^2\right)\,\left(2\,\mathbf{ky}^2\,\left(\lambda+2\,\mu\right)+\mathbf{kx}^2\,\left(\lambda+3\,\mu\right)\right)\Big)\\
&\quad\mathbf{ky}\Big/\sqrt{\mathbf{kx}^2+\mathbf{ky}^2}\,*\,(\lambda+\mu)\,\Big/\,\left(\lambda+3*\mu\right)\,*\,\Big(\mathbf{Conjugate[vint]}+\mathbf{kx}\,/\,\mathbf{ky}*\mathbf{Conjugate[uint]}+\\
&\qquad\mathbf{I}*\sqrt{\mathbf{kx}^2+\mathbf{ky}^2}\Big/\mathbf{ky}*\mathbf{Conjugate[wint]}\Big)\Big),\;\mathbf{Re}\Big[\sqrt{\mathbf{kx}^2+\mathbf{ky}^2}\Big]>0\Big]
\end{aligned}$$

$$\begin{aligned}
&\frac{1}{2\,\left(\text{kx}^2+\text{ky}^2\right)\,\left(\lambda+3\,\mu\right)}\\
&\mu\,\Big(\Big(2\,\mathbb{i}\,\text{kx}^3\,\text{wint}\,\mu+2\,\text{kx}^2\,\sqrt{\text{kx}^2+\text{ky}^2}\;\text{uint}\,\left(\lambda+2\,\mu\right)+\text{ky}^2\,\sqrt{\text{kx}^2+\text{ky}^2}\;\text{uint}\,\left(\lambda+3\,\mu\right)+\\
&\qquad\text{kx}\,\text{ky}\,\Big(2\,\mathbb{i}\,\text{ky}\,\text{wint}\,\mu+\sqrt{\text{kx}^2+\text{ky}^2}\;\text{vint}\,\left(\lambda+\mu\right)\Big)\Big)\,\text{Conjugate[uint]}+\\
&\quad\Big(\text{kx}\,\text{ky}\,\sqrt{\text{kx}^2+\text{ky}^2}\;\text{uint}\,\left(\lambda+\mu\right)+2\,\text{ky}^2\,\Big(\mathbb{i}\,\text{ky}\,\text{wint}\,\mu+\sqrt{\text{kx}^2+\text{ky}^2}\;\text{vint}\,\left(\lambda+2\,\mu\right)\Big)+\\
&\qquad\text{kx}^2\,\Big(2\,\mathbb{i}\,\text{ky}\,\text{wint}\,\mu+\sqrt{\text{kx}^2+\text{ky}^2}\;\text{vint}\,\left(\lambda+3\,\mu\right)\Big)\Big)\,\text{Conjugate[vint]}+\\
&\quad2\,\left(\text{kx}^2+\text{ky}^2\right)\,\Big(-\mathbb{i}\,\left(\text{kx}\,\text{uint}+\text{ky}\,\text{vint}\right)\,\mu+\sqrt{\text{kx}^2+\text{ky}^2}\;\text{wint}\,\left(\lambda+2\,\mu\right)\Big)\,\text{Conjugate[wint]}\Big)
\end{aligned}$$

Now, we replace the Lame coefficients with their expressions as function of the Young modulus and the Poisson ratio of the substrate:

```
energybisbis =
 FullSimplify[(1 / (2 (kx^2 + ky^2) (Young * ν / ((1 + ν) * (1 - 2 * ν)) + 3 Young / 2 / (1 + ν))))
   Young / 2 / (1 + ν) ((2 ⅈ kx^3 wint Young / 2 / (1 + ν) +
        2 kx^2 √(kx^2 + ky^2) uint (Young * ν / ((1 + ν) * (1 - 2 * ν)) + 2 Young / 2 / (1 + ν)) +
        ky^2 √(kx^2 + ky^2) uint (Young * ν / ((1 + ν) * (1 - 2 * ν)) + 3 Young / 2 / (1 + ν)) +
        kx ky (2 ⅈ ky wint Young / 2 / (1 + ν) + √(kx^2 + ky^2) vint
            (Young * ν / ((1 + ν) * (1 - 2 * ν)) + Young / 2 / (1 + ν)))) Conjugate[uint] +
      (kx ky √(kx^2 + ky^2) uint (Young * ν / ((1 + ν) * (1 - 2 * ν)) + Young / 2 / (1 + ν)) +
        2 ky^2 (ⅈ ky wint Young / 2 / (1 + ν) +
            √(kx^2 + ky^2) vint (Young * ν / ((1 + ν) * (1 - 2 * ν)) + 2 Young / 2 / (1 + ν))) +
        kx^2 (2 ⅈ ky wint Young / 2 / (1 + ν) + √(kx^2 + ky^2) vint
            (Young * ν / ((1 + ν) * (1 - 2 * ν)) + 3 Young / 2 / (1 + ν)))) Conjugate[vint] +
      2 (kx^2 + ky^2) (-ⅈ (kx uint + ky vint) Young / 2 / (1 + ν) + √(kx^2 + ky^2) wint
          (Young * ν / ((1 + ν) * (1 - 2 * ν)) + 2 Young / 2 / (1 + ν))) Conjugate[wint])]
```

$$\frac{1}{4\sqrt{\text{kx}^2+\text{ky}^2}\,\left(-3+\nu+4\,\nu^2\right)}\,\text{Young}\\
\Big(\Big(4\,\text{kx}^2\,\text{uint}\,(-1+\nu)+\text{ky}^2\,\text{uint}\,(-3+4\,\nu)-\text{kx}\left(\text{ky}\,\text{vint}-2\,i\,\sqrt{\text{kx}^2+\text{ky}^2}\,\text{wint}\,(-1+2\,\nu)\right)\Big)\\
\text{Conjugate}[\text{uint}]+\Big(-\text{kx}\,\text{ky}\,\text{uint}+\text{kx}^2\,\text{vint}\,(-3+4\,\nu)+\\
2\,\text{ky}\left(2\,\text{ky}\,\text{vint}\,(-1+\nu)+i\,\sqrt{\text{kx}^2+\text{ky}^2}\,\text{wint}\,(-1+2\,\nu)\right)\Big)\,\text{Conjugate}[\text{vint}]+\\
2\,\Big(\text{ky}\left(i\,\sqrt{\text{kx}^2+\text{ky}^2}\,\text{vint}\,(1-2\,\nu)+2\,\text{ky}\,\text{wint}\,(-1+\nu)\right)+\\
i\,\text{kx}\,\sqrt{\text{kx}^2+\text{ky}^2}\,\text{uint}\,(1-2\,\nu)+2\,\text{kx}^2\,\text{wint}\,(-1+\nu)\Big)\,\text{Conjugate}[\text{wint}]\Big)$$

In this section, we confirm our results by performing the same calculation with the terms associated with exp[k*z] (we must be careful and integrate the energy from 0 to infinity):

```
u2[z_] = (c1 * ky + c3 * kx * z) * Exp[- Sqrt[kx^2 + ky^2] * z];
v2[z_] = (- kx * c1 - I * Sqrt[kx^2 + ky^2] * c2 +
      c3 * (- Sqrt[kx^2 + ky^2] / ky * (λ + 3 * μ) / (λ + μ) + ky * z)) *
    Exp[- Sqrt[kx^2 + ky^2] * z];
w2[z_] = (c2 * ky + c3 * I * Sqrt[kx^2 + ky^2] * z) * Exp[- Sqrt[kx^2 + ky^2] * z];
uconj2[z_] = (Conjugate[c1] * ky + Conjugate[c3] * kx * z) * Exp[- Sqrt[kx^2 + ky^2] * z];
vconj2[z_] = (- kx * Conjugate[c1] + I * Sqrt[kx^2 + ky^2] * Conjugate[c2] +
      Conjugate[c3] * (- Sqrt[kx^2 + ky^2] / ky * (λ + 3 * μ) / (λ + μ) + ky * z)) *
    Exp[- Sqrt[kx^2 + ky^2] * z];
wconj2[z_] = (Conjugate[c2] * ky - Conjugate[c3] * I * Sqrt[kx^2 + ky^2] * z) *
    Exp[- Sqrt[kx^2 + ky^2] * z];
```

```
(λ + μ) * (- kx^2 * u2[z] - kx * ky * v2[z] + I * kx * w2 '[z]) +
  μ * (- kx^2 * u2[z] - ky^2 * u2[z] + u2 ''[z]) // Simplify
```

```
0
```

Again we inject the expressions of the displacements into the expression of the substrate energy:

```
energy2 = Simplify[1 / 2 * Integrate[(2 * μ + λ) *
       (kx^2 * u2[z] * uconj2[z] + ky^2 * v2[z] * vconj2[z] + wconj2 '[z] * w2 '[z]) +
      λ * (ky * kx * u2[z] * vconj2[z] + kx * ky * uconj2[z] * v2[z] +
          I * kx * u2[z] * wconj2 '[z] - I * kx * uconj2[z] * w2 '[z] +
          I * ky * v2[z] * wconj2 '[z] - I * ky * vconj2[z] * w2 '[z]) +
      μ * ((I * ky * u2[z] + I * kx * v2[z]) * (- I * ky * uconj2[z] - I * kx * vconj2[z]) +
          (I * kx * w2[z] + u2 '[z]) * (- I * kx * wconj2[z] + uconj2 '[z]) +
          (I * ky * w2[z] + v2 '[z]) * (- I * ky * wconj2[z] + vconj2 '[z])), {z, 0, Infinity}]]
```

$$
\begin{aligned}
&\text{ConditionalExpression}\Big[\frac{1}{2\,\text{ky}^2\,(\lambda+\mu)^2}\sqrt{\text{kx}^2+\text{ky}^2}\;\mu\\
&\Big(\text{ky}\,(\lambda+\mu)\,\Big(\text{c1}\,\text{ky}\,\big(\text{kx}^2+\text{ky}^2\big)\,(\lambda+\mu)+\text{kx}\sqrt{\text{kx}^2+\text{ky}^2}\,\big(\mathbb{i}\,\text{c2}\,\text{ky}\,(\lambda+\mu)+\text{c3}\,(\lambda+3\,\mu)\big)\Big)\\
&\quad\text{Conjugate[c1]}+\text{ky}\,(\lambda+\mu)\,\Big(\text{ky}\,\Big(-\mathbb{i}\,\text{c1}\,\text{kx}\sqrt{\text{kx}^2+\text{ky}^2}+\text{c2}\,\big(\text{kx}^2+4\,\text{ky}^2\big)\Big)\,(\lambda+\mu)-\\
&\quad\quad\mathbb{i}\,\text{c3}\,\big(\text{kx}^2+2\,\text{ky}^2\big)\,(\lambda+3\,\mu)\Big)\,\text{Conjugate[c2]}+(\lambda+3\,\mu)\\
&\quad\Big(\text{ky}\,\Big(\text{c1}\,\text{kx}\sqrt{\text{kx}^2+\text{ky}^2}+\mathbb{i}\,\text{c2}\,\big(\text{kx}^2+2\,\text{ky}^2\big)\Big)\,(\lambda+\mu)+\text{c3}\,\big(2\,\text{ky}^2\,(\lambda+2\,\mu)+\text{kx}^2\,(\lambda+3\,\mu)\big)\Big)\\
&\quad\text{Conjugate[c3]}\Big),\ \text{Re}\Big[\sqrt{\text{kx}^2+\text{ky}^2}\,\Big]>0\Big]
\end{aligned}
$$

$$\mathbf{Simplify}\left[\mathbf{energy2},\ \mathbf{Re}\left[\sqrt{\mathbf{kx}^2+\mathbf{ky}^2}\right]>0\right]$$

$$\begin{aligned}&\frac{1}{2\,ky^2\,\sqrt{kx^2+ky^2}\,(\lambda+\mu)^2}\,\mu\,\Big(ky\,(kx^2+ky^2)\,(\lambda+\mu)\\
&\quad\Big(c1\,ky\,(kx^2+ky^2)\,(\lambda+\mu)+kx\,\sqrt{kx^2+ky^2}\,\big(\mathrm{i}\,c2\,ky\,(\lambda+\mu)+c3\,(\lambda+3\,\mu)\big)\Big)\,\mathrm{Conjugate}[c1]+\\
&\quad ky\,(kx^2+ky^2)\,(\lambda+\mu)\,\Big(ky\,\big(-\mathrm{i}\,c1\,kx\,\sqrt{kx^2+ky^2}+c2\,(kx^2+4\,ky^2)\big)\,(\lambda+\mu)-\\
&\qquad\mathrm{i}\,c3\,(kx^2+2\,ky^2)\,(\lambda+3\,\mu)\Big)\,\mathrm{Conjugate}[c2]+\\
&\quad(\lambda+3\,\mu)\,\Big(ky\,\sqrt{kx^2+ky^2}\,\big(c1\,kx\,(kx^2+ky^2)+\mathrm{i}\,c2\,\sqrt{kx^2+ky^2}\,(kx^2+2\,ky^2)\big)\,(\lambda+\mu)+\\
&\qquad c3\,(kx^2+ky^2)\,\big(2\,ky^2\,(\lambda+2\,\mu)+kx^2\,(\lambda+3\,\mu)\big)\Big)\,\mathrm{Conjugate}[c3]\Big)\end{aligned}$$

$$\mathbf{FullSimplify}\left[\mathbf{energy2},\ \mathbf{Re}\left[\sqrt{\mathbf{kx}^2+\mathbf{ky}^2}\right]>0\right]$$

$$\begin{aligned}&\frac{1}{2\,ky^2\,(\lambda+\mu)^2}\,\sqrt{kx^2+ky^2}\,\mu\,\Big(ky\,(\lambda+\mu)\\
&\quad\Big(c1\,ky\,(kx^2+ky^2)\,(\lambda+\mu)+kx\,\sqrt{kx^2+ky^2}\,\big(\mathrm{i}\,c2\,ky\,(\lambda+\mu)+c3\,(\lambda+3\,\mu)\big)\Big)\,\mathrm{Conjugate}[c1]+\\
&\quad ky\,(\lambda+\mu)\,\Big(ky\,\big(c2\,kx^2+4\,c2\,ky^2-\mathrm{i}\,c1\,kx\,\sqrt{kx^2+ky^2}\big)\,(\lambda+\mu)-\mathrm{i}\,c3\,(kx^2+2\,ky^2)\,(\lambda+3\,\mu)\Big)\\
&\quad\mathrm{Conjugate}[c2]+(\lambda+3\,\mu)\,\Big(ky\,\big(c1\,kx\,\sqrt{kx^2+ky^2}+\mathrm{i}\,c2\,(kx^2+2\,ky^2)\big)\,(\lambda+\mu)+\\
&\qquad c3\,\big(2\,ky^2\,(\lambda+2\,\mu)+kx^2\,(\lambda+3\,\mu)\big)\Big)\,\mathrm{Conjugate}[c3]\Big)\end{aligned}$$

Now, we replace the constants c1 c2 and c3 with their expressions as functions of the displacements at the top surface of the substrate (z=0):

energy3 =

$$\begin{aligned}
&\frac{1}{2\,\mathrm{ky}^2\,(\lambda+\mu)^2}\sqrt{\mathrm{kx}^2+\mathrm{ky}^2}\;\mu\,\Bigg(\mathrm{ky}\,(\lambda+\mu)\,\Bigg(\mathrm{uint}/\mathrm{ky}\;\mathrm{ky}\,\left(\mathrm{kx}^2+\mathrm{ky}^2\right)(\lambda+\mu)+\mathrm{kx}\sqrt{\mathrm{kx}^2+\mathrm{ky}^2}\\
&\quad\Bigg(\mathrm{i}\,\mathrm{wint}/\mathrm{ky}\;\mathrm{ky}\,(\lambda+\mu)+\left(-\mathrm{kx}\Big/\sqrt{\mathrm{kx}^2+\mathrm{ky}^2}*\mathrm{uint}-\mathrm{I}*\mathrm{wint}-\mathrm{ky}\Big/\sqrt{\mathrm{kx}^2+\mathrm{ky}^2}*\right.\\
&\quad\quad\left.\mathrm{vint}\right)*(\lambda+\mu)\Big/\left(\lambda+3*\mu\right)\,\left(\lambda+3\,\mu\right)\Bigg)\Bigg)\;\mathrm{Conjugate}[\mathrm{uint}]/\mathrm{ky}+\\
&\quad\mathrm{ky}\,(\lambda+\mu)\,\Bigg(\mathrm{ky}\left(\mathrm{wint}/\mathrm{ky}\;\mathrm{kx}^2+4\;\mathrm{wint}/\mathrm{ky}\;\mathrm{ky}^2-\mathrm{i}\;\mathrm{uint}/\mathrm{ky}\;\mathrm{kx}\sqrt{\mathrm{kx}^2+\mathrm{ky}^2}\right)(\lambda+\mu)-\\
&\quad\quad\mathrm{i}\left(-\mathrm{kx}\Big/\sqrt{\mathrm{kx}^2+\mathrm{ky}^2}*\mathrm{uint}-\mathrm{I}*\mathrm{wint}-\mathrm{ky}\Big/\sqrt{\mathrm{kx}^2+\mathrm{ky}^2}*\mathrm{vint}\right)*\\
&\quad\quad(\lambda+\mu)\Big/\left(\lambda+3*\mu\right)\,\left(\mathrm{kx}^2+2\,\mathrm{ky}^2\right)\left(\lambda+3\,\mu\right)\Bigg)\;\mathrm{Conjugate}[\mathrm{wint}]/\mathrm{ky}+\\
&\quad\left(\lambda+3\,\mu\right)\Bigg(\mathrm{ky}\left(\mathrm{uint}/\mathrm{ky}\;\mathrm{kx}\sqrt{\mathrm{kx}^2+\mathrm{ky}^2}+\mathrm{i}\;\mathrm{wint}/\mathrm{ky}\left(\mathrm{kx}^2+2\,\mathrm{ky}^2\right)\right)(\lambda+\mu)+\\
&\quad\quad\left(-\mathrm{kx}\Big/\sqrt{\mathrm{kx}^2+\mathrm{ky}^2}*\mathrm{uint}-\mathrm{I}*\mathrm{wint}-\mathrm{ky}\Big/\sqrt{\mathrm{kx}^2+\mathrm{ky}^2}*\mathrm{vint}\right)*\\
&\quad\quad(\lambda+\mu)\Big/\left(\lambda+3*\mu\right)\,\left(2\,\mathrm{ky}^2\left(\lambda+2\,\mu\right)+\mathrm{kx}^2\left(\lambda+3\,\mu\right)\right)\Bigg)\Bigg)\\
&\quad\left(-\mathrm{kx}\Big/\sqrt{\mathrm{kx}^2+\mathrm{ky}^2}*\mathrm{Conjugate}[\mathrm{uint}]+\mathrm{I}*\mathrm{Conjugate}[\mathrm{wint}]-\right.\\
&\quad\quad\left.\mathrm{ky}\Big/\sqrt{\mathrm{kx}^2+\mathrm{ky}^2}*\mathrm{Conjugate}[\mathrm{vint}]\right)*(\lambda+\mu)\Big/\left(\lambda+3*\mu\right)\right)\;\text{// FullSimplify}
\end{aligned}$$

$$\begin{aligned}
&\frac{1}{2\sqrt{\mathrm{kx}^2+\mathrm{ky}^2}\,(\lambda+3\,\mu)}\\
&\mu\,\Bigg(\left(2\,\mathrm{kx}^2\,\mathrm{uint}\,(\lambda+2\,\mu)+\mathrm{ky}^2\,\mathrm{uint}\,(\lambda+3\,\mu)+\mathrm{kx}\left(-2\,\mathrm{i}\sqrt{\mathrm{kx}^2+\mathrm{ky}^2}\;\mathrm{wint}\,\mu+\mathrm{ky}\,\mathrm{vint}\,(\lambda+\mu)\right)\right)\\
&\quad\mathrm{Conjugate}[\mathrm{uint}]+\\
&\quad\left(\mathrm{kx}\,\mathrm{ky}\,\mathrm{uint}\,(\lambda+\mu)+\mathrm{kx}^2\,\mathrm{vint}\,(\lambda+3\,\mu)+2\,\mathrm{ky}\left(-\mathrm{i}\sqrt{\mathrm{kx}^2+\mathrm{ky}^2}\;\mathrm{wint}\,\mu+\mathrm{ky}\,\mathrm{vint}\,(\lambda+2\,\mu)\right)\right)\\
&\quad\mathrm{Conjugate}[\mathrm{vint}]+2\left(\mathrm{i}\,\mathrm{kx}\sqrt{\mathrm{kx}^2+\mathrm{ky}^2}\;\mathrm{uint}\,\mu+\mathrm{kx}^2\,\mathrm{wint}\,(\lambda+2\,\mu)+\right.\\
&\quad\quad\left.\mathrm{ky}\left(\mathrm{i}\sqrt{\mathrm{kx}^2+\mathrm{ky}^2}\;\mathrm{vint}\,\mu+\mathrm{ky}\,\mathrm{wint}\,(\lambda+2\,\mu)\right)\right)\mathrm{Conjugate}[\mathrm{wint}]\Bigg)
\end{aligned}$$

wconj2'[z] * w2'[z] // Simplify

$$\begin{aligned}
&e^{-2\sqrt{\mathrm{kx}^2+\mathrm{ky}^2}\;z}\left(\mathrm{kx}^2+\mathrm{ky}^2\right)\left(\mathrm{c2}\,\mathrm{ky}+\mathrm{i}\,\mathrm{c3}\left(-1+\sqrt{\mathrm{kx}^2+\mathrm{ky}^2}\;z\right)\right)\\
&\quad\left(\mathrm{ky}\,\mathrm{Conjugate}[\mathrm{c2}]-\mathrm{i}\left(-1+\sqrt{\mathrm{kx}^2+\mathrm{ky}^2}\;z\right)\mathrm{Conjugate}[\mathrm{c3}]\right)
\end{aligned}$$

$$\begin{aligned}
&\mathbf{FullSimplify}\Big[\\
&\frac{1}{2\,ky^{2}\sqrt{kx^{2}+ky^{2}}\,(\lambda+\mu)^{2}}\,\mu\,\Big(ky\,(\lambda+\mu)\,\Big(c1\,ky\,\big(kx^{4}+ky^{3}+kx^{2}\,ky\,(1+ky)\big)\,(\lambda+\mu)+\\
&\qquad kx\sqrt{kx^{2}+ky^{2}}\,\big(\mathbb{i}\,c2\,ky\,\big(kx^{2}+ky\,(-1+2\,ky)\big)\,(\lambda+\mu)+\\
&\qquad\quad c3\,\big(kx^{2}\,(\lambda+3\,\mu)+ky\,(-\lambda+2\,ky\,\lambda-\mu+4\,ky\,\mu)\big)\big)\Big)\,\mathrm{Conjugate}[c1]+\\
&\quad (kx^{2}+ky^{2})\,\Big(ky\,(\lambda+\mu)\,\Big(ky\,\Big(-\mathbb{i}\,c1\,kx\sqrt{kx^{2}+ky^{2}}+c2\,(kx^{2}+4\,ky^{2})\Big)\,(\lambda+\mu)-\\
&\qquad\quad \mathbb{i}\,c3\,(kx^{2}+2\,ky^{2})\,(\lambda+3\,\mu)\Big)\,\mathrm{Conjugate}[c2]+\\
&\qquad (\lambda+3\,\mu)\,\Big(ky\,\Big(c1\,kx\sqrt{kx^{2}+ky^{2}}+\mathbb{i}\,c2\,(kx^{2}+2\,ky^{2})\Big)\,(\lambda+\mu)+\\
&\qquad\quad c3\,\big(2\,ky^{2}\,(\lambda+2\,\mu)+kx^{2}\,(\lambda+3\,\mu)\big)\Big)\,\mathrm{Conjugate}[c3]\Big)\Big)\Big]
\end{aligned}$$

$$\begin{aligned}
&\frac{1}{2\,ky^{2}\sqrt{kx^{2}+ky^{2}}\,(\lambda+\mu)^{2}}\,\mu\\
&\quad\Big(ky\,(\lambda+\mu)\,\Big(c1\,ky\,(kx^{2}+ky)\,(kx^{2}+ky^{2})\,(\lambda+\mu)+kx\sqrt{kx^{2}+ky^{2}}\,\big(\mathbb{i}\,c2\,ky\,\big(kx^{2}+ky\,(-1+2\,ky)\big)\\
&\qquad\quad (\lambda+\mu)+c3\,\big(kx^{2}\,(\lambda+3\,\mu)+ky\,(-\lambda+2\,ky\,\lambda-\mu+4\,ky\,\mu)\big)\big)\Big)\,\mathrm{Conjugate}[c1]+\\
&\quad (kx^{2}+ky^{2})\,\Big(ky\,(\lambda+\mu)\,\Big(ky\,\Big(c2\,kx^{2}+4\,c2\,ky^{2}-\mathbb{i}\,c1\,kx\sqrt{kx^{2}+ky^{2}}\Big)\,(\lambda+\mu)-\\
&\qquad\quad \mathbb{i}\,c3\,(kx^{2}+2\,ky^{2})\,(\lambda+3\,\mu)\Big)\,\mathrm{Conjugate}[c2]+\\
&\qquad (\lambda+3\,\mu)\,\Big(ky\,\Big(c1\,kx\sqrt{kx^{2}+ky^{2}}+\mathbb{i}\,c2\,(kx^{2}+2\,ky^{2})\Big)\,(\lambda+\mu)+\\
&\qquad\quad c3\,\big(2\,ky^{2}\,(\lambda+2\,\mu)+kx^{2}\,(\lambda+3\,\mu)\big)\Big)\,\mathrm{Conjugate}[c3]\Big)\Big)
\end{aligned}$$

Finally, we replace the Lame coefficients with their expressions as functions of the Young modulus and Poisson ratio.

energy4 =

$$\frac{1}{2\sqrt{kx^2+ky^2}\,\left(\text{Young}*\nu/\left(\left(1+\nu\right)*\left(1-2*\nu\right)\right)+3\,\text{Young}/2/\left(1+\nu\right)\right)}\,\text{Young}/2/\left(1+\nu\right)$$

$$\Big(\Big(2\,kx^2\,\text{uint}\,\left(\text{Young}*\nu/\left(\left(1+\nu\right)*\left(1-2*\nu\right)\right)+2\,\text{Young}/2/\left(1+\nu\right)\right)+ky^2$$

$$\text{uint}\,\left(\text{Young}*\nu/\left(\left(1+\nu\right)*\left(1-2*\nu\right)\right)+3\,\text{Young}/2/\left(1+\nu\right)\right)+$$

$$kx\,\Big(-2\,i\,\sqrt{kx^2+ky^2}\,\text{wint}\,\text{Young}/2/\left(1+\nu\right)+ky\,\text{vint}$$

$$\left(\text{Young}*\nu/\left(\left(1+\nu\right)*\left(1-2*\nu\right)\right)+\text{Young}/2/\left(1+\nu\right)\right)\Big)\Big)\,\text{Conjugate[uint]}+$$

$$\Big(kx\,ky\,\text{uint}\,\left(\text{Young}*\nu/\left(\left(1+\nu\right)*\left(1-2*\nu\right)\right)+\text{Young}/2/\left(1+\nu\right)\right)+$$

$$kx^2\,\text{vint}\,\left(\text{Young}*\nu/\left(\left(1+\nu\right)*\left(1-2*\nu\right)\right)+3\,\text{Young}/2/\left(1+\nu\right)\right)+$$

$$2\,ky\,\Big(-i\,\sqrt{kx^2+ky^2}\,\text{wint}\,\text{Young}/2/\left(1+\nu\right)+$$

$$ky\,\text{vint}\,\left(\text{Young}*\nu/\left(\left(1+\nu\right)*\left(1-2*\nu\right)\right)+2\,\text{Young}/2/\left(1+\nu\right)\right)\Big)\Big)$$

$$\text{Conjugate[vint]}+2\,\Big(i\,kx\,\sqrt{kx^2+ky^2}\,\text{uint}\,\text{Young}/2/\left(1+\nu\right)+$$

$$kx^2\,\text{wint}\,\left(\text{Young}*\nu/\left(\left(1+\nu\right)*\left(1-2*\nu\right)\right)+2\,\text{Young}/2/\left(1+\nu\right)\right)+$$

$$ky\,\Big(i\,\sqrt{kx^2+ky^2}\,\text{vint}\,\text{Young}/2/\left(1+\nu\right)+ky\,\text{wint}\,\left(\text{Young}*\nu/\left(\left(1+\nu\right)*\left(1-2*\nu\right)\right)+\right.$$

$$\left.2\,\text{Young}/2/\left(1+\nu\right)\right)\Big)\Big)\,\text{Conjugate[wint]}\Big)\ //\ \text{FullSimplify}$$

$$\frac{1}{4\sqrt{kx^2+ky^2}\,\left(-3+\nu+4\,\nu^2\right)}\,\text{Young}$$

$$\Big(\Big(4\,kx^2\,\text{uint}\,\left(-1+\nu\right)+ky^2\,\text{uint}\,\left(-3+4\,\nu\right)-kx\,\Big(ky\,\text{vint}+2\,i\,\sqrt{kx^2+ky^2}\,\text{wint}\,\left(-1+2\,\nu\right)\Big)\Big)$$

$$\text{Conjugate[uint]}+$$

$$\Big(-kx\,ky\,\text{uint}+2\,ky\,\Big(i\,\sqrt{kx^2+ky^2}\,\text{wint}\,\left(1-2\,\nu\right)+2\,ky\,\text{vint}\,\left(-1+\nu\right)\Big)+kx^2\,\text{vint}\,\left(-3+4\,\nu\right)\Big)$$

$$\text{Conjugate[vint]}+2\,\Big(2\,kx^2\,\text{wint}\,\left(-1+\nu\right)+i\,kx\,\sqrt{kx^2+ky^2}\,\text{uint}\,\left(-1+2\,\nu\right)+$$

$$ky\,\Big(2\,ky\,\text{wint}\,\left(-1+\nu\right)+i\,\sqrt{kx^2+ky^2}\,\text{vint}\,\left(-1+2\,\nu\right)\Big)\Big)\,\text{Conjugate[wint]}\Big)$$